Biomimetic Fabrication of Organic-Inorganic Composite Materials

Von der Fakultät für Lebenswissenschaften

der Technischen Universität Carolo-Wilhelmina

zu Braunschweig

zur Erlangung des Grades eines

Doktors der Naturwissenschaften

(Dr. rer. nat.)

genehmigte

D i s s e r t a t i o n

von Sajjad Mahmood Waraich

aus Mandi Bahauddin / Pakistan

1. Referent: Professor Dr. Henning Menzel
2. Referent: Professor Dr. Peter Behrens
eingereicht am: 27.02.2012
mündlich Prüfung (Disputation) am: 23.04.2012

Druckjahr 2012

Vorveröffentlichungen der Dissertation:

Teilergebnisse aus dieser Arbeit wurden mit Genehmigung der Fakultät für Lebenswiss-enschaften, vertreten durch den Mentor der Arbeit, in folgenden Beiträgen vorabveröffentlicht:

Publikationen:

Waraich, S. M., Hering, B., Burghard, Z., Bill, J., Behrens, P. & Menzel, H., Fabrication and characterization of biocompatible nacre-like structures from α-zirconium hydrogen phosphate hydrate and chitosan. J. Colloid Interface Sci. 367: 74-82 (2012).

Tagungsbeiträge:

Menzel, H., Waraich, S. M., Wißmann, G., Hering, B. & Behrens, P.: Fabrication and characterization of nacre like composites from zirconium hydrogenphosphate hydrate and chitosan. (Poster). Jahrestagung der Deutschen Gesellschaft für Biomaterialien e.V. (DGBM), Heilbad Heiligenstadt (2010).

Waraich, S. M., Hering, B., Behrens, P. & Menzel, H.: Preparation of mother-of-pearl like materials for the biomedical applications by layer by layer deposition. (Poster). Jahrestagung der Deutschen Gesellschaft für Biomaterialien e.V. (DGBM), Tübingen (2009).

Waraich, S. M., Hering, B., Behrens, P. & Menzel, H.: Mimicking nacre as bio-inspired implant material. (Poster). European Polymer Congress, Graz/Austria (2009).

Waraich, S. M., Hering, B., Behrens, P., Helmecke, O., Menzel, H., Moral, A. I., van der Meer, M., Richter, B., Ostermeier, S. & Hurschler, C.: Creating nacre-like composite materials for biomedical applications. (Vortrag). ZFM-Festkörpernachmittag, Hanover 2009.

Waraich, S. M., Hering, B., Behrens, P. & Menzel, H.: Nacre as model for bio-inspired implant materials: Synthetic Approaches. (Poster). Hybrid Materials, Tours/France (2009).

Waraich, S. M., Hering, B., Behrens, P., Helmecke, O. & Menzel, H.: Nacre as model for bio-inspired implant materials: Synthetic Approaches. (Poster). Jahrestagung der Deutschen Gesellschaft für Biomaterialien e.V. (DGBM), Hamburg (2008).

Menzel, H., Helmecke, O., Waraich, S. M., Hering, B., Behrens, P., Denkena, B., van der Meer, M., Ostermeier, S. & Hurschler, C.: Nacre as bio-inspired model for implant material. (Poster). Jahrestagung der Deutschen Gesellschaft für Biomaterialien e.V. (DGBM), Hanover (2007).

Acknowledgments

First and foremost I would like to express my gratitude and sincere regards to my advisor Prof. Dr. Henning Menzel for giving me the opportunity to pursue my thesis work. I appreciate his invaluable guidance, advice, encouragement and funding to make this work productive. I am thankful to Prof Dr. Peter Behrens (Institute of Inorganic Chemistry, Leibniz University Hanover) for the cooperation and useful discussions within the SFB 599 sub project D9 “Biomimetic Ceramics” and for his willingness to be the co-referee.

My thanks and appreciations go to Dr. Britta Hering (Institute of Inorganic Chemistry, Leibniz University Hanover) for her excellent collaboration, synthesizing inorganic material and performing SEM. Furthermore, the cooperation from the collaborating colleagues of D9 throughout the project is appreciated as well. Valuable contributions from Dr. Zaklina Burghard (Max Planck Institute for Metal Research, Stuttgart) in performing the nanoindentation and Matthias Boettger (Laboratory for Electro Optics, TU Braunschweig) for making it possible to perform the profilometer measurements are much appreciated.

I thank all the members of the research group Menzel for making the working environment friendly and productive. Especially I would like to thank Ansgar Niehoff, my office colleague, for his readiness to help. I wish to record my thanks to Dr. Olaf Helmecke for optimizing the dip robot. Andreas Bertz is thankfully acknowledged for performing the GPC measurements. My special thanks are due to Corinna Lorenz for her quick proof reading and valuable suggestions to the thesis.

My stay in Braunschweig during Master and PhD work was wonderful and joyous which I will never forget. I am indebted to many of my colleagues and friends who supported me directly or indirectly during my whole stay.

Finally I would like to thank my family, particularly my parents, who raised me and supported me in all my pursuits. Above all, my wife, who took care of Hassan and Mueez who, with their endless energy, were ever ready to play with me whenever I was working on my thesis at home.

Table of Contents

1 Introduction

Osteoarthritis takes place as a result of joint wearing along with pain as a usual presenting feature. In extreme case of damage an artificial joint is implanted, that's why this disease is responsible for more than 95% of joint and knee replacements. It has been estimated that around 120 000 total hip and 136 000 knee implants respectively are being implanted in Germany and UK annually.[1-2] One of the major clinical problems related to the total hip and knee surgery is associated with prosthetic failure (Figure 1-1). There is a need of revision in cases where degradation of the implants occurs. A steady increase has been observed between 1990 and 2002 for the revisions and the numbers are expected to increase rapidly.[3] This has resulted in a burden on the healthcare system and there is need to improve the implant performance. Main focus is on the quality and lifetime of the implant to reduce both cost and painful procedures which a patient has to go through.

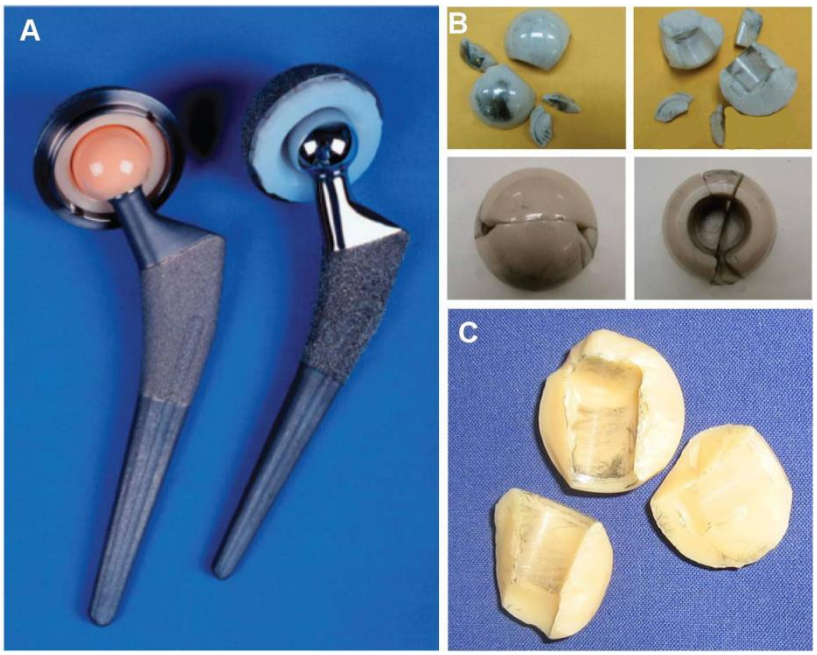

Figure 1-1: (A) Prosthetic hip implants, (B) failure of ceramic femoral head[4] and (C) disrupted head of hip prosthesis*

* adapted from Dr. S. Ostermeier, Medical School Hanover

A common problem of failure is the breakdown of implants under repetitive loading cycles. The average life time of prosthetic devices is 10-15 years. This life time is even shorter in case of younger patients who are more active than older. Around 25% of the implants for hip and knee joint replacements need to go through second surgery as a result of premature failure.[5-6]

Implant performance can be improved by the construction of new hybrid composite materials. Copper, chromium with ultrahigh molecular weight polyethylene material combination has been substituted by ceramics as an alternative for knee and hip total prosthesis for many years.[7-8] Zirconia and alumina were used for orthopedic bearings; particularly the later one is by far the most widely used ceramic. The brittle nature of the ceramic material has proved to be particularly problematic, because it may cause catastrophic failure of the implants. Low fracture toughness of ceramics along with their susceptibility to failure by slow crack growth remains a concern for the reliability of such materials.

The ideal implant must be able to withstand high cyclic loads for several decades without failure and must have reliable biocompatibility. For the search of a new class of materials which can fulfill high demands, hybrid materials are best choice. Many examples of such materials can be taken from nature where organic and inorganic building blocks are distributed on the macro molecular or nano scale. Generally the inorganic part contributes mechanical strength and structure to the natural objects and the organic counterpart ensures bonding between these building blocks. Well known examples of such materials are silk, antler, hedgehog spines, bone and nacre (mother of pearl).[9] These materials are studied extensively by the researchers to copy the ideas as found in nature and transfer them to artificial materials in a so called biomimetic approach.

Under the banner of collaborative research centre 599, “Sustainable bioresorbable and permanent implants of metallic and ceramic materials” sub project D9 “biomimetic ceramics” explores the possibilities of new biomimetic hybrid materials on the design principle of nacre. The choice for nacre was obvious because of the specific mechanical properties owing to the complex hierarchical structure of elastic organic and hard inorganic component. It was a collaborative effort which is explained schematically in Figure 1-2. Institute of Technical Chemistry (TU Braunschweig) in cooperation with Institute of Inorganic Chemistry (Leibniz University Hanover) were responsible to synthesize polymer and inorganic nano particles from which composite materials were prepared. The machinability and mechanical behavior

of new material can be tested at Institute of Production Engineering and Machine Tools (Hanover). The Department of Orthopedics at the Medical School of Hanover has conducted experiment regarding sliding, wear and fracture toughness of the nacre material.

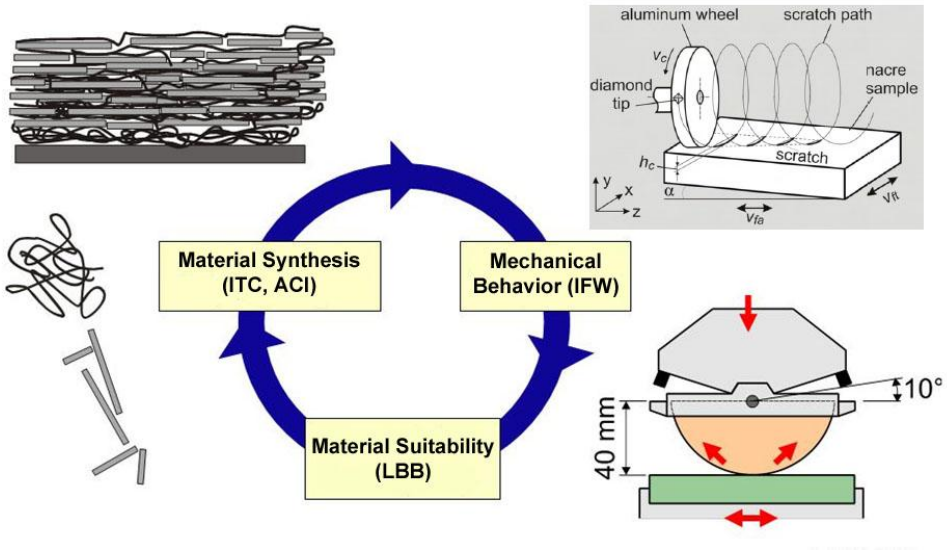

Figure 1-2: Schematic presentation of sub project D9 "Biomimetic Ceramics"*

Natural hybrid materials are often characterized as "hard" biological substances which are stiff, resistant to crack and hard. These materials are formed by nature combining minerals into a soft protein network for example calcium carbonate in sea shells, hydroxyapatite in teeth and bones and silica in diatoms. The presence of mineral makes these structures 100-5000 times stiffer than soft proteins as antler bone is 100 time stiffer than collagen and is made up of 30% of mineral.[10] This means mechanical properties can be improved by increasing the mineral or inorganic content. However, higher mineral content makes the material fragile which is not the case as found in these natural materials. The key behind this better mechanical performance is the arrangement to form these structures. Natural composites have evolved over the years with features found from macro to micro to nano scale. The overall performance observed at the macro scale level is the result of the synergy of processes that are operational at several scales to transfer loads and stresses, distribute damage, dissipate energy and stop the crack.

* adapted from SFB 599

Hybrid material includes two moieties, organic and inorganic, combined at molecular scale. These materials can be classified depending on the type of interaction connecting the inorganic and organic species. Materials showing the weak interactions between the two phases like van der Waals, hydrogen bonding or weak electrostatic interactions belong to class I, while class II hybrid materials are those that show strong chemical interactions between the constituting components (Figure 1-3).

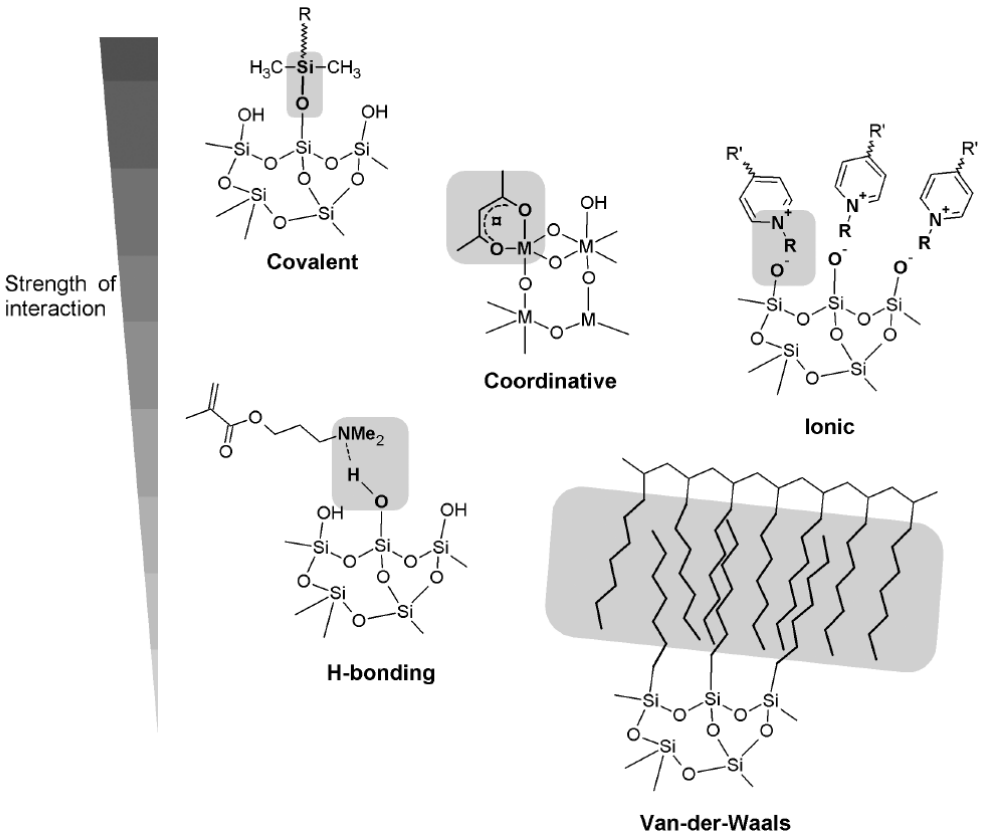

Figure 1-3: Interactions typically applied in hybrid materials and their relative strength[11]

Hybrid materials favorably combine the often dissimilar properties of both components into one material. This field is very creative because of the possibility of many combinations of the components with known and unknown properties. Changing composition at the molecular level leads to the modification of the material properties. Properties like toughness or scratch resistance can be tailored if hard inorganic nano particles are included into the polymer matrix.

1.1 Nacre

Medical materials are one typical area of hybrid materials where while retaining biocompatibility, mechanical properties can be adjusted according to the requirement. Nacre is an exceptional hybrid material with its structure and related mechanical properties and taken here as model to mimic the construction of new material. Nacre has been tested for the suitability of the material to be used as an implant material. Modulus, bending strength and fracture toughness of nacre are compared with a synthetic alumina ceramic material.[12]

In order to develop new methods for new generation materials a biomimetic approach is followed which investigates biological structures and establishes a relationship between structure and properties. Nacre shell is an attractive target for such a process with its inner nacreous layer composed of aragonite platelets and proteins.

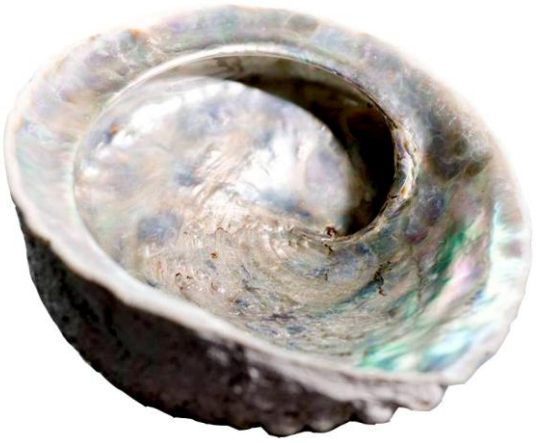

Figure 1-4: Abalone inner shell*

An adult abalone shell is around 15-20 cm in diameter and composed of two layers. A brittle and hard layer lies on the outer side and is composed of large crystals of calcite while the inner layer “nacre” is 95% volume of aragonite and 5% volume of proteins and polysaccharides.[13] Nacre is capable of dissipating energy via inelastic deformations while the outer layer is hard thus making the whole construction an ideal armor design.

* adapted from M. van der Meer, Leibniz University Hanover

The nacre is a layered composite structure of aragonite platelets of 200 to 600 nm thicknesses and 1 to 5 µm wide with bio-macromolecule such as hydrophobic proteins and chitin. The structure of nacre can be described as brick and mortar (Figure 1-5).

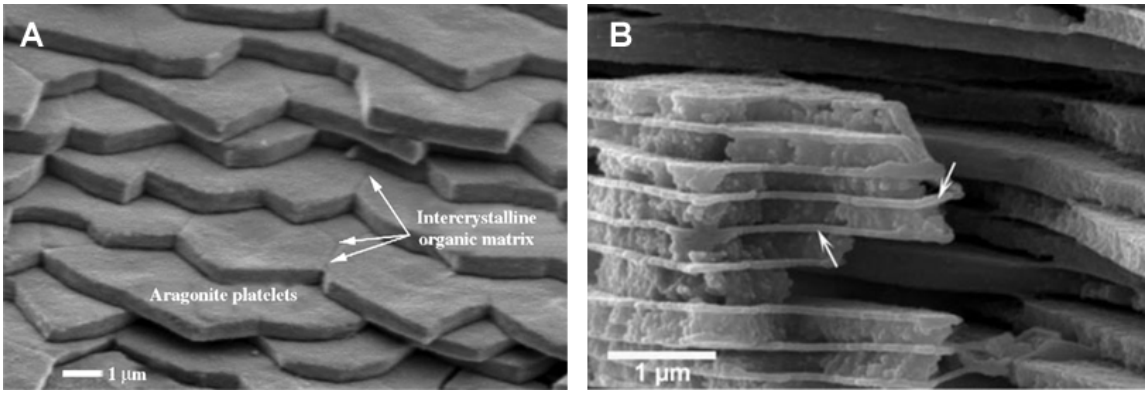

Figure 1-5: (A) SEM of nacre[14], (B) fracture section of nautilus nacre (arrows showing interlamellar organic layer after etching[15]

There is a very high degree of crystallographic texture characterized by a nearly perfect "c-axis" alignment normal to the plane of the tiles. The proteins laying in between aragonitic pseudo hexagonal platelets have not yet been fully identified. It is a mixture of different compounds rich in aspartic acid along with other amino acids.[9] This organic thin film termed as matrix covers the inorganic component on all sides with great adherence to the inorganic phase as shown schematically in Figure 1-6.

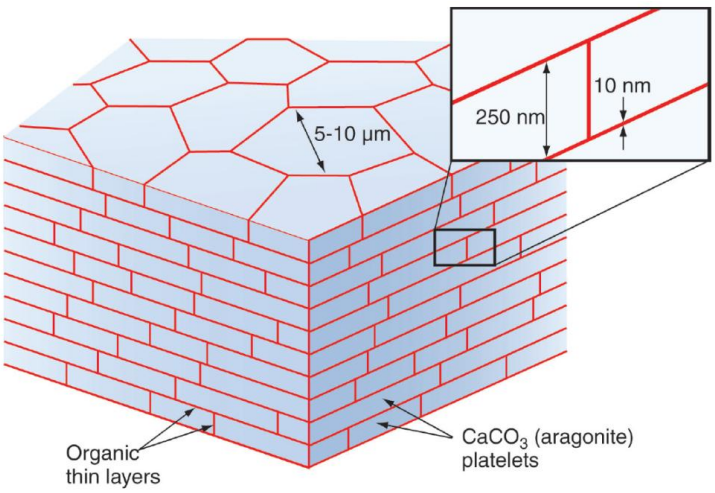

Figure 1-6: Schematic diagram of nacreous structure[16]

The complex layered structure of aragonite platelets and biomacromolecules is formed in the presence of soluble proteins, insoluble hydrophobic proteins and polysaccharides. Crystal habit, size and shape of the aragonite is controlled by the formation of pre organized sheets of organic matrices as presented schematically in Figure 1-7.[17]

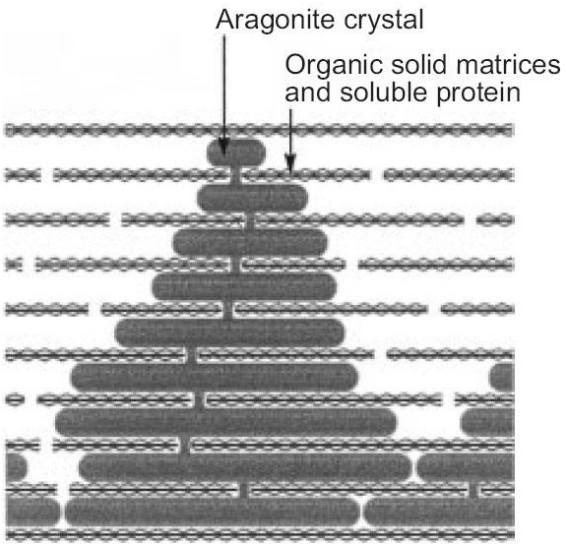

Figure 1-7: Schematic illustration of nacre growth[17]

1.2 Mechanical Strength

Nacre is special due to organic material arranged in a highly precise manner in combination with aragonite thus making it superior to most other artificial composite ceramics regarding stiffness, strength and toughness.[18] Various reports have been published on the mechanical properties of the nacre and underlying mechanisms. First measurements of this kind were performed by Curry on a variety of bivalves, gastropods and cephalopods. He measured a fracture strength in bending varying between 56 and 116 MPa and described a stress strain curve of nacre in tension which indicates a linear (elastic) region until a sharp yield point at about 0.2% strain followed by failure at about 0.6% strain.[19] Young's modulus of 70 GPa and 60 GPa were obtained with dry and wet samples respectively by Jackson et al.[18] Similarly a tensile strength of 170 MPa was observed for dry and 140 MPa for a wet sample. Nacre has a work of fracture which is around 3000 times greater than that of aragonite which constitutes around 95% of the structure.[19]

The performance of nacre is controlled by mechanisms at the interface between the aragonite platelets particularly one generating resistance to shearing and hardening. Tensile stress is transferred via platelet through shear stress in the platelet overlapping regions. At the time of failure all possible sliding sites are activated as shown in Figure 1-8.

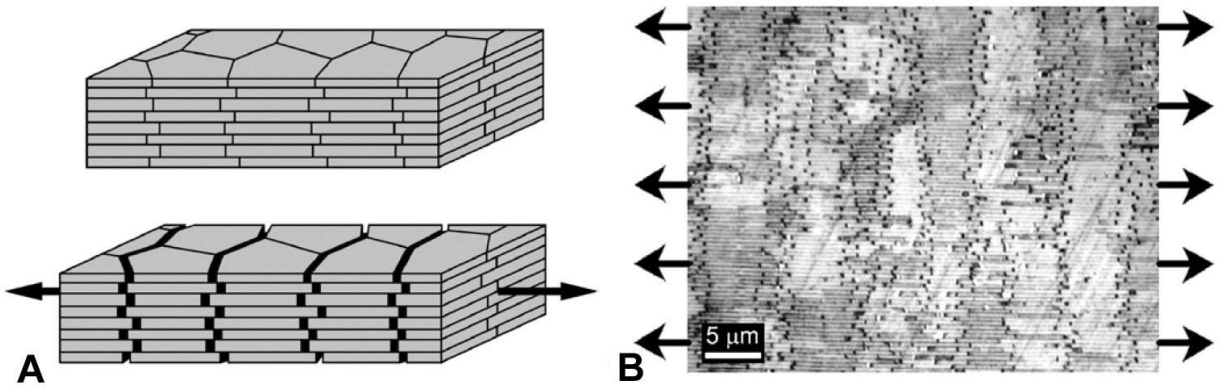

Figure 1-8: (A) Schematic tablet sliding mechanism, (B) tensile specimen showing that all the potential sliding sites were activated[20]

Deformations are spread over larger areas as higher stresses are required to slide platelets further, therefore, favoring the material to initiate new sliding sites. Under tensile stress the platelets interfaces start to yield in shear and the tablets slide on one another with local deformation. Once the sliding sites are exhausted, the material fails by pullout of the platelets which takes place after a local sliding distance of 100-200 nm. This mechanism is considered to be the main source of the superior mechanical properties and is unique to nacre.[21]

A possible strengthening process is anchoring of the organic adhesive phase to the inorganic component. Unfolding of chains, breaking of cross links and perhaps permanent reorientation of the organic phase during deformation helps in the strengthening mechanism. An uncontrolled crack growth is prevented if a stress normal to the platelet plane is applied. This is due to the organic fraction that glues the crystals and shows high ductility.[22] Importance of soft organic phase is clear as it plays a key role in alleviating impact damage to aragonite platelets[23], however, Meyers et al. has reported importance of organic layer in the growth of the aragonite crystal, while having only a minor role in the mechanical strength.[24]

Another nano scale mechanism is due to the presence of nanoasperites on the opposed platelets surfaces. These nanoasperites provide frictional resistance against pull out of the tablets.[25]

Waved surface of inorganic platelets in nacre progressively locks tablets sliding, making it more difficult to separate the tablets from their interfaces.[10] The tablets must have to climb on each other's waviness during the course of sliding. This results in an increased resistance to sliding and progressive platelet interlocking. Three dimensional finite element models based on the microstructure have proved the significance of waviness in nacre hardening mechanism.[20]

Song et al. confirmed the existence of mineral bridges between aragonite platelets, distributed among the organic matrix.[26] The presence of bridges reinforces the weak interfaces, such that the interfaces become just suitable for the crack to extend in itself. Successive layers of aragonite are not simply laying one over another but there are interlocks present between the layers. Simulation by Katti et al. showed that the existence of such interlocking has significant role in the deformation behavior and the progressive failure of interlocks helps in limiting catastrophic failure.[27]

Different mechanisms discussed above are depicted schematically in Figure 1-9. It is unknown, how much energy is dissipated and under what conditions they are triggered to operate by each of the above mentioned mechanisms.

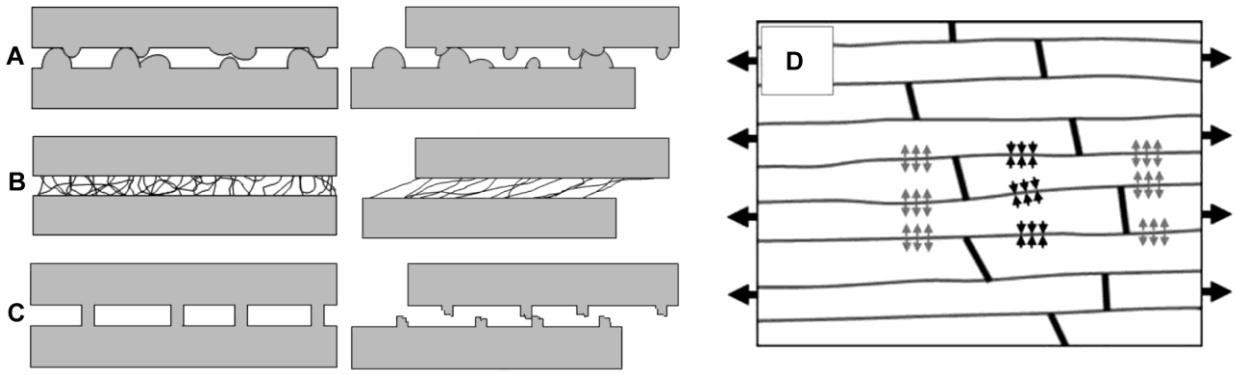

Figure 1-9: Nanoscale mechanisms controlling the shearing of the tablet's interface: (A) asperities, (B) biopolymer stretching, (C) mineral bridges, (D) schematic waviness mechanism[10, 25]

1.3 Synthetic Nacre

The technology transfer from nature to synthetic material is often called biomimetics, biomimicry or bionics. Artificial nacre has been prepared by different methods and scientific groups. In all approaches specific material which is found in nature is not copied, but only the architectural configurations and the material characteristics. The biggest hurdle lies in copying the architecture found at micro and nano scales in a way which allows the preparation of real, macro scale samples at reasonable cost.

1.3.1 Bottom up Approach

Researchers have dealt with the problem of mimicking nacre with the bottom up approach. This approach involves the use of organic macromolecules as template for inorganic crystals to nucleate and grow from supersaturated solutions. Crystal growth is either accelerated or inhibited by the presence of organic phase. This process is dependent on the functionality, molecular weight, concentration and density of functional groups on the polymer chains. Nacre mimicking structures can be produced in the presence of appropriate polymers with inorganic crystals. Composites of chitosan and polygalacturonic acid with hydroxyapatite have been synthesized by allowing precipitation of hydroxyapatite in the presence of these biopolymers.[28] Layered hybrid films showing high tensile strength and ductile behavior have been synthesized based on a bottom up colloidal assembly of alumina platelets with chitosan.[29] Gehrke et al. prepared nacre that looks morphologically similar with the help of amorphous precursor particles.[30] These approaches are helpful, but in respect of design, orientation, material choice and constructing complex structures are not yet good enough.

1.3.2 Layer-by-Layer Assembly

Hybrid material can be build up by a simple but versatile technique called “layer-by-layer” (LbL) deposition. This method relies on surface charges and their interaction with counter ions. Different charges on the surfaces of inorganic and organic polyelectrolytes helps in constructing a hybrid inorganic-organic material. Typically, anionic charges on a flat surface can be used to deposit a polyelectrolyte which is positively charged. After polymer deposition

the original surface charge is overcompensated thus allowing to deposit a next layer of negatively charged inorganic building blocks (Figure 1-10).[31-32]

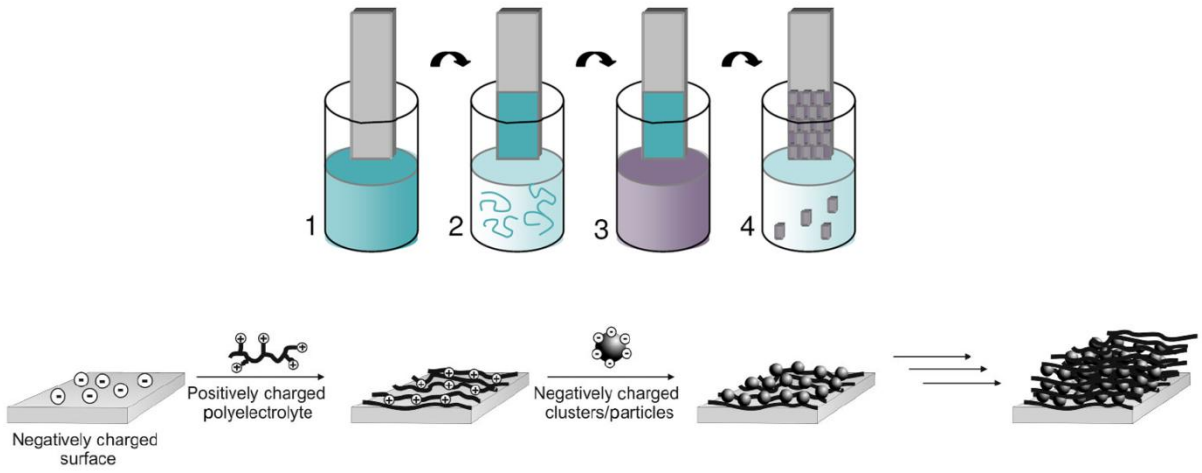

Figure 1-10: Layer-by-layer deposition[11]

Following the same procedure another layer of polymer is deposited and so on. This technique enables the sequential deposition of oppositely charged material to attain complex multilayer hybrid structures. An advantage employing this technique lies in the choice of building blocks which could be in the form of clusters, particles or platelets. In addition it allows the control of the layer thickness, composition and function. A wide variety of materials have been constructed with this technique.[33-37]

LbL assembly can also be constructed by another simple technique called spin coating. It is a fast method to construct homogenous, thin films out of a solution on the surface of flat surfaces. An excess amount of the depositing material solution is dispensed on the substrate followed by spinning the substrate at high speed typically around 3000 rpm. Material is spread on the surface of the substrate under the influence of centrifugal force. A desired film thickness is achieved by high rotations during which the fluid is spun off the edges of the substrate. A big issue in this technique is repeatability as the film homogeneity depends on factors like evaporation rate of solvent, viscosity, solution concentration, rotation speed and time. Additionally this method is manual and therefore not optimal for the construction of thicker materials.

1.3.3 Electrophoretic Deposition

Novel and complex material combinations can be achieved by the low cost approach of electrophoretic deposition.[38-39] Charged nanoparticles are deposited in suspension upon application of an external electric field as presented in Figure 1-11. Nacre like composites have been prepared by Wang et al. utilizing electrodeposition of a clay dispersion in water containing poly(amic acid).[40]

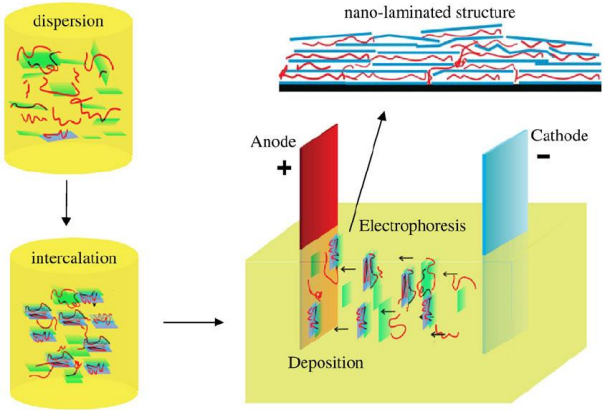

Figure 1-11: Scheme showing electrophoretic assembly to construct nanolaminated film[38]

1.3.4 Controlled Freezing

This method is based on the fact that, during the formation of ice, the solutes present in the water are expelled and are entrapped within channels between the ice crystals (Figure 1-12). Nacre like material can be prepared by this method using ceramic particles dispersed in water.[41]

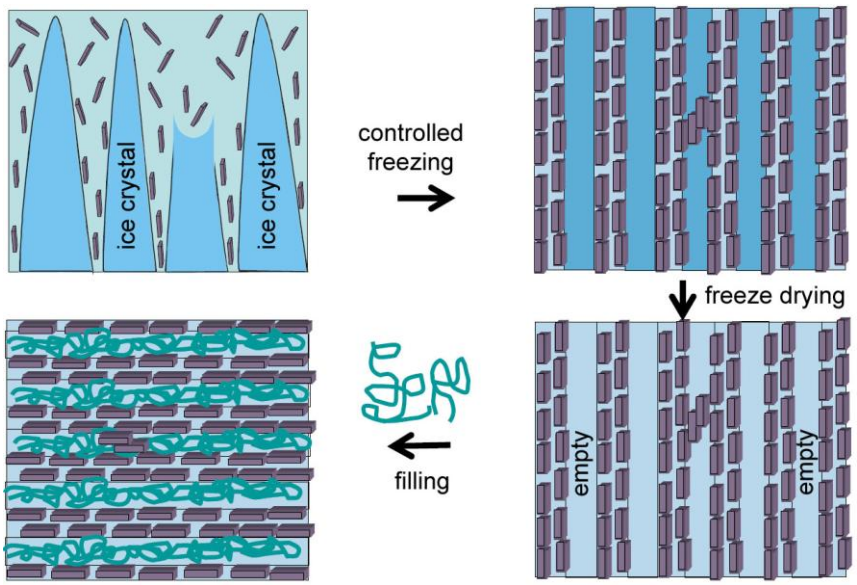

Figure 1-12: Schematic controlled freeze drying[42]

To construct ordered structures as artificial nacre, the freezing process has to be controlled very carefully thus the channels are ordered within the ice. In the first stage this method yields a very porous material which has to be processed further. This porous scaffold can be filled with an organic component thus resulting in a dense composite material.

1.3.5 Centrifugal Deposition

Chen et al. prepared hybrid nanocomposites from clay nanoplatelets and polyimide with the help of a centrifugal deposition process.[43] Hydrophilic montmorillonite (MMT) was converted into hydrophobic MMT called organic MMT and dispersed with strong ultrasonic. The silicate was covered by imide monomers followed by in situ polymerization and layered deposition on glass substrate by centrifugation. As potential energy is minimized under the centrifugal force it helps to align MMT platelets parallel to the surface of the substrate. This procedure resulted in an ordered nanostructure with alternating organic and inorganic layers as depicted schematically in Figure 1-13.

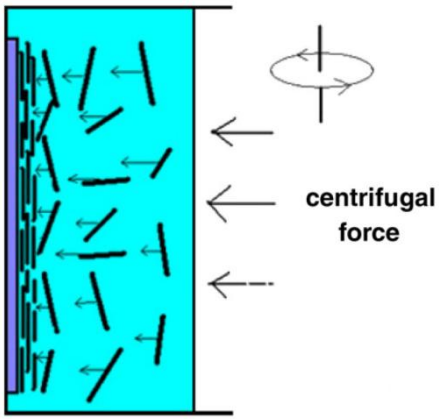

Figure 1-13: Automatic alignment of clay platelets under the centrifugal force[43]

1.3.6 Vacuum Filtration

Yao et al. has recently introduced a simple, fast, time saving process as depicted in Figure 1-14.[44] Artificial nacre like nanocomposite film is prepared by mixing an aqueous suspension of exfoliated MMT and an aqueous solution of chitosan.

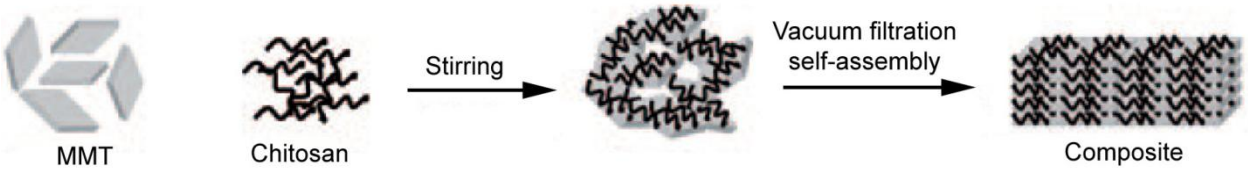

Figure 1-14: Schematic diagram, vacuum filtration[44]

Stirring of the suspension guarantees full adsorption of chitosan on MMT sheets. Both building blocks were aligned to a nacre like structure by self assembly induced by vacuum filtration. This method proved to be simple, fast and time efficient.

References

[1] Jennissen, H. P., *Materialwissenschaft*, Wissenschaftsverlag Universität Essen: (2000); Vol. 13, pp 78.

[2] Murnaghan, J. M.; Hamer, A. J., *Surgery (Oxford)*, (2010) **28**, 508.

[3] Affatato, S.; Spinelli, M.; Zavalloni, M.; Mazzega-Fabbro, C.; Viceconti, M., *Med. Eng. Phys.*, (2008) **30**, 1305.

[4] Rahaman, M. N.; Yao, A.; Bal, B. S.; Garino, J. P.; Ries, M. D., *J. Am. Ceram. Soc.*, (2007) **90**, 1965.

[5] Emery, D. F. G.; Clarke, H. J.; Grover, M. L., *J. Bone Joint Surg. (Br)*, (1997) **79-B**, 240.

[6] Adden, N., Dissertation Technische Universität Braunschweig (2007).

[7] Garino, J. P., *Clin. Orthop. Rel. Res.*, (2000) **379**, 41.

[8] Akagi, M.; Nakamura, T.; Matsusue, Y.; Ueo, T.; Nishijyo, K.; Ohnishi, E., *J. Bone Joint Surg. (Am)*, (2000) **82**, 1626.

[9] Lin, A.; Meyers, M. A., *Mater. Sci. Eng., A*, (2005) **390**, 27.

[10] Barthelat, F., *Philos. Trans. R. Soc. London, Ser. A* (2007) **365**, 2907.

[11] Kickelbick, G., *Hybrid Materials. Synthesis, Characterization, and Applications.*, Wiley-VCH Verlag GmbH & Co. KGaA, Weinheim: (2007).

[12] Richter, B.; Kellner, S.; Menzel, H.; Behrens, P.; Denkena, B.; Ostermeier, S.; Hurschler, C., *Arch Orthop Trauma Surg.*, (2011) **131**, 191.

[13] Sarikaya, M.; Aksay, I., *Biomimetics, design and processing of materials. Polymers and complex materials.*, American Institute of Physics, Woodbury, NY: (1995).

[14] Stempflé, P.; Brendlé, M., *Tribol. Int.*, (2006) **39**, 1485.

[15] Addadi, L.; Joester, D.; Nudelman, F.; Weiner, S., *Chem. Eur. J.*, (2006) **12**, 980.

[16] Mayer, G., *Science*, (2005) **310**, 1144.

[17] Kato, T.; Sugawara, A.; Hosoda, N., *Adv. Mater.*, (2002) **14**, 869.

[18] Jackson, A. P.; Vincent, J. F. V.; Turner, R. M., *J. Mater. Sci.*, (1990) **25**, 3173.

[19] Currey, J. D., *Proc. R. Soc. London, B*, (1977) **196**, 443.

[20] Barthelat, F.; Tang, H.; Zavattieri, P. D.; Li, C. M.; Espinosa, H. D., *J. Mech. Phys. Solids*, (2007) **55**, 306.

[21] Espinosa, H. D.; Rim, J. E.; Barthelat, F.; Buehler, M. J., *Prog. Mater. Sci.*, (2009) **54**, 1059.

[22] Sumitomo, T.; Kakisawa, H.; Owaki, Y.; Kagawa, Y., *J. Mater. Res.*, (2008) **23**, 1466.

[23] Gao, H.; Ji, B.; Jager, I. L.; Arzt, E.; Fratzl, P., *Proc. Natl. Acad. Sci. U. S. A.*, (2003) **100**, 5597.

[24] Meyers, M. A.; Lin, A. Y.-M.; Chen, P.-Y.; Muyco, J., *J. Mech. Behav. Biomed.*, (2008) **1**, 76.

[25] Wang, R. Z.; Suo, Z.; Evans, A. G.; Yao, N.; Aksay, I. A., *J. Mater. Res.*, (2001) **16**, 2485.

[26] Song, F.; Soh, A. K.; Bai, Y. L., *Biomaterials*, (2003) **24**, 3623.

[27] Katti, K. S.; Katti, D. R., *Mater. Sci. Eng., C* (2006) **26**, 1317.

[28] Verma, D.; Katti, K. S.; Katti, D. R.; Mohanty, B., *Mater. Sci. Eng., C*, (2008) **28**, 399.

[29] Bonderer, L. J.; Studart, A. R.; Gauckler, L. J., *Science*, (2008) **319**, 1069.

[30] Gehrke, N.; Nassif, N.; Pinna, N.; Antonietti, M.; Gupta, H. S.; Colfen, H., *Chem. Mater.*, (2005) **17**, 6514.

[31] Luz, G. M.; Mano, J. F., *Philos. Trans. R. Soc. London, Ser. A* (2009) **367**, 1587.

[32] Decher, G.; Schlenoff, J. B., *Multilayer Thin Films*, Multilayer Thin Films, Wiley-VCH: Weinheim: (2003).

[33] Zhang, L.; Shen, Y. H.; Xie, A. J.; Li, S. K.; Li, Y. M., *J. Mater. Chem.*, (2009) **19**, 1884.

[34] Tang, Z.; Kotov, N. A.; Magonov, S.; Ozturk, B., *Nat. Mater.*, (2003) **2**, 413.

[35] Srivastava, S.; Kotov, N. A., *Acc. Chem. Res.*, (2008) **41**, 1831.

[36] Tang, Z.; Wang, Y.; Podsiadlo, P.; Kotov, N. A., *Adv. Mater.*, (2006) **18**, 3203.

[37] Lee, H.; Lee, Y.; Statz, A. R.; Rho, J.; Park, T. G.; Messersmith, P. B., *Adv. Mater.*, (2008) **20**, 1619.

[38] Lin, W.; Wang, C.-a.; Le, H.; Long, B.; Huang, Y., *Mater. Sci. Eng., C*, (2008) **28**, 1031.

[39] Lin, T.-H.; Huang, W.-H.; Jun, I.-K.; Jiang, P., *Chem. Mater.*, (2009) **21**, 2039.

[40] Wang, C.-A.; Long, B.; Lin, W.; Huang, Y.; Sun, J., *J. Mater. Res.* , (2008) **23**, 1706.

[41] Deville, S.; Saiz, E.; Nalla, R. K.; Tomsia, A. P., *Science*, (2006) **311**, 515.

[42] Hering, B., Dissertation Leibniz Universität Hannover (2010).

[43] Chen, R.; Wang, C.-A.; Huang, Y.; Le, H., *Mater. Sci. Eng., C* (2008) **28**, 218.

[44] Yao, H.-B.; Tan, Z.-H.; Fang, H.-Y.; Yu, S.-H., *Angew. Chem., Int. Ed.*, (2010) **49**, 10127.

2 Biomimetic Materials

2.1 Aim of the Thesis

The goal of this study is the development of biomimetic materials based on the structural pattern found in nacre. This class of biomimetic materials shall be tested if their properties will allow the use in endoprosthetics applications like hip or knee joints. Traditional ceramic material used for this purpose show lower inelastic deformability despite their low wear level. Nacre is a hard and elastic composite material made up of biopolymers as elastic and inorganic particles as stiffer components. A special hierarchical arrangement of these components delivers special mechanical properties. In our model system, inorganic part is found in the form of thin platelets that are aligned more or less in a parallel fashion. Organic matter controls the formation of these platelets during growth process. LbL deposition will be used to align the platelets and a polyelectrolyte is used to secure adhesion of the platelets.

Firstly, different phosphonic acid or phosphonate functional (co-)polymers have to be synthesized which are capable of controlling the crystallization of the inorganic component. The polymers have to be optimized as nucleation controlling agent to obtain a platelet morphology for hydroxyapatite (HA) and zirconium hydrogenphosphate (ZrP). In order to control the composition of the copolymers, knowledge about the reactivity ratios of the constituting monomers is inevitable. Polymers which have shown crystallization control of inorganic components as platelets are to be used for the synthesis of inorganic component. Hydroxyapatite and zirconium hydrogen phosphate are considered as inorganic components, whereas former resembles component of natural bone while the later is known to have a layered structure and being biocompatible. Under the influence of synthesized phosphorous functional (co-)polymers, either nanoparticles of HA or platelets of ZrP are obtained and should be analyzed with SEM and XRD.

As a next step a composite material shall be fabricated using ZrP platelets in combination with a cationic (anchoring) polymer. This has to be done with a dip robot according to layer-by-layer assembly in order to produce a hierarchical pattern as found in model system nacre. Additionally alumina in the form of platelets is used as inorganic part in the construction of a hierarchical material with an anchoring polymer functionalized with dopamine as found in the mussels. The hybrid composite materials need to be characterized by profilometer, nanoindentation, scanning electron microscopy, atomic force microscopy

and ellipsometry for the thickness, morphology and importantly associated mechanical properties.

2.2 Thesis Organization

In addition to the first chapter, which gave a brief introduction into ceramics as implant materials, and nacre as biomimetic model for materials with a micro structure, which is the basis for a strengthening mechanism, the thesis comprises seven chapters. Some of them are publications submitted or already published.

The third chapter *"Characterization Methods"* is devoted to the experimental techniques used to elucidate the composite materials structure and mechanical properties.

Chapter 4 *"Synthesis, Characterization, Monomer Reactivity Parameters and Thermal Properties of Phosphonate and Phosphonic Acid Functional Copolymers"* deals with the synthesis of copolymers of phosphonic acid or phosphonate ester monomers with different comonomers, determination of the reactivity parameters, and their thermal degradation behavior.

Chapter 5 named *"Polymer Tailoring"* describes synthesis of bisphosphonic acid and incorporation of these functional groups to commercially available cationic polymers. Additionally tailor made polymers are synthesized with phosphate and phosphonate ester functional groups.

The next chapter 6 *"Synthesis of Inorganic Particles under the Influence of Polymer Additives"* summarizes the controlled crystal growth of α-Zirconium hydrogenphosphate hydrate and hydroxyapatite under the influence of polymers discussed in chapter 4 and 5 as these are capable of interacting with the surface of inorganic growing crystals. These crystallization experiments have been performed by B. Hering within the project collaboration.

Chapter 7 *"Preliminary Dipping Experiments"* describes the fabrication of composite materials according to LbL assembly as model system to check the suitability of different applied analytical methods for the composite construction, characterization and its mechanical properties.

Chapter 8 *"Fabrication and Characterization of Biocompatible Nacre-like Structures from α-Zirconium hydrogenphosphate hydrate and Chitosan"* has been published in *J. Colloid Interface Sci.*[*]. The co-author B. Hering has contributed with the synthesis of inorganic platelets and SEM while Z. Burghard and J. Bill have performed the nanoindentation. P. Behrens and H. Menzel were the supervisors of this work. This chapter discusses in detail the experimental results obtained for the LbL assembled composite material from chitosan and α-zirconium hydrogenphosphate hydrate. Results are discussed regarding different concentrations and pH of the constituting components for the composite growth. Furthermore, the elucidation of the mechanical properties is described.

Chapter 9 "Nacre Inspired Assembly of Organic- Inorganic Composites, Characterization and Mechanical Properties" highlights the results based on a new system of LbL assembled composite material. Growth of the composite with additional layers and the mechanical behaviour for this nacre like biomimetic material is discussed.

[*] Waraich, S. M.; Hering, B.; Burghard, Z.; Bill, J.; Behrens, P.; Menzel, H., *J. Colloid Interface Sci.*, (2012) **367**, 74.

3 Characterization Methods

Composite materials are substituting the conventional materials because of their comparable and even better performance. The mechanical, chemical, and structural properties of these materials are very important for the next generation materials. The fabrication of new materials requires a critical process of characterization. Thin films are very important for their industrial use in different areas like optics, electronics, medicals and as future new hybrid materials. These new material are constructed in smaller dimensions and as complex hierarchical geometries. This mode of construction requires analytical methods which provide knowledge of material at this scale. Within this chapter, underlying principles for characterization techniques used in this work are described. These techniques are capable of measuring the mechanical properties, thickness, degradation behavior and structural details of the deposited films.

3.1 Nanoindentation

Nanoindentation is one of the methods used widely for measuring the mechanical properties of materials in small dimensions. This technique is specially used in situations where traditional methods cannot be applied for the evaluation of mechanical properties.

Tensile testers are employed to determine elastic modulus, stress and strain values for bulk samples. However, it is very difficult to evaluate mechanical properties of thin films, especially when attached to bulky surfaces. Nanoindentation has been applied for such situations quite successfully.

Conceptually it is based on pushing a tip of known geometry into the surface under investigation. After reaching a predefined maximum load, it is reduced until complete relaxation occurs. The surface of material is indented with the same procedure many times. High resolution sensors and actuators measure precisely load (P) and displacement (h) during the course of pushing in and withdrawing from the material. From this data the load and displacement curve is constructed as given exemplary in Figure 3-1. Making use of established models, mechanical properties can be determined.

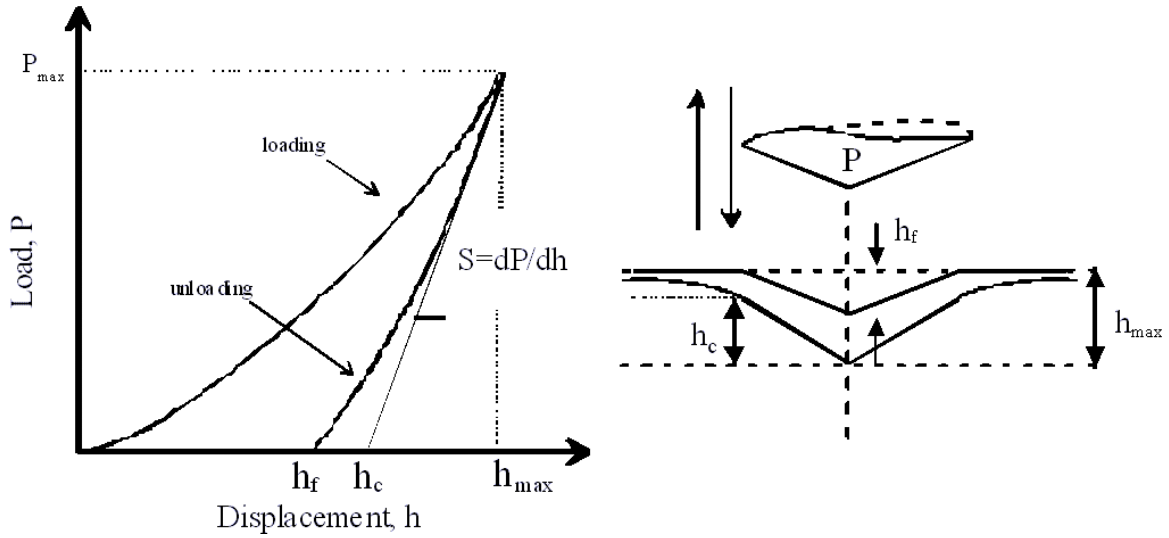

Figure 3-1: Typical load-displacement curve obtained from indentation and area under the indenter tip*

Important parameters measured are given in Figure 3-1, where P_{max} is the maximum load and h_{max} corresponds to the distance at maximum load. The slope S = dP/dh corresponds to the elastic unloading stiffness. During the indentation process, both elastic and plastic deformations have occurred. A steeper unloading curve indicates a larger modulus. Material resistance against the penetrating probe is shown by the loading curve with both elastic and plastic properties. On removal of the load from the indenter, the material recovers elastically thus presenting the unloading curve.

From these load-displacement curve different mechanical properties can be evaluated.[1] Typically, hardness and Young's modulus of the material can be calculated from the curve. Hardness is measured as maximum load applied divided by the projected contact area.[2]

$$H = \frac{P_{max}}{A_c}$$

Where

H hardness

P_{max} maximum loading

A_c area of the tip in dependency on the contact depth (area function)

* adapted from Z. Burghard, Max Planck Institute for Metal Research Stuttgart

The reduced elastic modulus is calculated as follows:

$$E_r = \frac{\sqrt{\pi}}{2\sqrt{A_c}} S$$

E_r Reduced modulus

S contact stiffness dP/dh

From this value Young's modulus can be calculated according to the equation:

$$\frac{1}{E_r} = \frac{(1-{\nu_i}^2)}{E_i} + \frac{(1-{\nu_s}^2)}{E_s}$$

In the above equation ${\nu_i}^2$ and E_i denote the Poisson ratio and Young's modulus for the indenter material supplied by the manufacturer whereas ${\nu_s}^2$ and $E_s$represents Poisson ratio and Young's modulus for the sample.

This mode of measurement is very sensitive to the substrate influence on which indentation takes place, particularly for indentation depths larger than 20% of the total thickness of the sample under observation.[3] For the same reason it is advisable to restrict measuring depth within 10-20% of the overall sample thickness.

In order to determine the above mentioned parameters, is important to know the exact contact area (A_c) and this requires exact knowledge of the shape of the indenter being used. Various models are suggested for the calculation of contact area from the geometry of indenter and *P-h* curve. However, the method suggested by Oliver and Pharr is most frequently used and will be applied here too.[2]

There is a wide variety of indenter tips with different geometries and advantages available. They include cube corner, cone, sphere, vickers and berkovich as shown in Figure 3-2. To obtain reproducible and reliable results, the indenter type is selected depending on the sample.

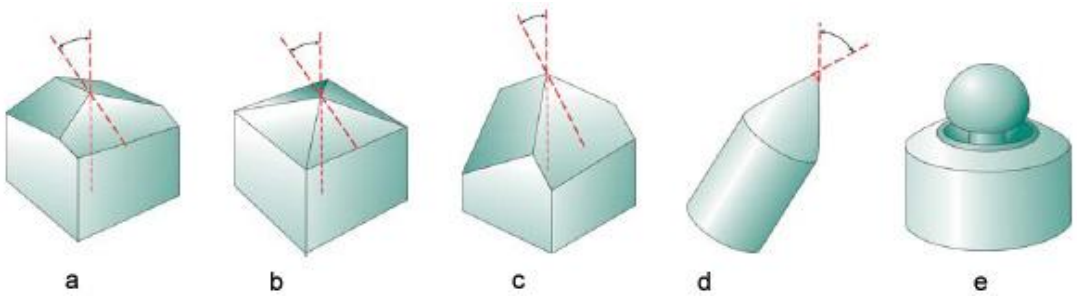

Figure 3-2: Indenting tips (a) Berkovich, (b) Vickers, (c) cube corner, (d) cone, (e) sphere[4]

The Berkovich type indenter with a trigonal pyramidal geometry is most frequently used. The included angle is 142.3° with a radius of curvature around 150 nm. This indenter type can be used for films of thickness greater than 100 nm. Cube corner indenter with an included angle of 90° and average radius of curvature from 40-100 nm are suitable for ultra thin films of thickness less than 100 nm. Spherical or cono-spherical indenters do not have a very low radius of curvature in comparison to other types and are used in the analysis of soft polymeric or biological samples.[5] All measurements in this work were performed with Berkovich indenters whose sharpness can be exploited to analyze rough surfaces in a better way in comparison to other types.

Even very sharp indenters are not perfectly sharp at the end of their tip which has to be taken into account during the indentation process at smaller depths. This is important to calculate the area function (A_c) which is a function of the distance from the end of the indenter, the contact depth (h_c). The tip shape area function can be represented as follows;

$$A_c = f(h_c)$$

Contact area (A_c) can be related to contact depth (h_c) by the tip calibration function as given below;

$$A_c = C_0 h_c^2 + C_1 h_c + C_2 \sqrt{h_c}$$

The values of C_0, C_1 and C_2 can be determined empirically using load-displacement curve of fused quartz.[6] A typical indentation on the surface of a composite material is shown in Figure 3-3.

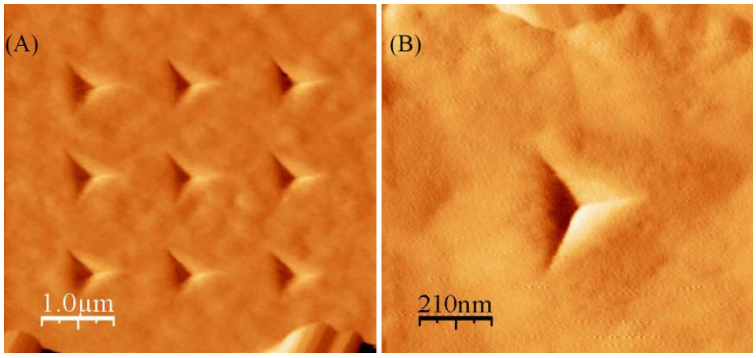

Figure 3-3: AFM image of Berkovich indenter (A) indentation array, (B) single indentation[7]

This method of calculating hardness and Young's modulus has been applied to a variety of solid supported materials (films) such as metal oxide coatings[8], transition metal nitrides layers[3] and films of polyelectrolytes.[9]

In Figure 3-4 a nanoindenter is presented schematically. Force is applied through electromagnetic actuation from the top with the help of a system of a coil and a magnet. In other systems force can be applied via electrostatic actuation. Besides pushing the indenter with a known force, it is necessary to determine the displacement accurately. This is done by a capacitance displacement gage.

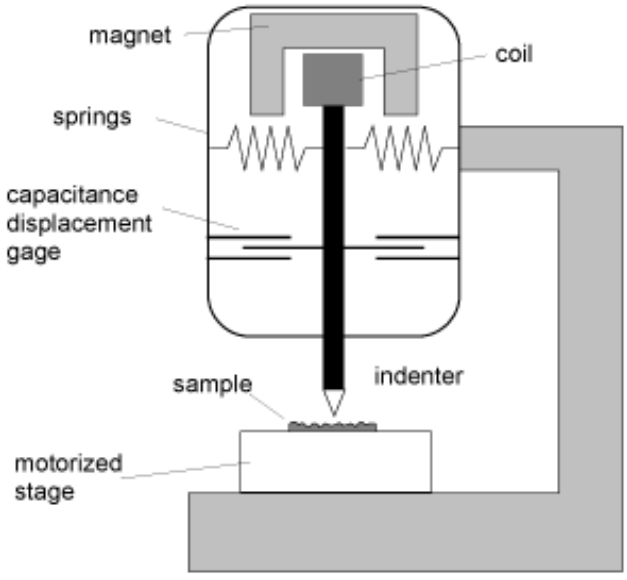

Figure 3-4: Schematic of a nanoindenter, for explanation see text[10]

The gage is a parallel plate capacitor with constant voltage and plate area. When indenter moves from the top, distance between the fixed plates of the capacitor changes. This movement is responsible for the change in current that can be related to the distance. As an alternative, laser beams can also be used to monitor any change in the tip position.

Mechanical properties of the composite materials fabricated within this thesis were determined by Zaklina Burghard at Max Planck Institute for Metal Research Stuttgart with a nanoindenter XP from MTS Nano Instrument using a Berkovich indenter.

3.2 Ellipsometry

Ellipsometry uses polarized light to determine the thickness of thin films deposited on a surface. Modern instruments make it possible to determine thickness and refractive index of films with an ease without involving mathematics of the underlying principles. A very brief working principle is discussed here and for detailed mathematical and physical description the reader is referred to literature.[11-12]

Light can be described as an electromagnetic wave with the electric and magnetic field vector being perpendicular to each other and to the propagation direction. Light is linear polarized when the electric field vector is oriented in one direction. Two such waves can be combined in phase leading to a circular polarized light. These waves can be combined out of phase resulting in an elliptically polarized wave. Thus every polarized wave can be described by two components of linearly polarized waves. This is the basis for ellipsometry.

When linearly polarized light interacts with a surface it is resolved into parallel (p) and perpendicular (s) components. Due to a phase shift of the incident light at the transition from one medium to second medium the two components are reflected differently. The difference is dependent on the nature of sample under investigation like thickness, complex refractive index, and dielectric function. Δ and Ψ are most important parameters where Δ is the change in the phase difference between the perpendicular and parallel components of the incident light (δ_1) and the reflected light (δ_2).

$$\Delta = \delta_1 - \delta_2$$

Additionally there is a change in the amplitude presented by the angle Ψ with values between 0° and 90° and whose tangent is the ratio of the reflectance for s- and p-polarized light.

$$tan\Psi = \left|\frac{R^p}{R^s}\right|$$

On reflection, change of the phase and amplitude of the polarized light are measured and by using following fundamental equation of ellipsometry

$$tan\Psi e^{i\Delta} = \frac{R^p}{R^s}$$

and in combination with an adequate model for the material to be measured, thickness and the refractive index of the sample can be calculated.[11-12]

3.3 Scanning Electron Microscopy (SEM)

SEM is a non destructive topographical analytical tool with high resolution. It is preferred over the conventional microscope with resolution restriction due to the wave length of light. It is based on analyzing the surface with a beam of electrons generated by an electron gun cathode made up of a tungsten filament or LaB_6 crystal (Figure 3-5). Electrons are accelerated in the presence of an electric field between the Wehnelt cylinder and the anode. After acceleration, the electron beam is focused within a depth of 1 to 10 nm by condenser lenses and astigmatism is corrected by coils. The electron beam passes through a pair of deflection coils which can move the beam in a xy plane over the sample called scanning. Any gas particles are removed from the chamber by evacuating the column. This helps to avoid any expansion of electron beam by impact on gas particles. The cross section of the layer-by-layer coated samples can be mounted perpendicularly on the object holder. To avoid high negative charge deposition the sample was coated with a thin gold layer of around 30 nm.

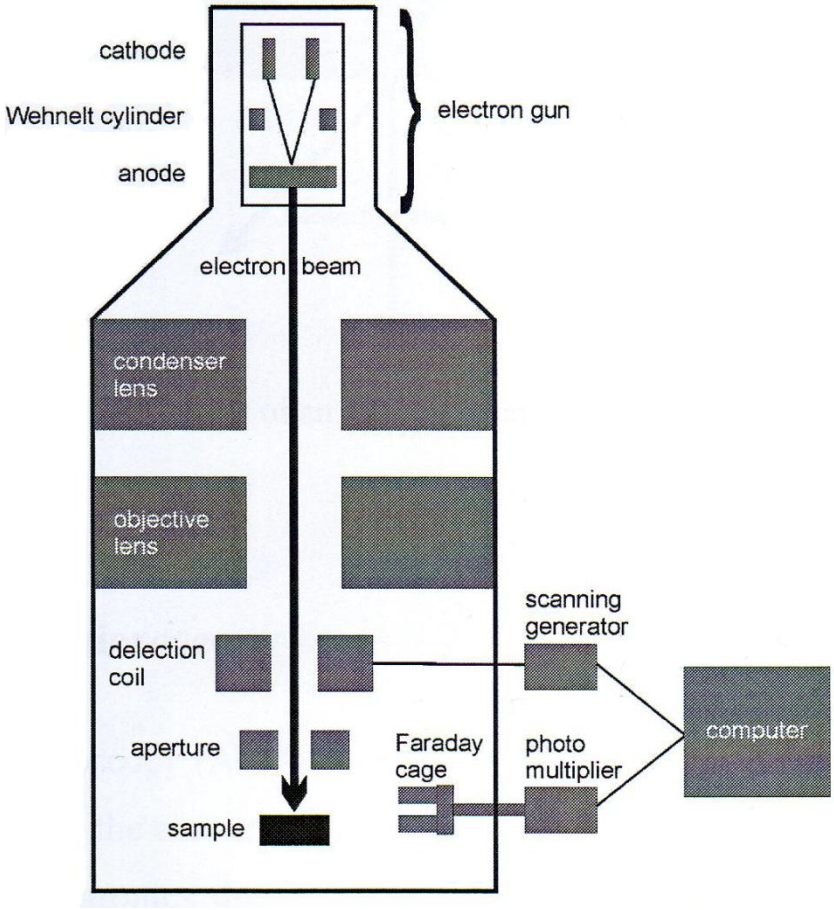

Figure 3-5: Schematic of the vacuum chamber of a SEM[13]

Due to elastic and inelastic scattering different emission products are emitted. Out of these, secondary and Auger electrons are with low energy of less than 50 eV. They are generated by impact ionization or the Auger effect. These electrons are deflected and amplified by a multiplier due to their weak electric field. Back scattering electrons are produced by elastic scattering processes and have high energy. Beside these types there are various other products produced during the electron beam impact at the sample surface as shown in Figure 3-6.[13]

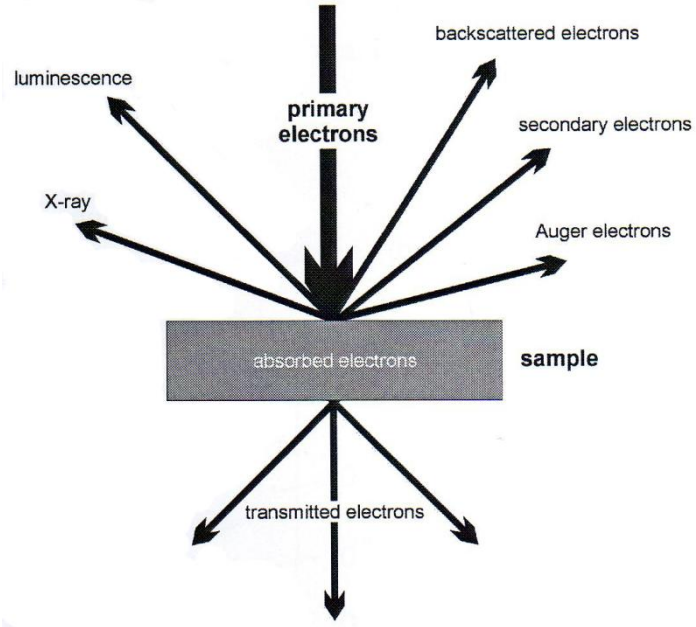

Figure 3-6: Emission products of an electron beam in the SEM

Secondary electrons and back scattered electrons are more frequently used for imaging the samples. Morphology and topographical details are elucidated with secondary electrons, whereas back scattered electrons are valuable for illustrating contrast in composition in multiphase samples as explained in Figure 3-7 for a metallurgical cross section of lead-tin solder. The solder separates out into two phases and the brighter areas in the backscattered image correspond to the lead phase of the solder.

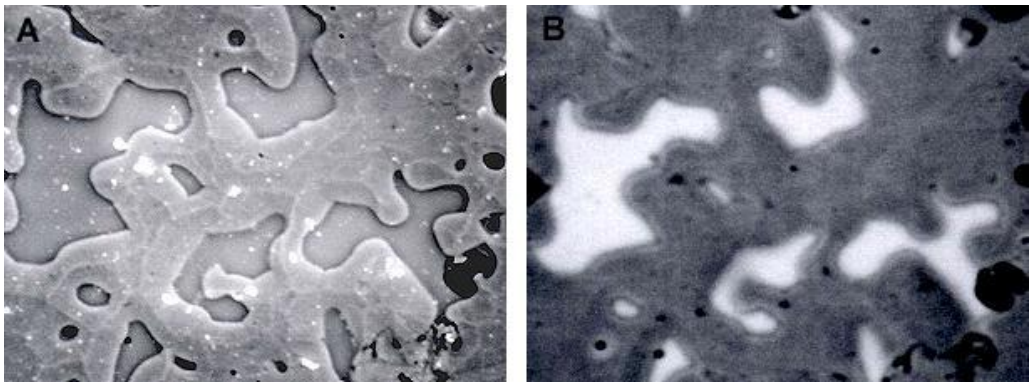

Figure 3-7: SEM image of solder 2500X (A) secondary electron image and (B) back scattered electron image[14]

Photons in the form of characteristic X-rays which are produced as a result of inelastic collision can be used for elemental analysis. The emission products mentioned above are detected by special detectors placed in the sample chamber leading to an electronic signal. The intensity of the detected signal is displayed on a monitor according to its brightness.

3.4 Atomic Force Microscopy (AFM)

AFM is a scanning force microscopy and measures different forces like attractive, repulsive, magnetic, electrostatic and Van Der Waals forces between a sharp tip of the instrument and the surface of sample. A detailed view of different types of forces at the tip is shown in Figure 3-8. A number of publications with detailed information are dedicated to this technique.[13, 15-16]

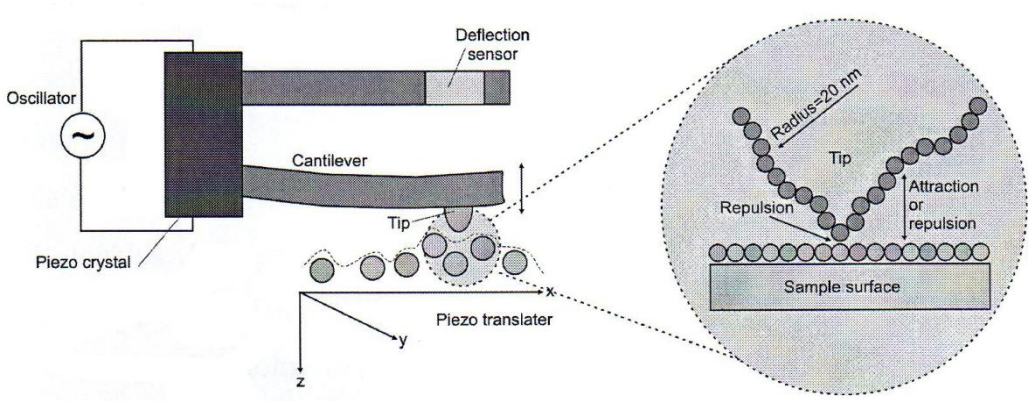

Figure 3-8: Schematic of AFM tip with acting forces[13]

Fundamentally, the sample surface is scanned with the help of an extremely small tip placed on a flexible cantilever. The size of tip is around 10 µm with radius of curvature ideally terminated only by a single atom. Depending on the instrument type a piezoelectric scanner moves the cantilever or the substrate as shown in Figure 3-9.

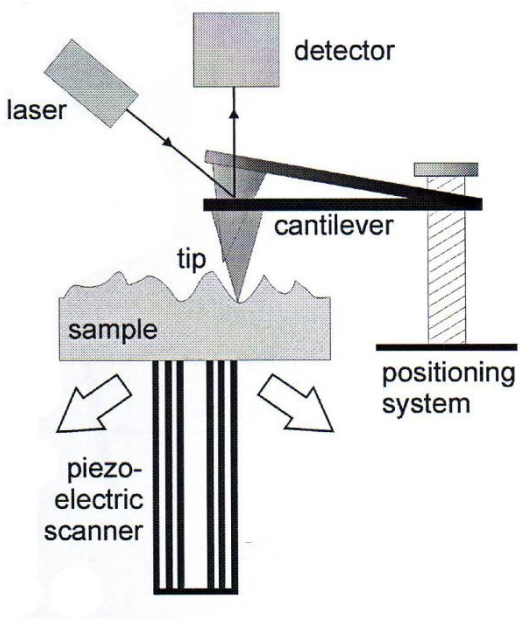

Figure 3-9: Schematic drawing of an AFM[13]

During the scan vertical deflections of the cantilever are monitored and recorded by a laser beam on the photodiodes. These data points are converted into an image with the help of an imaging system.

AFM can be used in different modes like contact mode where the tip is in direct contact with the surface and repulsive forces are dominant. In the non contact mode, the tip lies at a height of 5 to 10 nm from the surface and is oscillated on the cantilever. The attractive Van der Waals field is used in this mode and is useful for analyzing soft surfaces. In the tapping mode the tip touches the surface at each oscillation as the cantilever oscillates at its resonance frequency, resulting in temporary repulsive forces as found in the contact mode. The cantilever oscillation is reduced due to energy loss caused by the tip contacting the surface. The reduction in oscillation amplitude is used to identify and measure surface features.

3.5 Profilometry

A surface profilometer can be used to measure the vertical profile of thin film, wafers, solar cells, ceramics and surface finish coatings etc. In comparison to other film thickness

measurement techniques such as ellipsometry, interferometry or laser ultrasound spectroscopy this technique is simple and does not require very expensive hardware.

The principle of this technique is rather simple. A diamond stylus is in contact with the surface and is moved laterally across the sample surface. Any change in the vertical height of the stylus is monitored and signals are transferred to show height with reference to scanned distance with very high precision and repeatability. In different instruments either the stylus moves or the surface of interest can be moved.

Although simple, this technique can measure thickness ranging in height from 1nm to 2 mm. Vertical resolution is an important factor to be considered with this wide range of thickness measurement. There is user adjustable vertical range setting that needs to be selected accordingly. In a similar way horizontal resolution is selected depending on the stylus size, scan speed and scan length. Another important parameter is stylus force which is selected depending on the stylus radius and material hardness. Using very high stylus force can cause plastic or elastic deflection of the testing material thus effecting repeatability. On the other hand a stylus with very low force can "hop" over large steps.[17] Stylus size can be from few nm to 25 µm radius used for different purposes. Although this technique looks similar to AFM, the sensitivity and working principle are different as shown in Figure 3-10.

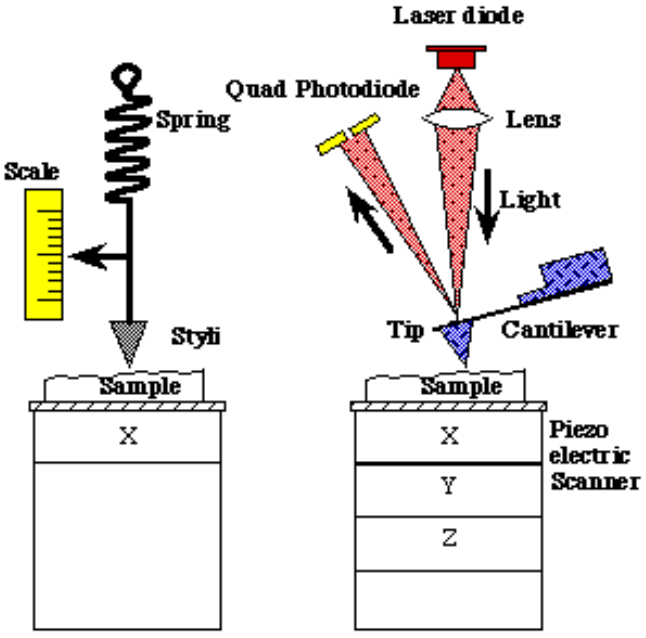

Figure 3-10: Schematic comparison of profilometer and AFM[18]

3.6 Thermogravimetry (TGA)

TGA measures the weight loss or gain of a sample as function of temperature. It is used to determine the thermal stability and fraction of volatile components with reference to the weight change while heating. Therefore, the sample is heated in an inert gas or in air and the weight is monitored as a function of increasing temperature. The sample is typically heated from ambient temperature to 700 °C with an increment of 10 °C per minute. The maximum temperature is selected so that the sample weight is stable at the end of experiment. Drying, structural water release, decomposition, gas evolution etc can be measured from the obtained curve.

References

[1] Fischer-Cripps; C., A., *Nanoindentation*, Springer-Verlag (New York): (2002).

[2] Oliver, W. C.; Pharr, G. M., *J. Mater. Res.*, (1992) **7**, 1564.

[3] Wang, J.; Li, W.-Z.; Li, H.-D.; Shi, B.; Luo, J.-B., *Thin Solid Films*, (2000) **366**, 117.

[4] www.agilent.com/find/nanoindenter, In (2011).

[5] www.hysitron.com, In (2011).

[6] Larkin, A. L.; Davis, R. M.; Rajagopalan, P., *Biomacromolecules*, (2010) **11**, 2788.

[7] Burghard, Z.; Zini, L.; Srot, V.; Bellina, P.; Aken, P. A. v.; Bill, J., *Nano Lett.*, (2009) **9**, 4103.

[8] Burghard, Z.; Tucic, A.; Jeurgens, L. P. H.; Hoffmann, R. C.; Bill, J.; Aldinger, F., *Adv. Mater.*, (2007) **19**, 970.

[9] Pavoor, P. V.; Bellare, A.; Strom, A.; Yang, D.; Cohen, R. E., *Macromolecules*, (2004) **37**, 4865.

[10] www.nanoindentation.cornell.edu, In (2011).

[11] Tompkins, H. G., *A User's Guide to Ellipsometry*, Academic Press, Boston: (1993).

[12] Jenkins, T. E., *J. Phys. D: Appl. Phys.* , (1999) **32**, R45.

[13] Helmecke, O., Dissertation Technische Universität Braunschweig (2008).

[14] http://www.seallabs.com/hiw6.htm, In (2012).

[15] Bubert, H.; Rivière, J. C.; Arlinghaus, H. F.; Hutter, H.; Jenett, H.; Bauer, P.; Palmetshofer, L.; Fabry, L.; Pahlke, S.; Quentmeier, A.; Hinrichs, K.; Hill, W.; Gruska, B.; Arthur, R.; Friedbacher, G., *Surface and Thin-Film Analysis*, Wiley-VCH Verlag GmbH & Co. KGaA: (2000).

[16] Adden, N., Dissertation Technische Universität Braunschweig (2007).

[17] Chi, T., *Veeco Application Note*, *Veeco Metrology Group*, (2010),

[18] www.probe.olympus-global.com, In (2011).

4 Synthesis, Characterization, Monomer Reactivity Parameters and Thermal Properties of Phosphonate and Phosphonic Acid Functional Copolymers

4.1 Abstract

Polymers containing phosphate or phosphonate groups are interesting because of their strong interaction with surfaces of inorganic materials. They are used to modify surface chemistry and to control crystal growth. Copolymerization with other monomers allows further adjustment of the properties. These copolymers are potential candidates for controlled crystallization of α-Zirconium hydrogenphosphate hydrate. Copolymers of phosphonic acid or phosphonate ester containing monomers with different other monomers were synthesized by free radical polymerization and characterized by ^{1}H- and ^{31}P-NMR spectroscopy. The copolymer composition was evaluated from the N/C content as determined with elemental analysis. The reactivity values were determined according to the Kelen-Tüdos and Finemann-Ross method. Beside almost alternating copolymers, there were monomer pairs with higher differences in the r-values. The average molecular weight was determined by GPC and all copolymers have a monomodal distribution. Additionally, thermal decomposition behavior was studied with TGA and copolymers with higher content of phosphorous monomers have shown lower mass loss up to 700 °C.

4.2 Introduction

By introduction of functional groups into copolymers new materials with tailored properties and specific applications are possible.[1-2] Phosphorous containing polymers have attained attention because of their technological applications. Surface modification of metal oxide is possible with copolymers having phosphonic acid groups.[3] Functional copolymers with phosphonic acid groups also found application as flame retardants, ion exchange resins and chelating agents for heavy metal salts.[4] Adhesive and anticorrosive properties can be

enhanced by the use of copolymers of phosphonate and phosphonic acid containing monomers and methyl methacrylate.[5]

Phosphonic acid functional copolymers have presented promising proton conductivity.[6-7] The level of energy efficiency in fuel cells is related to the velocity of protons that are transferred through fuel cell membranes. This required high proton transport efficiency is displayed by phosphonic acid functional copolymers and they have successfully been used as fuel cell membranes [8-10]. Phosphonic acid copolymers being biocompatible and biodegradable have been proposed for use in tissue engineering and drug controlled release [11-13]. A biocompatible organic-inorganic composite has been synthesized by reactions between tetracalcium phosphate and polyvinylphosphonic acid.[14] Dental application is an area strongly dominated by phosphonate ester and phosphonic acid containing polymers because of the strong interaction with calcium containing minerals as found in teeth.[15-16]

Copolymerization of phosphorous containing monomers provides the possibility of introducing different organic functionalities in addition to the phosphorous moiety. This leads to the design of copolymers with controlled composition which can be used for a particular application. Phosphorous containing copolymers are also used as $CaCO_3$ and calcium phosphate (CaP) crystallization controlling agents.[17-18] Copolymers of vinylphosphonic acid with 4-vinylimidazole have been used to influence the crystallization of hydroxyapatite.[19]

Properties of the basic polymer chains can be altered by copolymerization to get desired properties. An important aspect of the copolymerization is to acquire knowledge of the reactivity parameters of the constituting components. These reactivity parameters are obtained by establishing the relationship between the compositions of the copolymers produced by different initial monomer concentrations. In this report different phosphonate or phosphonic acid containing copolymers are synthesized by free radical polymerization and characterized by ^{1}H- and ^{31}P-NMR and elemental analysis. The copolymerization parameters were calculated according to Kelen-Tüdos and Finemann-Ross methods.

4.3 Experimental

4.3.1 Materials

Vinylphosphonic acid (VPA) (97%, Aldrich), acrylamide (AAM) (≥ 99%, Sigma), bromotrimethylsilane (TMSBr) (97%, Aldrich) were used as received. Ethyl 2-[4-(dihydroxyphosphoryl)-2-oxabutyl] acrylate (EDOA), whose synthesis is described elsewhere was a kind gift from Ivoclar Vivadent, Liechtenstein.[16] N,N dimethylacrylamide (DMAA, 99% Aldrich and 1-vinylimidazole (1-VI, ≥ 99% Aldrich) were distilled under vacuum and 4-vinylpyridine (VP, 95% Acros) was dried by distilling from CaH_2 prior to use. DMF (99.5%) and 1,4-dioxane (99.5%) were obtained from Acros and used as received. Millipore water with resistivity of 17 MΩ was used for all polymerizations. *α,α′*-azobisisobutyronitrile (AIBN, 98%, Acros), *α,α′*-Azodiisobutyramidine dihydrochloride (ADIBA, 97%, Aldrich), dibenzoyl peroxide (BPO, 75% Acros) and sodium persulfate (98%, Acros) were used without any further treatment. THF was distilled, while methanol and dicholoromethane (HPLC grade, Fisher Scientific) were used directly. Diethyl *p*-vinylbenzylphosphonate (VBP) and dimethyl (2-methacryloyloxyethyl) phosphonate (DMEP) were synthesized according to the literature.[5, 20] Roth ZelluTrans dialysis tubes with a molecular weight cut off (MWCO) 12000-14000 were used for purification.

4.3.2 Copolymerizations

Poly (vinylphosphonic acid)-co-(acrylamide), p(VPA-co-AAM) **1** (see Figure 4-1) was synthesized by a method adapted from the literature with a slight modification in the amount of BPO as initiator.[21] Vinyl phosphonic acid and acrylamide stock solutions (1.5M) were prepared in dioxane and copolymerization was carried out in capped tubes using different proportions of both monomers as shown in Table 4-1. For each polymerization reaction 0.3 mol% of BPO with respect to the monomers was added and the mixture was purged with nitrogen for 30 minutes followed by polymerization at 80 °C. After the required time the polymerization was stopped, the contents of the polymerization mixture were dialyzed against distilled water followed by freeze drying of the copolymer. In all experiments unless mentioned, conversions were determined gravimetrically and restricted to less than 15% by adjusting the polymerization time accordingly.

^{1}H-NMR (D_2O): δ = 2.9-1.1 (CH, CH_2 back none)

^{31}P-NMR (D_2O): δ = 29.3

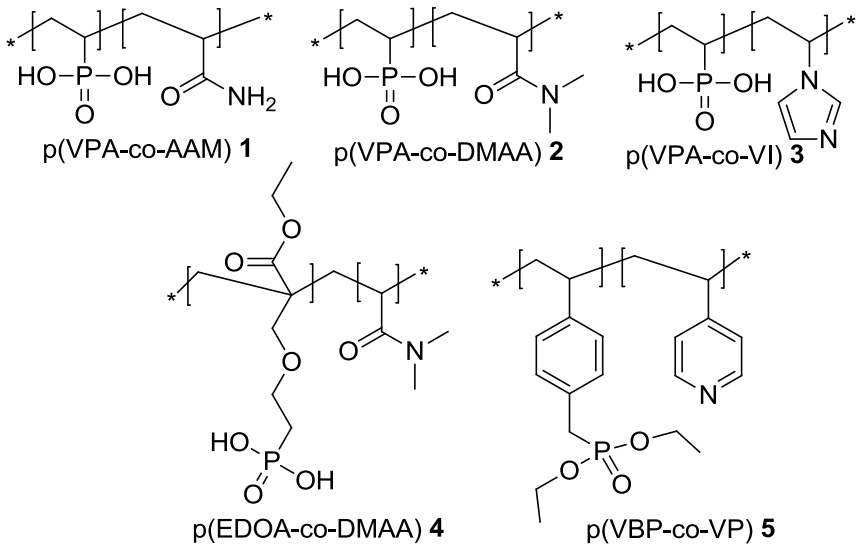

Figure 4-1: Phosphorous containing copolymers

In a similar way poly (vinylphosphonic acid)-co-(dimethyl acrylamide), p(VPA-co-DMAA) **2** was synthesized from stock solutions (1.5 M) in water. For each polymerization reaction 0.3 mol% $Na_2S_2O_8$ was added as initiator and purged with nitrogen for 30 minutes followed by polymerization at 60 °C. Purification of the polymers was performed by dialysis against distilled water followed by freeze drying of the copolymer.

^{1}H-NMR (D_2O): δ = 3.4-2.4[(N-$(CH_3)_2$], 2.4-1.1 (CH, CH_2 back none)

^{31}P-NMR (D_2O): δ = 29.4, 21

Table 4-1: Copolymerization data of VPA with AAM, DMAA and 1-VI

System	**M_1**[a]	**Conv.%**	**m_1**[b]
p(VPA-co-AAM) **1**			
1	0.1	10	0.07
2	0.2	12	0.15
3	0.3	13	0.21
4	0.4	14	0.27
5	0.5	9	0.33
6	0.6	14	0.42
7	0.7	15	0.48
8	0.8	13	0.57
9	0.9	15	0.70
p(VPA-co-DMAA) **2**			
1	0.2	15	0.03
2	0.3	13	0.05
3	0.4	13	0.08
4	0.5	14	0.15
5	0.6	11	0.19
6	0.7	14	0.29
7	0.8	12	0.42
p(VPA-co-1-VI) **3**			
1	0.2	11	0.45
2	0.3	7	0.48
3	0.4	6	0.51
4	0.5	7	0.55
5	0.6	7	0.59
6	0.7	7	0.66
7	0.8	6	0.73

[a] The mol fraction of VPA in feed.

[b] The mol fraction of VPA in copolymer, obtained from elemental analysis.

Poly (vinylphosphonic acid)-co-(1-vinylimidazole), p(VPA-co-1VI) **3** was prepared according to a method originally described for 4-vinylimidazole.[22] Copolymers were synthesized from stock solutions (3.5 M) of both monomers in DMF. For each polymerization reaction 0.5 mol% AIBN was added as initiator and purged with nitrogen for 30 minutes followed by polymerization at 60 °C. Isolated yellow colored precipitates were filtered, washed with DMF and dissolved in water acidified by adding an appropriate amount

of 2 M HCl until they are solubilized. Purification of the polymers was performed by dialysis against distilled water followed by freeze drying of the copolymer. Monomer concentrations in the feed and the copolymers synthesized are summarized in Table 4-1.

^{1}H-NMR (D_2O): δ = 8.7 (N-CH-N), 7.4 (N-CH), 2.9-1.0 (back bone)

^{31}P-NMR (D_2O): δ = 29

Poly (ethyl 2-[4-(dihydroxyphosphoryl)-2-oxabutyl] acrylate-co-dimethylacrylamide, p(EDOA-co-DMAA) **4** was synthesized from stock solutions (1 M) of both monomers in water. For each polymerization reaction 0.3 mol% $Na_2S_2O_8$ was added as initiator and the mixture was purged with nitrogen for 30 minutes followed by polymerization at 60 °C. Purification of the polymers was performed by dialysis against distilled water followed by freeze drying of the copolymer. Contents of the monomer incorporated within the polymer chains are depicted in Table 4-2.

^{1}H-NMR (D_2O): δ = 4.4-3.3 ($CH_2\underline{CH_2}O$, $CH_3\underline{CH_2}O$, $\underline{CH_2}C$-C), 3.3-2.4 [(N-$(CH_3)_2$], 2.4-1.0 (CH_2P, back bone H)

^{31}P-NMR (D_2O): δ = 22.5

Poly (vinylbenzyl phosphonic acid)-co-(4-vinylpyridine), p(VBP-co-VP) **5** was synthesized from stock solutions (2 M) of both monomers in THF. For each polymerization reaction 1 mol% AIBN was added as initiator and purged with nitrogen for 30 minutes followed by polymerization at 60 °C. Polymerization was terminated by precipitation in diethyl ether resulting in a white polymer. The products were filtered and dried overnight under reduced pressure at room temperature. Copolymers with conversion up to 44% were obtained.

^{1}H-NMR (CDCl3): δ = 8.3, (2H, aromat. CH (4-VP)), 7.1 (2H, aromat. CH (VBP)), 6.3 (2H, aromat. CH (4-VP)), 6.3 (2H, aromat. CH (VBP)), 4.0 (4H, -O-$\underline{CH_2}$-CH_3), 3.1 (2H, -CH_2-P), 1.6 (6H, -P(O)(OCH_2-$\underline{CH_3}$)$_2$

Table 4-2: Copolymerization data of EDOA and VBP with DMAA and VP

System	M_1[a]	Conv.%	m_1[b]
p(EDOA-co-DMAA) **4**			
1	0.2	7	0.34
2	0.3	7	0.52
3	0.4	6	0.63
4	0.5	4	0.73
5	0.6	5	0.80
6	0.7	3	0.86
7	0.8	3	0.90
p(VBP-co-VP) **5**			
1	0.31	44	0.33
2	0.50	24	0.46
3	0.70	35	0.63
4	0.85	25	0.79
5	0.95	28	0.89

[a] The mol fraction of EDOA and VBP in feed.

[b] The mol fraction of EDOA and VBP in copolymer, obtained from elemental analysis.

Poly (2-methacryloyloxyethyl) phosphonic diacid, pMEPD (Figure 4-2) was synthesized in a two step reaction.

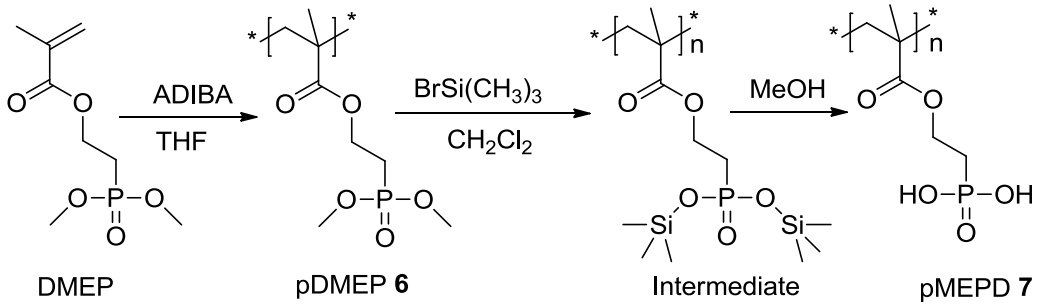

Figure 4-2: Synthetic scheme for methacrylic diphosphonic acid polymer

In a 25 ml schlenk tube, 2.2 g (10 mmol) of dimethyl (2-methacryloyloxyethyl) phosphonate (DMEP) dissolved in a mixture of 6 ml methanol (HPLC quality) and 4 ml Millipore water were degassed with a stream of nitrogen for 30 minutes. Water soluble azo initiator

α,α′-azodiisobutyramidine dihydrochloride (ADIBA) 27.12 mg, (1 mol%) was added to start polymerization at 55 °C. After 18 hours the polymerization was stopped and the reaction mixture was dissolved in water and dialyzed against deionized water. Finally the polymer was freeze dried. The yield was up to 87%. The polymer was analyzed by ^{1}H- and ^{31}P-NMR. In the next step the phosphonate ester polymer (pDMEP) 1.21 g, (5.4 mmol) was added to a 100 ml three necked flask fitted with condenser. Polymer was dissolved by the addition of 25 ml dichloromethane under nitrogen flow. After complete dissolution of the polymer, 2.15 ml (16.3 mmol) of $BrSi(CH_3)_3$ was added dropwise with a syringe through a septum. The mixture was stirred at room temperature overnight. The solvents and volatile residues were evaporated resulting into a solid material. The dealkylation was realized by adding 15 ml of methanol and stirring at room temperature for another 12 hours. The residue was dialyzed and freeze dried to yield a white phosphonic acid polymer. The conversion was 92%.

p(DMEP) ^{1}H-NMR (CD_3OD): δ = 4.4-4.0 (-O-CH_2), 4.0-3.6 [-P(O)(OCH_3)$_2$], 2.6-1.4 (-CH_2-P and –$\underline{CH_2}$-C(CH_3), 1.4-0.43 (–CH_2-C($\underline{CH_3}$)

^{31}P-NMR (CD_3OD): δ = 32

p(MEPD) ^{1}H-NMR (D_2O): δ = 4.4-3.9 (-O-CH_2), 2.6-1.4 (-CH_2-P and –$\underline{CH_2}$-C(CH_3), 1.4-0.43 (-CH_2-C($\underline{CH_3}$)

^{31}P-NMR (D_2O): δ = 25

4.3.3 Analytics

The copolymers were analyzed by ^{1}H- and ^{31}P-NMR spectroscopy on a Bruker AM400 instrument. The amount of monomeric units in the copolymer was determined from the carbon and nitrogen content via elemental analysis with Thermo Quest CE Instruments Flash EA 1112. Molecular weights were determined by GPC equipped with PSS Suprema columns (10µm pre-column) and DAWN DSP light scattering detector Wyatt (Santa Barbara USA) with water in presence of 0.01 wt% phosphate buffer pH 7.4 and sodium azide 0.05 wt% at 40 °C. The thermal stability of the copolymers was investigated by thermogravimetric analysis performed with a Netzsch Thermal Analysis TG209 instrument.

4.3.4 Determination of the Monomer Reactivity Values

Reactivity values were determined according to conventional linearization methods such as Kelen-Tüdos and Finemann-Ross method.[23-24] As monomer with high reactivity is consumed sooner and the monomer mixture becomes progressively poorer in that monomer, the conversion in the copolymerization reaction was kept around 15%. However it is reported that the reactivity ratios can be calculated using Kelen-Tüdos method even at high conversions up to 50% which is an advantage over the other methods.[25-26]

4.4 Results and Discussion

Polymers containing phosphonate or phosphate groups are interesting because of their interaction with inorganic material surfaces. They are important because of their acidic and proton conducting behavior. The properties can be tailored by copolymerization with other monomers. Phosphonic acid containing monomers undergo copolymerization virtually with all vinyl monomers.[27] To design a copolymer with desired composition, reactivity parameters play a central role and therefore, need to be determined.

Vinyl phosphonic acid (VPA) is the simplest monomer with a phosphonic acid group and is commercially available. Water soluble and non-ionic acrylamide (AAM) was chosen for copolymerization which act as “diluent” to reduce VPA density along the polymer chain. The polymers of VPA with AAM were characterized by ^{1}H- and ^{31}P-NMR spectroscopy. Back bone hydrogen can be seen from 1.1 ppm to 3.0 ppm but no further signals are detected as there are no other active protons. In ^{31}P-specta there is a major peak at 29.3 ppm which corresponds to the $RPO(OH)_2$ groups. Although p(VPA-co-AAM) has been prepared earlier [21], no copolymerization parameters have been reported so far. Therefore, the compositions of the different copolymers were determined using elemental analysis and are summarized in

Table 4-1. With the compositions as function of the monomer feed ratio the reactivity ratios can be determined using the method of Finemann-Ross and Kelen-Tüdos (Figure 4-3).

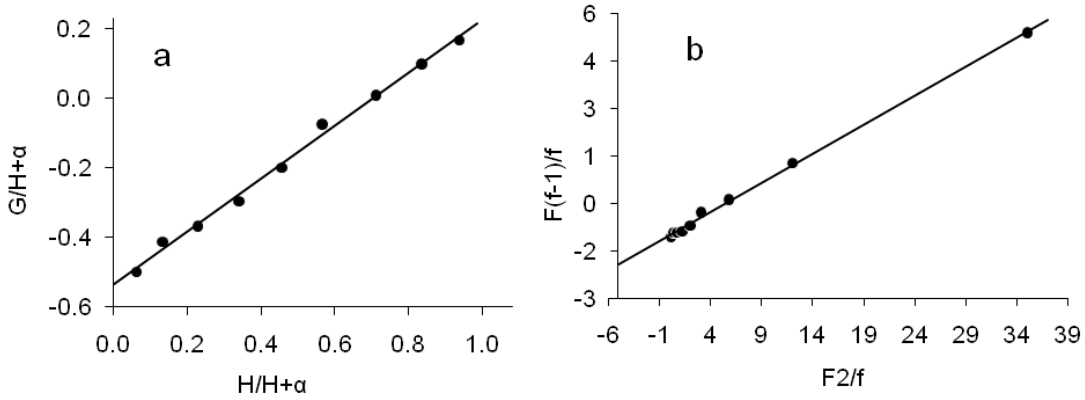

Figure 4-3: (a) Kelen-Tüdos and (b) Finemann-Ross plots for copolymer p(VPA-co-AAM) **1**

The r-values calculated from experimental data are r_1(VPA)=0.20 and r_2(AAM)=1.35 respectively according to the Kelen-Tüdos method. These values are indicative of a preferred incorporation of the AAM compared to VPA. Copolymer microstructure is build up of longer AAM sequences and solitary VPA groups.

Dimethylacrylamide (DMAA), another water soluble monomer, was used to substitute acrylamide for the copolymerization with vinylphosphonic acid. As the hydrophilic character of DMAA is less pronounced than for AAM, the copolymers of p(VPA-co-DMAA) **2** are less hydrophilic in comparison to the p(VPA-co-AAM) **1**. Copolymers of VPA with DMAA were also characterized by ^{1}H- and ^{31}P-NMR spectroscopy. There are two main regions of the ^{1}H-NMR spectra: 3.4 to 2.4 ppm due to the dimethyl group which are shifted downfield due to the presence of nitrogen atom attached directly to the methyl group, and 2.4 to 1.1 ppm due to the -CH- and CH_2 backbone. It was possible to determine the content of each monomer from the ^{1}H-NMR spectrum because of the well identified peak for the dimethyl groups. The composition determined from the ^{1}H-NMR integral (not presented here) were close to those calculated from elemental analysis. Beside a major peak at 29.4 ppm in ^{31}P-NMR, a minor peak around 21 ppm appeared. The minor peak can be attributed to the phosphonic acid group of residual monomer.[14, 28] Additionally the formation of anhydride groups R(HO)OP-O-PO(OH)R bond could also result in a similar peak.[29-30]

The composition of the copolymers elucidated by elemental analysis was used to determine the r-parameters. A prominent difference was found in the reactivity ratios of the two monomers; r_1=0.29 and r_2=7.63 for VPA and DMAA, respectively. This is indicative of very

high reactivity of DMAA in comparison to the co monomer, thus favoring the incorporation of more DMAA in the polymer chains in comparison to VPA. The copolymers obtained are poor in VPA content compared to the monomer mixture (see Table 4-1).

Heterocyles such as vinylimadazole (VI) are interesting because of the nitrogen acting as strong proton acceptor resulting in protonic charge carriers. This property makes them an important candidate for the synthesis of anhydrous proton conducting polymer electrolytes.[7] The imidazole ring is part of an important amino acid "histidine" and unlike amines, it is not completely protonated at low pH and very active in donor acceptor and hydrogen bonding.[31] Combination of VPA with VI brings together acidic and basic units within a polymer chain. Copolymers of pVPA-co-4-vinylimidazole have been reported to control the crystal growth of hydroxyapatite, depending on the phosphorous content of the copolymer.[19] These copolymers, therefore, might have a potential for controlled crystallization of other inorganic materials too.

The copolymer composition was determined from the elemental analysis data (Table 4-1) and used to calculate the reactivity values. The r-values for p(VPA-co-1VI) **3** are r_1=0.40 and r_2=0.11 for VPA and 1-vinylimidazole (1VI) respectively. For this pair of monomers both r_1 and r_2 are less than one and roughly similar, which indicates that the system copolymerizes almost statistically with a tendency to be alternating. Each monomer has nearly the same ability to react with an active polymer chain. A comparable copolymer of VPA with 4-vinylimidazole (4VI) has been reported however the authors have not mentioned r-values for this pair.[22] The polymers are soluble in aqueous solution of HCl and their solubility decreases with increasing VPA content in the copolymer. This could be related to the formation of inter and intra molecular complexation due to the protonation of nitrogen in the imidazole ring forming imidazolium ion when copolymerized with VPA.[22] A similar donor-acceptor interaction has been observed between imidazole and carboxylate in the copolymer of poly(1-vinyl imidazole-co-acrylic acid).[32]

Ethyl 2-[4-(dihydroxyphosphoryl)-2-oxabutyl]acrylate (EDOA) is a water soluble, phosphonic acid monomer with hydrolytically stable bonds between the methacrylic and the strongly acidic phosphoric acid group. This monomer is capable of adhering to the dentine surface and dental replacement composite and therefore used as primer for dental applications.[16] Being active towards inorganic ions, for example calcium, it is interesting to copolymerize it with another water soluble monomer like N,N dimethylacrylamide (DMAA).

The copolymers with different compositions and therefore different concentrations of active phosphonic acid groups can be tested for their efficiency as morphology directing agent in the crystallization of inorganic compounds. Spectra of a copolymer of p(EDOA-co-DMAA) **4** are shown in Figure 4-4.

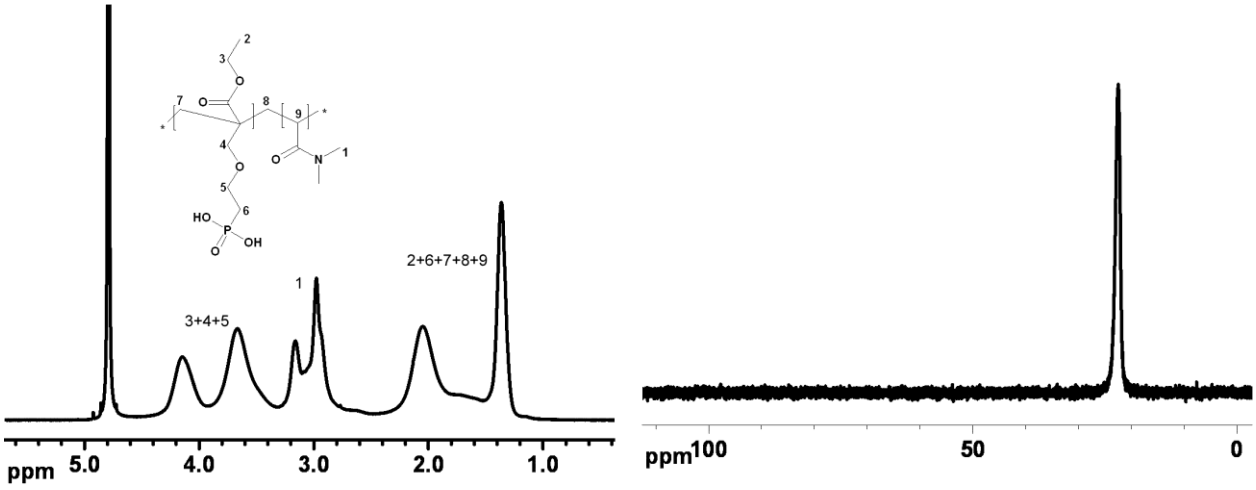

Figure 4-4: ^{1}H- and ^{31}P-NMR spectra of p(EDOA-co-DMAA) **4**

The ^{1}H-NMR spectrum exhibits the presence of the characteristic dimethyl amide protons from DMAA in the 3.3-2.4 ppm range. Signals from different alkyl protons of EDOA can be seen shifted downfield to 4.4-3.3 ppm due to the vicinity of the oxygen and the acrylic group, while the backbone protons are found between 2.4 and 1.0 ppm. A major peak is found at 22.5 ppm in ^{31}P-NMR spectrum for the phosphonic acid group. The composition of the different copolymers was determined by elemental analysis and is summarized in (Table 4-2). With the compositions as function of the monomer feed ratio the reactivity ratios can be determined using the method of Finemann-Ross and Kelen-Tüdos (Table 4-3).

In this monomer pair the phosphonic acid containing monomer has a higher reactivity than DMAA and the r-values have resulted in 2.45 and 0.40 for EDOA and DMAA respectively. Copolymers are always with higher content of EDOA in comparison to the starting mixture composition because of their greater tendency to be incorporated within the polymer chain. The reactivity ratios provide a tool for the estimation of sequence of EDOA and DMAA

along the polymer chain. Longer sequences of EDOA monomer separated by very short sequences of DMAA are expected in the polymeric chains.

Vinylbenzyl phosphonate (VBP) is a phosphonate ester and can be copolymerized with 4-vinylpyridine (4-VP). Phosphonate ester of VBP can be hydrolyzed resulting in a phosphonic acid copolymer. Such phosphonic acid functional polymer are proton conducting polyelectrolytes[33] while poly(vinylpyridine) is also proton conductive, but only in the presence of a proton donor.[6] Thus an alternating copolymer with both monomers as donor and acceptor would be an ideal model. Polymers and copolymers of VBP can be also used as chelating agent for heavy metal salts, as fire retardants and as ion exchange resins.[4] Copolymer of VBP and 4-VP were prepared and characterized by ^{1}H-NMR and elemental analysis. The ^{1}H-NMR integral of the aromatic CH-groups next to 4-vinylpyridine nitrogen at 8.3 ppm has been used for determination of the copolymer 4-VP content. For determination of the copolymer VBP content, the integral of the CH_2-groups within the phosphonic acid ester group at 4.0 ppm as well as the integral of the CH_2-group next to VBP phosphorus at 3.1 ppm have been utilized.

Values obtained from ^{1}H-NMR perfectly matched with those data obtained from elemental analysis using the carbon to nitrogen ratio as presented in Table 4-2. As reaction conversions have been beyond values suitable for the Finemann-Ross plot this method has not been applied here. Determination of the copolymerization parameters according to the method of Kelen-Tüdös resulted in r_1= 0.45 for VBP and r_2= 0.58 for 4-VP, indicating that the copolymer add the monomers in a statistical manner with a tendency to be alternating. Based on previously described copolymerizations, Table 4-3 summarizes the calculated reactivity ratios r_1 and r_2 for all.

Table 4-3: Comparison of reactivity ratios of monomer pairs by different methods

System	Method	r_1	r_2	r_1r_2
p(VPA-co-AAM) **1**	KT	0.20	1.35	0.26
	FR	0.18	1.31	0.24
p(VPA-co-DMAA) **2**	KT	0.29	7.63	2.21
	FR	0.29	7.64	2.24
p(VPA-co-1-VI) **3**	KT	0.40	0.11	0.05
	FR	0.43	0.15	0.06
p(EDOA-co-DMAA) **4**	KT	2.45	0.40	0.99
	FR	2.22	0.28	0.62
p(VBP-co-VP) **5**	KT	0.45	0.58	0.26

Copolymerization diagrams can be constructed from the experimental r-parameters (Figure 4-5). The solid line in the centre represents ideal situation where reactivity ratios are 1 for both monomers. The experimental curves are lying above or below the ideal curve except for p(VPA-co-1VI) **3** and p(VBP-co-VP) **5**, where both are initially above the ideal line until they cut it at certain point and then lying below the ideal line.

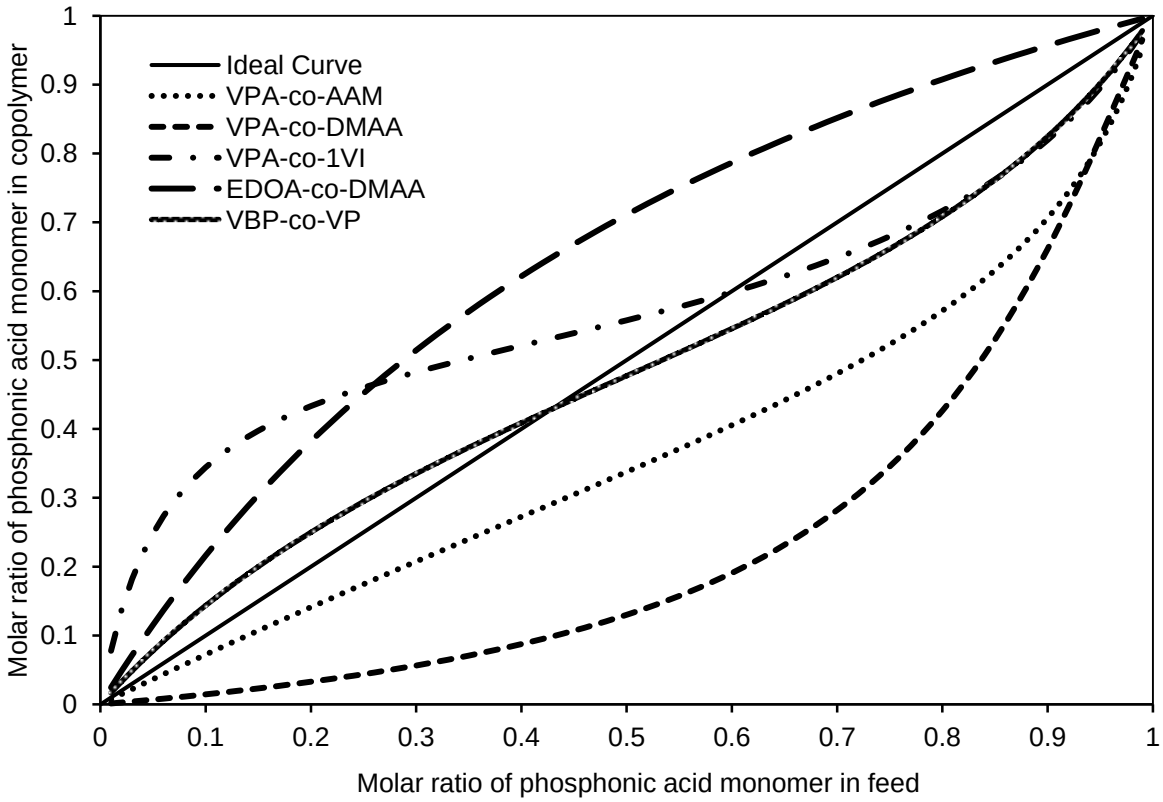

Figure 4-5: Copolymerization diagram according to r-parameters

For curves either above or below the ideal line, the r-values are not close to each other and particularly higher than one whereas the second value is less than one, thus forcing the curve away from the ideal line. The bigger the difference in r-values, for example in case of p(VPA-co-DMAA) **2** is, the higher the deviation from ideal curve. To synthesize a copolymer with same monomeric composition, either a very high initial monomer ratio of VPA is required or feeding the batch continuously with VPA monomer during the course of polymerization.

Poly(VPA-co-1VI) **3** has both values less than 1 with an azeotropic point at 0.6 where the monomer feed results in the formation of a copolymer with the same monomeric composition. The same is true for p(VBP-co-VP) **5**, showing an azeotropic point at a monomer feed of 0.4. Poly (VBP-co-VP) **5** is characterized by a statistical incorporation of the monomers into the polymer chain and its copolymerization behavior is much closer to ideal behavior than for p(VPA-co-VI) **3**.

Besides copolymers, also homopolymers of dimethyl(2-methacryloyloxyethyl)phosphonate (DMEP) and (2-methacryloyloxyethyl)phosphonic diacid (MEPD) were synthesized and characterized. These polymers are adhesion promoters for fluoropolymers and act as anticorrosive agents on the galvanized steel.[5] Poly(2-methacryloyloxyethyl)phosphonic diacid (pMEPD) **7** was obtained via the dealkylation of the corresponding phosphonate ester (pDMEP) **6**. In literature only copolymers of DMEP and MEPD with high content of MMA have been reported. The authors have discussed the difficulty of copolymerizing MEPD because of the condensation of the phosphonic acid group.[5] We were also unable to homopolymerize MEPD directly from the monomer, however the synthesis by polymerizing DMEP followed by the hydrolysis was successful (Figure 4-2). ^{1}H-NMR of phosphonate ester and phosphonic acid polymers are presented in Figure 4-6.

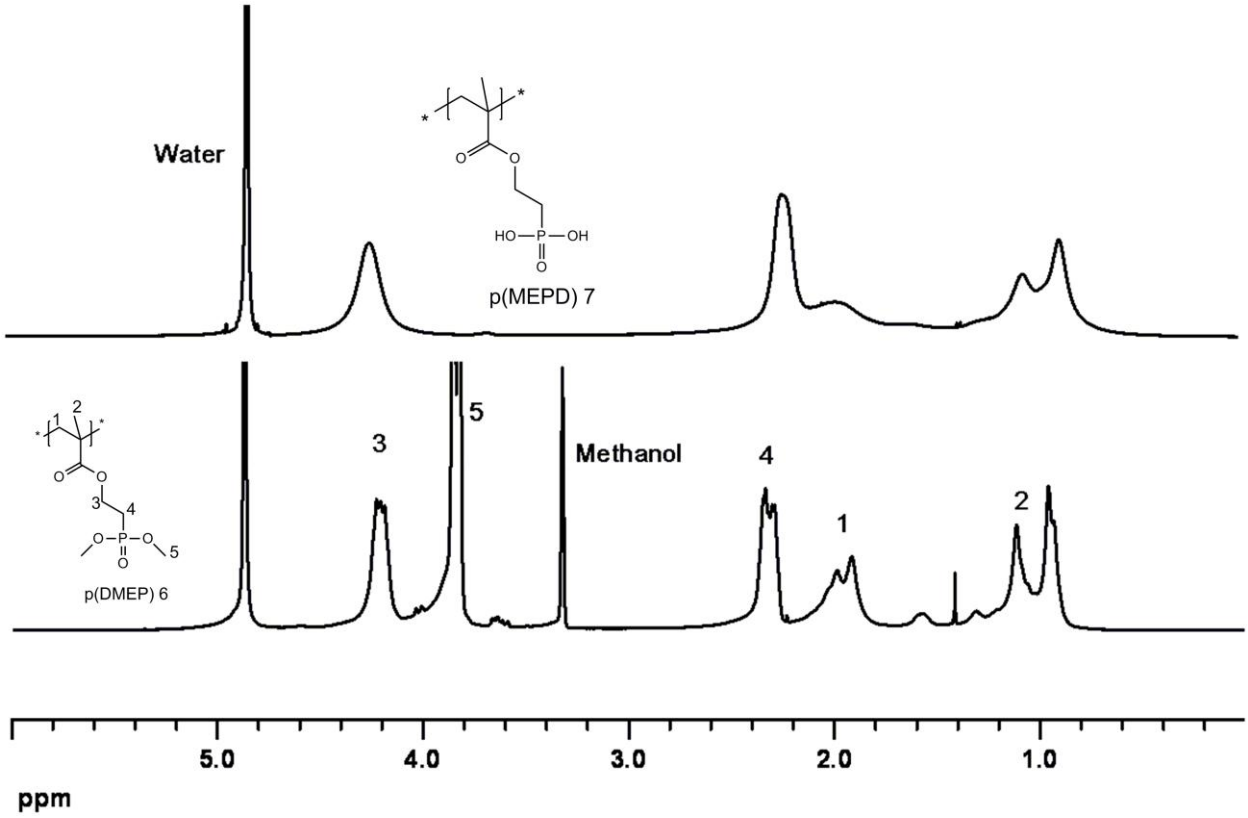

Figure 4-6: ^{1}H-NMR spectra of p(DMEP) **6** and p(MEPD) **7**

The peak at (δ) 4.0-3.6 ppm corresponds to the protons of phosphonate ester group. In the spectrum of p(MEPD) **7** this peak cannot be detected, which indicates complete hydrolysis of

the methyl ester. Additionally the ^{31}P-NMR spectrum of the p(DMEP) **6** exhibits one single peak at (δ) 32 ppm characteristic of a phosphonate ester while the resulting phosphonic acid shows a single peak at (δ)25 ppm (Figure 4-7).

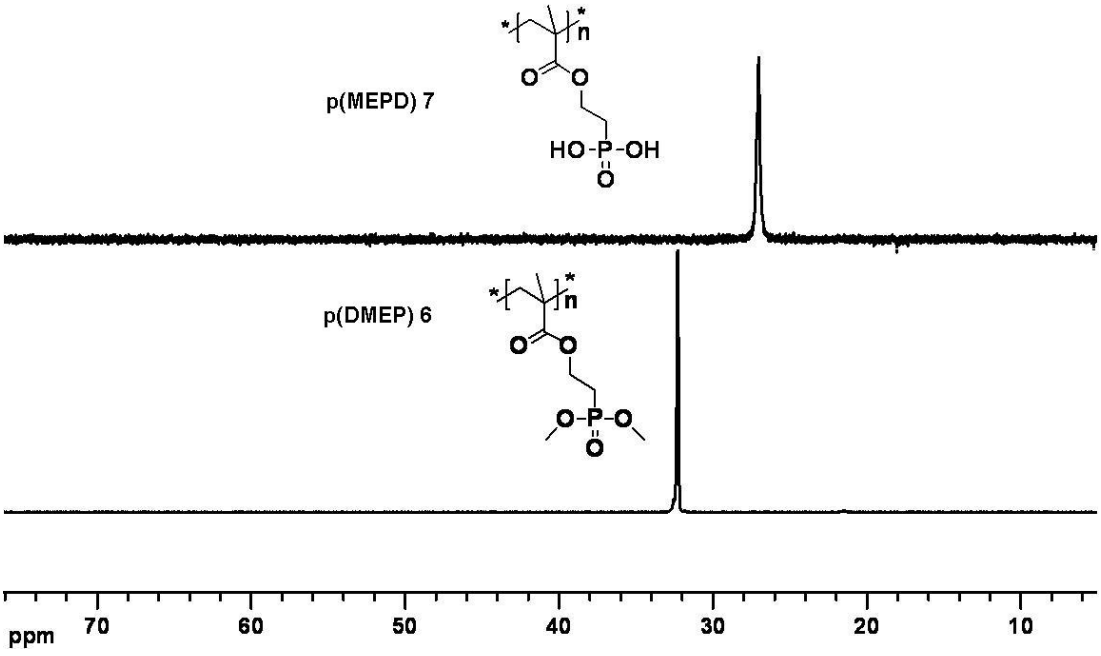

Figure 4-7: ^{13}P-NMR spectra of p(DMEP) **6** and p(MEPD) **7**

4.4.1 GPC Analysis

Aqueous SEC was performed to evaluate the molecular weight and molecular weight distribution. SEC indicates a monomodal distribution. Two representative chromatograms are depicted in Figure 4-8.

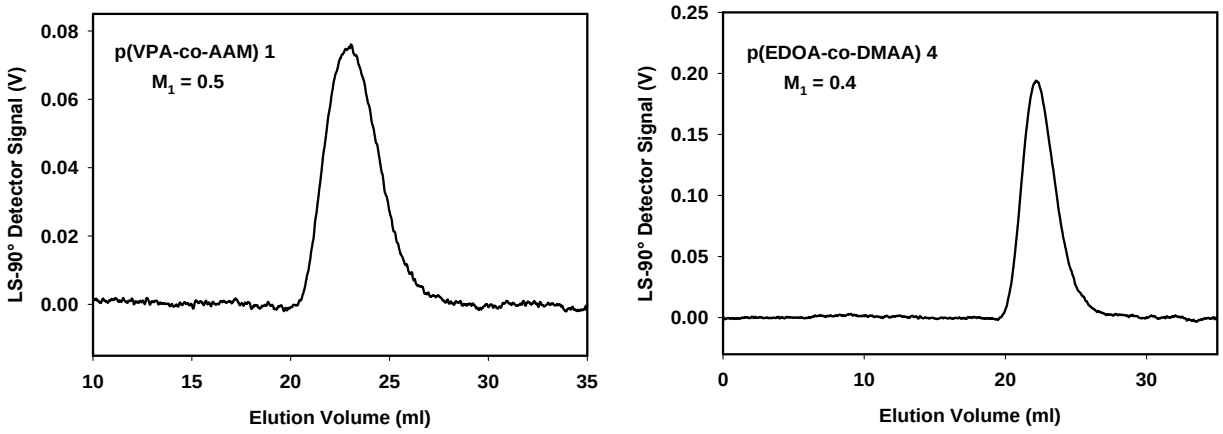

Figure 4-8: Typical GPC curves of copolymers

Molecular weight data for different copolymers is given in Table 4-4.

Table 4-4: GPC results for different copolymers

Sample	**M_1**[a]	**M_n (kg/mol)**	**M_w (kg/mol)**	**PDI**
p(VPA-co-AAM) **1**	0.3	115.7	177	1.53
p(VPA-co-AAM) **1**	0.5	90.2	121.2	1.34
p(VPA-co-DMAA) **2**	0.7	257.0	405.3	1.52
p(VPA-co-DMAA) **2**	0.8	101.3	141.7	1.40
p(EDOA-co-DMAA) **4**	0.4	258.5	329.1	1.27
p(EDOA-co-DMAA) **4**	0.7	115.6	238.7	2.06
pMEPD	-	342.1	427.0	1.25

[a] The mol fraction of VPA and EDOA in feed.

The molecular weight for one copolymer series decreases with increasing content of the phosphonic acid moieties. This might be due to the chain transfer properties of phosphorous functional monomers. A large number of organophosphorous monomers have been found to

be chain transfer agents due to the formation of stable conformations of the growing chain end with a greater proximity between the phosphoryl group of the penultimate unit and radical centre. Abstraction of radical takes place because of the possibility of intramolecular substitution, leading to the termination of the old chain and the generation of new one without the termination of the kinetic chain (Figure 4-9).[27]

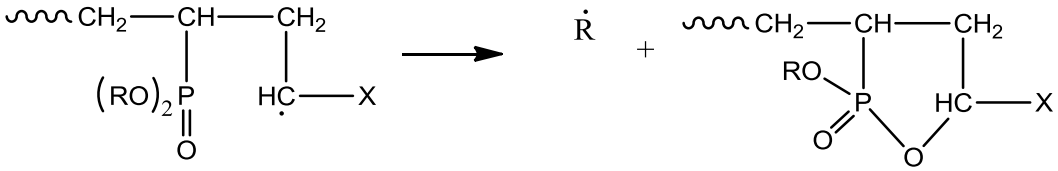

Figure 4-9: Chain transfer mechanism of organophosphorous monomer[27]

As discussed earlier copolymers of VPA-co-1VI were soluble only in acidic water and molecular weight of these copolymers therefore could not be determined on the existing SEC system with a buffered eluent.

4.4.2 Crystallization Control of α-Zirconium Hydrogenphosphate Hydrate

It is well-known that polymers, especially charged ones, are capable of influencing the morphology of inorganic crystals by interaction with charged building units, either by influencing the nucleation process, complexation equilibria in solution or by specific adsorption to crystal surfaces. α-Zirconium hydrogenphosphate hydrate (α-ZrP) possesses a layered structure so that the crystallization with a platelet-like morphology should be possible. The synthesized polymers were investigated if they can favour platelet morphology of α-ZrP if added as morphology directing agent in the ZrP crystallization.

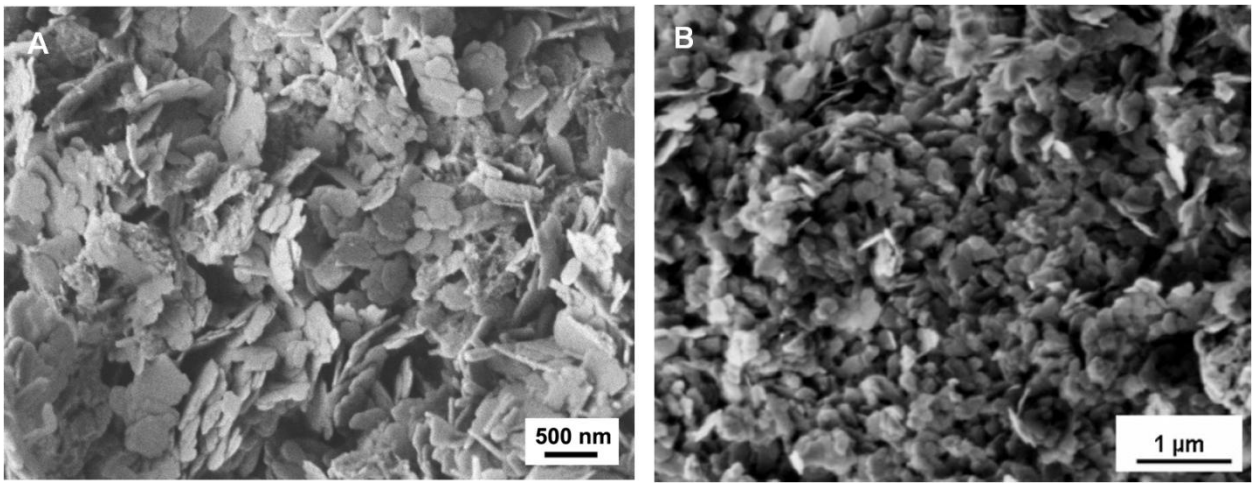

Figure 4-10: SEM image of α-ZrP synthesized under the influence of (A) p($VPA_{0.25}$-co-$AAM_{0.75}$) **1**, (B) pMEPD **7**

Addition of p($VPA_{0.25}$-co-$AAM_{0.75}$) has resulted in nano-sized platelets of high aspect ratio (Figure 4-10A). The concentration of the copolymer was adjusted in a way that the number of zirconium cations to phosphonic acid groups of the copolymer (Zr/P ratio) was 9.4:1. Platelets obtained by this way can be dispersed by ultrasonication and used in the synthesis of nacre like organic-inorganic hybrid materials according to well known process of layer-by-layer assembly.[34] A change either in copolymer composition or in the ratio of Zr/P has resulted in unspecific particle morphology. In a similar experiment with p(VPA-co-DMAA) and p(EDOA-co-DMAA), thick aggregated platelets with a rough surface and low aspect ratio were obtained. Presence of pMEPD as morphology directing agent at Zr/P ratio of 5:1 has resulted in small aggregated platelets with diameter of few hundred nanometres (Figure 4-10B). A detailed description of the effects of the functional copolymers on the nucleation of α-Zirconium hydrogenphosphate hydrate (α-ZrP) and hydroxyapatite is given by Hering.[35]

4.4.3 Decomposition Analysis

As phosphonic acid containing polymers are used as flame retardants it was of interest to measure their degradation by increasing temperature gradually. The investigation of the thermal stability was performed by thermogravimetric analysis (TGA). Analysis was

conducted at a heating rate of 10 °C/min in a nitrogen atmosphere up to 550 °C followed by air up to 700 °C.

All copolymers except p(VPA-AAM) were almost thermally stable up to approximately 300 °C with slight changes in the mass. Beyond 300 °C a major mass loss took place until 550 °C. The thermal stability for different copolymers was higher for higher amounts of phosphonic acid groups incorporated. TGA curves obtained for different samples are presented in Figure 4-11.

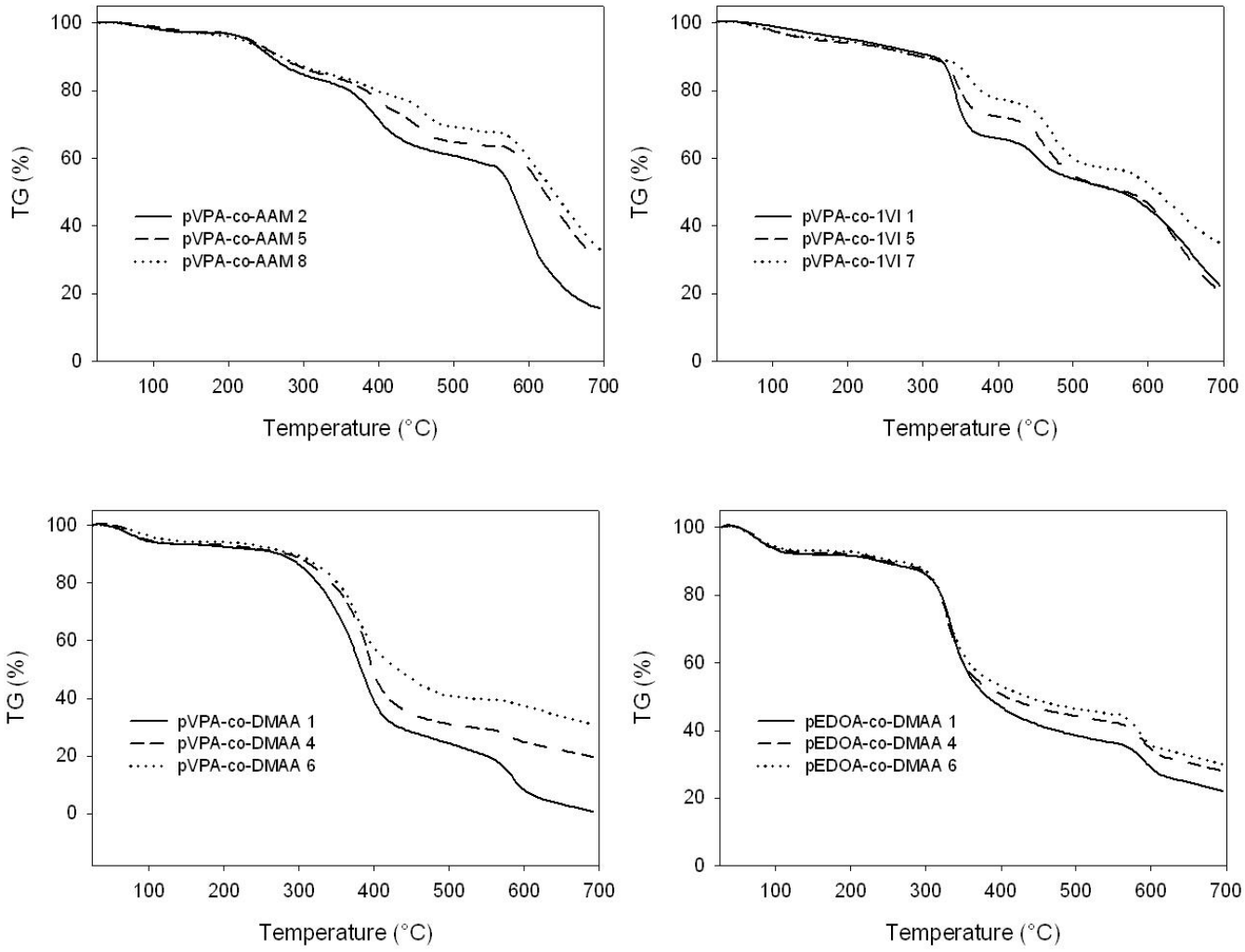

Figure 4-11: TGA curves of synthesized copolymers (number at the end of copolymer represent sample according to Table 4-1 and Table 4-2)

4.5 Conclusion

Phosphonic acid and phosphonate ester containing copolymers were synthesized. Their structures were verified with ^{1}H- and ^{31}P-NMR indicating the presence of both monomers. A series of experiments were conducted with increasing concentrations of the phosphorous monomer and restricted to low conversions. The reactivity ratios were determined by two different methods, which resulted in almost similar values. The r-values for p(VPA-co-1VI) and p(VBP-co-VP) indicate alternating monomer sequences and the corresponding copolymerization diagrams show azeotropic points at 60% and 40% VPA in the monomer mixture, respectively. The copolymers of VPA and EDOA with AAM and DMAA have resulted in significantly different r-values and thus copolymerization diagrams obtained were away from the ideal curve. The average molecular weight of the copolymer decreases with increasing content of the phosphonic acid moieties as measured by GPC. Copolymers with higher content of phosphonic acid were thermally more stable. These copolymers can interact with α-ZrP and act as morphology directing agent and thus can control the crystallization. Particularly a copolymer of p(VPA-co-AAM) has resulted in high aspect ratio platelets.

References

[1] Deen, G. R.; Gan, L. H., *Polymer*, (2006) **47**, 5025.

[2] Soykan, C.; Delibas, A.; Coskun, R., *React. Funct. Polym.* , (2008) **68**, 114.

[3] Zeller, A.; Musyanovych, A.; Kappl, M.; Ethirajan, A.; Dass, M.; Markova, D.; Klapper, M.; Landfester, K., *ACS Appl. Mater. Interfaces*, (2010) **2**, 2421.

[4] Boutevin, B.; Hervaud, Y.; Boulahna, A.; Hadrami, E. M. E., *Polym. Int.* , (2002) **51**, 450.

[5] Bressy-Brondino, C.; Boutevin, B.; Hervaud, Y.; Gaboyard, M., *J. Appl. Polym. Sci.*, (2002) **83**, 2277.

[6] Jiang, F.; Kaltbeitzel, A.; Meyer, W. H.; Pu, H.; Wegner, G., *Macromolecules*, (2008) **41**, 3081.

[7] Sevil, F.; Bozkurt, A., *J. Phys. Chem. Solids*, (2004) **65**, 1659.

[8] Schuster, M.; Rager, T.; Noda, A.; Kreuer, K. D.; Maier, J., *Fuel Cells*, (2005) **5**, 355.

[9] Yamada, M.; Honma, I., *Polymer*, (2005) **46**, 2986.

[10] Erdemi, H.; Bozkurt, A., *Eur. Polym. J.*, (2004) **40**, 1925.

[11] Iwasaki, Y.; Nakagawa, C.; Ohtomi, M.; Ishihara, K.; Akiyoshi, K., *Biomacromolecules*, (2004) **5**, 1110.

[12] Wang, J.; Mao, H.-Q.; Leong, K. W., *J. Am. Chem. Soc.*, (2001) **123**, 9480.

[13] Murphy, M. B.; Hartgerink, J. D.; Goepferich, A.; Mikos, A. G., *Biomacromolecules*, (2007) **8**, 2237.

[14] Greish, Y. E.; Brown, P. W., *Biomaterials*, (2001) **22**, 807.

[15] Moszner, N.; Zeuner, F.; Pfeiffer, S.; Schurte, I.; Rheinberger, V.; Drache, M., *Macromolecular Materials and Engineering*, (2001) **286**, 225.

[16] Moszner, N.; Zeuner, F.; Fischer, U. K.; Rheinberger, V., *Macromol. Chem. Phys.*, (1999) **200**, 1062.

[17] Huang, J.; Matyjaszewski, K., *Macromolecules*, (2005) **38**, 3577.

[18] Suzuki, S.; Whittaker, M. R.; Grondahl, L.; Monteiro, M. J.; Wentrup-Byrne, E., *Biomacromolecules*, (2006) **7**, 3178.

[19] Dogan, O.; Oner, M., *Langmuir*, (2006) **22**, 9671.

[20] Frantz, R.; Durand, J.-O.; Carré, F.; Lanneau, G. F.; Bideau, J. L.; Alonso, B.; Massiot, D., *Chem. Eur. J.*, (2003) **9**, 770.

[21] Chen, X.; Huang, R.; Pelton, R., *Ind. Eng. Chem. Res.*, (2005) **44**, 2078.

[22] Bozkurt, A.; Meyer, W. H.; Gutmann, J.; Wegner, G., *Solid State Ionics*, (2003) **164**, 169.

[23] Fineman, M.; Ross, S. D., *J. Polym. Sci.*, (1950) **5**, 259.

[24] Kelen, T.; Tüdős, F., *React. Kinet. Catal. Lett.* , (1974) **1**, 487.

[25] Rao, S. P.; Ponratnam, S.; Kapur, S. L.; Iyer, P. K., *J. Polym. Sci. Polym. Letter. Ed.*,, (1976) **14**, 513.

[26] Bajaj, P.; Sen, K.; Bahrami, S. H., *J. Appl. Polym. Sci.*, (1996) **59**, 1539.

[27] Shulyndin, S. V.; Levin, Y. A.; Ivanov, B. E., *Russ. Chem. Rev.*, (1981) **50**, 865.

[28] Braybrook, J. H.; Nicholson, J. W., *J. Mater. Chem.*, (1993) **3**, 361.

[29] Kim, Y. K.; Gu, L.-s.; Bryan, T. E.; Kim, J. R.; Chen, L.; Liu, Y.; Yoon, J. C.; Breschi, L.; Pashley, D. H.; Tay, F. R., *Biomaterials*, (2010) **31**, 6618.

[30] Millaruelo, M.; Steinert, V.; Komber, H.; Klopsch, R.; Voit, B., *Macromol. Chem. Phys.*, (2008) **209**, 366.

[31] Annenkov, V. V.; Danilovtseva, E. N.; Tenhu, H.; Aseyev, V.; Hirvonen, S. P.; Mikhaleva, A. I., *Eur. Polym. J.*, (2004) **40**, 1027.

[32] Belyayeva, V. V.; Skushnikova, A. I.; Pavlova, A. L.; Domnina, Y. S.; Brodskaya, E. I., *Poly. Sci. U.S.S.R.*, (1989) **31**, 2188.

[33] Li, S.; Zhou, Z.; Abernathy, H.; Liu, M.; Li, W.; Ukai, J.; Hase, K.; Nakanishi, M., *J. Mater. Chem.*, (2006) **16**, 858.

[34] Waraich, S. M.; Hering, B.; Burghard, Z.; Bill, J.; Behrens, P.; Menzel, H., *J. Colloid Interface Sci.*, (2012) **367**, 74.

[35] Hering, B., Dissertation Leibniz Universität Hannover (2010).

5 Polymer Tailoring

For the synthesis of inorganic platelets, different types of phosphonic acid functional polymers were synthesized. The details of the synthesis have been presented in chapter 4. Beside this, further polymers were prepared by polymer analogous modification with phosphate and bisphosphonate groups.

5.1 Modified Polyamines

Poly (allylamine) (PAA) and poly (ethylene imine) (PEI) were modified with bisphosphonic acid. Bisphosphonates are unique with two bonds located on the same carbon atom. Some bisphosphonate are used for the treatment of several bone related diseases. This class of compounds is capable of interacting with calcium ions present in the hydroxyapatite, a vital bone component and is ultimately taken up by the bone where they influence the calcium metabolism.[1-2] PAA and PEI were modified with a bisphosphonate in order to obtain polymers which might show strong interaction with hydroxyapatite to control the growth of mineral. A general reaction scheme for the modification of polyamine is given in Figure 5-1. A bisphosphonic moiety shall be synthesized first which will be added to polyamines by the activation of the double bond via Michael addition.

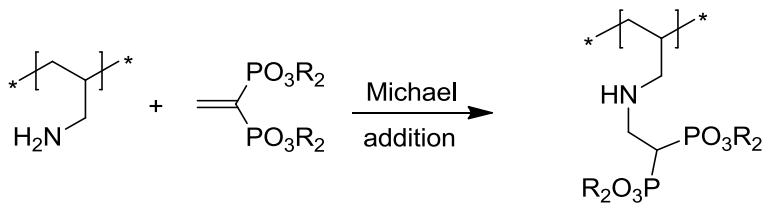

Figure 5-1: Reaction scheme for the modification of polyamines

5.2 Experimental

5.2.1 Synthesis of Ethenylidene Bisphosphonic Acid

An unsaturated bisphosphonic acid ester was synthesized in a two step reaction starting from tetramethylmethylene diphosphonate **1** as reported in Figure 5-2.[3]

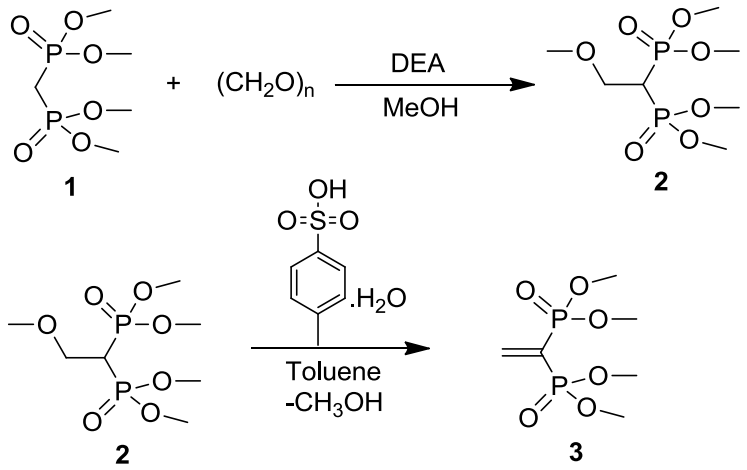

Figure 5-2: Synthesis of tetramethyl ethenylidene bisphosphonate

6.44 g (214.67 mmole) of paraformaldehyde and 3.15 g (43.08 mmole, 4.47 ml) of diethylamine were given to 124 ml of methanol in a nitrogen atmosphere. The mixture was warmed until it became clear. Contents were cooled to room temperature followed by the addition of 10 g (43.08 mmole) of tetramethylmethylene diphosphonate **1** with 2 hour refluxing. Methanol was removed and the resulting intermediate **2** was dissolved in 170 ml of dry toluene and 0.04 g of *p*-toluenesulfonic acid was added followed by 14 hours of refluxing. A Dean Stark trap was used to collect the methanol during refluxing. The crude product was diluted with 86 ml chloroform and washed twice with 13 ml of water. The organic phase was dried over magnesium sulfate and concentrated. Distillation of the crude product at $1x10^{-2}$ mbar (bp 98 °C) resulted in tetramethyl ethenylidene bisphosphonate **3** (49%) as clear liquid.

^{1}H-NMR ($CDCl_3$): δ = 7.1- 6.8 distorted dd (H_2C=), 3.7 distorted dd (12H, OCH_3)

^{13}C-NMR ($CDCl_3$): δ = 150.3 (H_2C=), 129.9 (PCP), 53.1 (OCH_3)

^{31}P-NMR ($CDCl_3$): δ = 16.1

In the second step, dealkylation of the product **3** was performed by dissolving 6.73 g (27.52 mmole) of **3** under nitrogen in 165 ml of dry chloroform. Bromotrimethyl silane (29.14 ml, 220.2 mmole) was added drop wise while stirring within 72 hours. Reaction sequences for the synthesis of bisphosphonic acid starting from the corresponding bisphosphonate ester are shown in Figure 5-3.

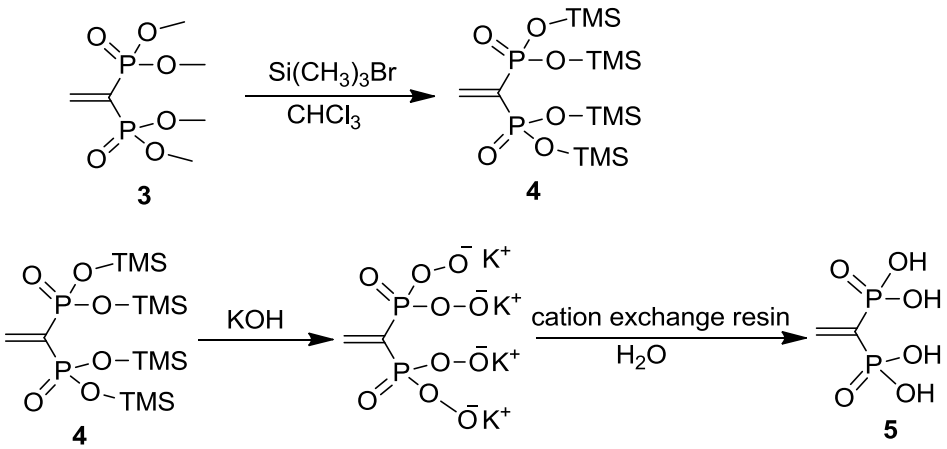

Figure 5-3: Synthesis of ethenylidene bisphosphonic acid

The mixture was concentrated and the crude product was dissolved in 83 ml of methanol. The product was precipitated on addition of methanolic KOH solution, filtered and dried under vacuum. The white solid product was dissolved in water and stirred overnight with excess of amberlite cation exchange resin. The resin was filtered off and the solution was freeze dried to obtain ethenylidene bisphosphonic acid **5** as white solid with 78% yield.

^{1}H-NMR (D_2O): δ = 6.6 (H_2C=)

^{13}C-NMR (D_2O): δ = 146.5 (H_2C=), 139.2 (PCP)

^{31}P-NMR (D_2O): δ = 11.9

5.2.2 Modification of Polyamine with Ethenylidene Bisphosphonic Acid

Bisphosphonic acid **5** (BP) was used to modify polyamine.[4] Polyallylamine hydrochloride (PAA, Mw 15 000) 0.198 g (2.12 mmole) or polyethyleneimine (PEI, Mw 1800) were dissolved in 8 ml of water and passed through a column filled with strongly basic anionic ion exchange resin (Dowex® 550 A, OH), respectively.

The solution was eluted until pH 8-10, having PAA or PEI as free base and concentrated to small volume. Bisphosphonic acid 0.4 g (2.12 mmole) was dissolved in 5 ml of water and mixed with concentrated solution of the polyamine. The mixture was heated under vacuum to 68 °C and further dried at 112 °C for 8 hours. After cooling, 13 ml of water and 0.37 ml (2.65 mmole) of triethylamine were added. The solution was stirred for 2 days. The polymer solution was filtered, diluted with 13 ml of water. To the solution 1.32 ml (15.9 mmole) of concentrated 37% hydrochloric acid was added followed by 22 ml of methanol. The modified polymer precipitated as white powder which was filtered and dried under vacuum. Samples with different amine/BP ratios were synthesized as given in Table 5-2 and Table 5-3 by adjusting the amounts of both components as required. Michael addition of BP to PAA and PEI is shown in Figure 5-4.

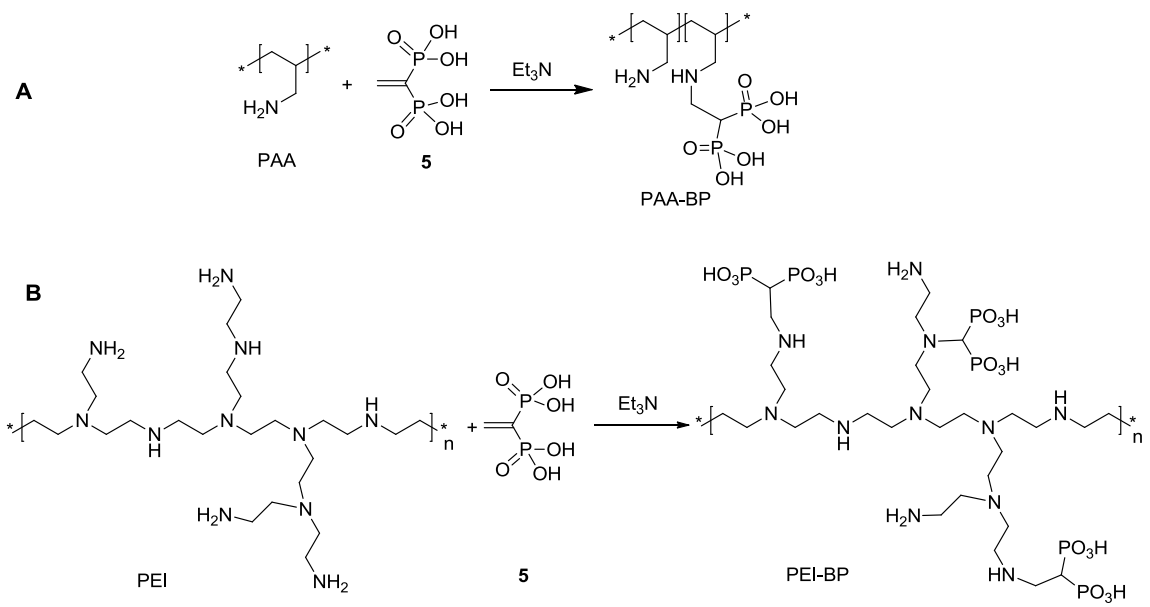

Figure 5-4: Michael addition of BP to (A) PAA, (B) PEI

5.2.3 Modification of Polyvinyl Alcohol

UV-PVA

PVA modified with UV cross linkable acryl groups was synthesized according to the literature.[5] In a 250 ml two necked flask fitted with condenser, 3 g (68 mmole) of PVA (88% hydrolyzed, Mw 88 000) was added to 60 ml of N-methylpyrrolidone (NMP).

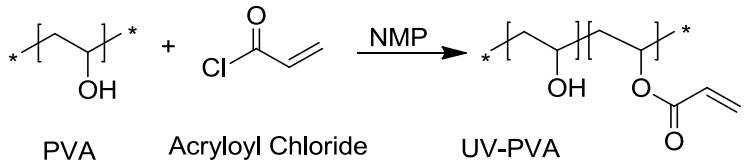

Figure 5-5: Synthetic pathway of UV active PVA[5]

The flask was flushed with nitrogen and heated for 2 hours at 110 °C to dissolve PVA. The mixture was cooled carefully to 4 °C and 1.10 ml (13.6 mmole) acryloyl chloride, dissolved in 15 ml of anhydrous NMP was added drop wise. Reaction contents were stirred for 12 hours at 4 °C followed by the precipitation of modified polymer in excess of methanol. Polymer was filtered and dried under vacuum with a yield of 87%.

^{1}H-NMR (D_2O): δ = 6.45-6.01 (H_2C=CH), 4.06 (H_2C=C**H,** PVA), 1.74 (**H_2**C=CH, PVA)

Polyvinyl Alcohol Phosphate

For the synthesis of polyvinyl alcohol phosphate (Figure 5-6), a three necked flask equipped with condenser was loaded with 12 g of polyphosphoric acid, 40 ml DMF and 25.6 ml of tributyl amine. Reaction mixture was stirred until polyphosphoric acid dissolves completely. PVA (4 g) was added slowly with stirring and heated for 6 h at 120 °C under nitrogen atmosphere. The viscous solution obtained was cooled down and added to approx. 500 ml of ethanol.

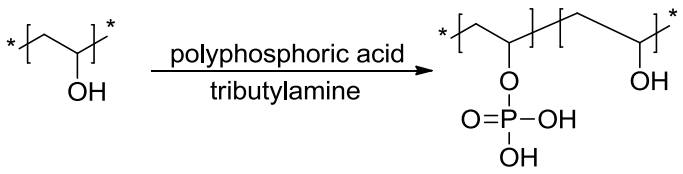

Figure 5-6: Synthesis of poly vinyl alcohol phosphate

Saturated NaCl solution was added drop wise to precipitate the polymer. The precipitate was redissolved in 300 ml of water and the pH was adjusted to 9-10 with 1N NaOH. The liberated tributyl amine was removed by evaporation under vacuum until a viscous solution was obtained which was filtered and dialyzed against de-ionized water. After dialysis the solution was concentrated and adjusted to pH 2 with 1N HCl. In the next step approx. 200 ml of ethanol was added followed by drop wise addition of saturated NaCl to precipitate the modified polymer. Finally, the precipitate was washed with 99.5% ethanol and dried under vacuum. This process resulted in poly vinyl alcohol phosphate with a yield up to 72%.

^{1}H-NMR (D_2O): δ = 4.68 (**H**C-O-P), 4.18 (**H**C-OH), 2.2-1.8 (C**H$_2$**)

5.2.4 Synthesis of Poly DMEP-co-DMAEMA

2-(dimethylamino)ethyl methacrylate (DMAEMA) is commercially available and was dried and distilled before use. Dimethyl(2-methacryloyloxethyl) phosphonate (DMEP) was synthesized and purified under high vacuum with a yield of 20% as cited elsewhere.[6] The copolymerization was carried out in THF with AIBN 0.1% as initiator (Figure 5-7).

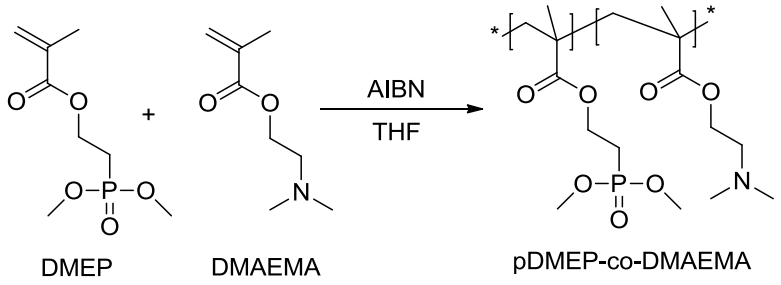

Figure 5-7: Copolymerization of DMEP with DMAEMA

Seven copolymers were synthesized with different monomer feed ratios. Stock solutions (1M) of both monomers were prepared in dry THF. Different amounts of monomers were used as mentioned in Table 5-1.

Table 5-1: Copolymerization of DMEP with DMAEMA

No.	DMEP mmole	DMAEMA mmole	Copolymer Net(g)	Copolymer Yield%
1	3.50	0.50	0.21	25
2	3.00	1.00	0.46	56
3	2.50	1.50	0.41	52
4	2.00	2.00	0.41	54
5	1.50	2.50	0.32	44
6	1.00	3.00	0.12	17
7	0.50	3.50	0.29	44

Mixtures were flushed for 30 minutes with nitrogen to obtain inert atmosphere. AIBN stock solution was prepared by adding 0.8 mmole (0.131g) of azoinitiator to 10 ml THF. To each reaction tube 0.5 ml of the AIBN solution was added to start polymerization at 60 °C. The polymerization was terminated after 5 hours by dipping the reaction tubes in ice cold water. Resulting highly viscous thick solution was diluted with methanol in case of sample 1 and 2 and precipitated in diethylether. Sample 6 and 7 were precipitated in cold petrol ether, filtered and dried under vacuum. All copolymers were redissolved in methanol, precipitated and dried until constant weight.

^{1}H-NMR (CD_3OD): δ = 4.6-4.3 (O**CH_2**-CH_2N), 4.3-3.9 (O**CH_2**-CH_2P), 3.9-3.7 [(-PO-$(CH_3)_2$], 3.7-3.5 [(N-$(CH_3)_2$], 2.9-2.5 (–CH_2N), 2.5-2.2 (-CH_2P), 2.2-0.5 (back bone hydrogen)

5.3 Results and Discussion

During the synthesis of tetramethyl ethenylidene bisphosphonate **3,** first step is a base catalyzed reaction of **1** with paraformaldehyde. In the next step, a double bond was

introduced by an acid catalyzed elimination of methanol which was collected in a Dean Stark trap to shift the equilibrium. Bisphosphonate ester **3** was treated with a silylating agent to enhance the reactivity of phosphonate groups towards hydrolysis. For this purpose, twice the required amount of bromotrimethyl silane was added for a complete dealkylation. In the next step, hydrolysis of the intermediate **4** was done in the presence of water and potassium cations were removed with ion exchange resin. The bisphosphonic acid modified product **5** can clearly be differentiated from **3** by the absence of peak at 3.7 ppm in ^{1}H-NMR. For these kinds of phosphorous compounds ^{31}P-NMR is very helpful in characterization. Compund **3** in the ester form presented a single peak at 16.9 ppm which was shifted upfield to 11.9 ppm in case of corresponding acid **5**.

Ethenylidene bisphosphonic acid **5** was added to modify polyallylamine (PAA) via a Michael addition. This organic reaction is a useful method for C-N bond formation with a nucleophilic addition of a nucleophile to α, β unsaturated carbonyl compound.[7] A detailed mechanism for PAA-BP is given in Figure 5-8.

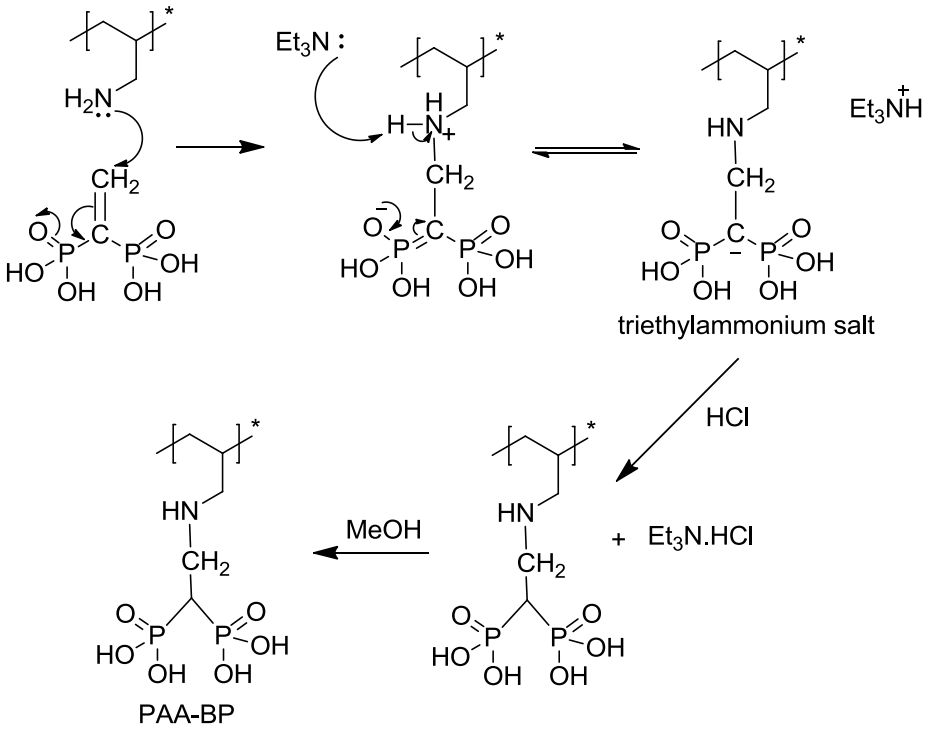

Figure 5-8: Michael addition of PAA to BP

Here polyallylamine is nucleophile and ethenylidene bisphosphonic acid is the Michael acceptor. Nucleophilic attack from PAA takes place on the β carbon of BP thus creating a bond between amine and carbon. The presence of Et_3N abstracts one hydrogen from the amine and forms a triethylammonium salt. Hydrochloric acid precipitates as white material ($Et_3N.HCl$) which was dissolved by the addition of MeOH leaving behind the substituted PAA-BP. Three samples of the PAA were substituted with different amounts of BP as given in Table 5-2.

Table 5-2: PAA tailoring with BP

Sample	PAA/BP	Yield%
1	1	1
2	1.18	36
3	1.5	55

A lower content of BP resulted in higher yield of the reaction. This observation is similar to the yield of other phosphonic acid copolymers discussed in chapter 4. Variations in the substitution degree of the PAA were performed to observe the effect (if any) on the nucleation of hydroxyapatite.

^{31}P-NMR of PAA-BP documented a strong peak at (δ) 17.6 ppm along with a small peak at 12.2 ppm characteristic of BP. The intensity of the peak for BP is very low in comparison to PAA-BP indicating a successful addition of BP to PAA. ^{1}H-NMR was difficult to interpret as proton signals are overlapping thus making ^{31}P-NMR an important characterization tool.

Branched polyethyleneimine (PEI) was also modified with bisphosphonic acid in different ratios as presented in Table 5-3. A low molecular weight PEI (1800 g/mole) was used for the modification[8] because the PEI and PAA modified with BP were soluble in water at pH 10. These modified polymers were tested as crystallization controlling agent to obtain platelets of either calcium or zirconium hydrogen phosphate.

Table 5-3: PEI tailoring with BP

Sample	PEI/BP	Yield%
1	0.85	82
2	1.06	91
3	1.27	85

^{31}P-NMR for PEI-BP show peaks at 17 and 18 ppm beside a small peak at 12.2 ppm. The peak at 12.2 ppm is indicative of the presence of a small amount of BP as impurity while rests of the signals are indicative of an addition product of PEI with BP. As PEI used was a branched polymer and it is expected that addition reaction took place at primary and secondary amine as shown in Figure 5-4 and has resulted in different phosphorus NMR signals at 17 and 18 ppm.

5.3.1 Cross linkable Polyvinyl Alcohol

Polyvinyl alcohol is a versatile polymer which can be used in the preparation of composite materials with promising mechanically properties. A combination of PVA with montmorillonite has resulted in mechanically strong composites. An increase in tensile strength and stiffness has been observed by cross linking with Al^{3+} and Cu^{2+}.[9] Poly vinylalcohol interacts with montmorillonite by hydrogen bonding which is consolidated by cross linking thus making this interaction even stronger. This phenomenon is helpful in the load transfer from the polymers matrix to the inorganic components. Exploiting hydrogen bonding, ultrathin layers of PVA and exfoliated graphene oxide have been fabricated with better mechanical strength in comparison to the constituting components.[10] Classically, polyelectrolytes with high charge density are used in layer-by-layer assembly for the fabrication of a composite material. Although polyvinyl alcohol is uncharged, it is capable of producing strong composite materials in comparison to electrostatic interaction with clay particles.[11-13] Podsiadlo et al. have reported ultra strong and stiff layered polymer nanocomposites of pVA/MMT that were cross linked with glutaraldehyde which forms covalent acetal bonds between hydroxyl groups of the PVA.[11] These characteristics of PVA provoked the fabrication of composite with zirconium hydrogen phosphate platelets. PVA can be modified with acryloyl chloride which makes it UV active as shown in Figure 5-5.

5.3.2 Phosphonic Acid Functional Polymers

Polyvinyl Alcohol Phosphate

In addition to the phosphonate and phosphonic acid, a phosphate of poly vinyl alcohol (Figure 5-6) was synthesized. The aim of this synthesis was to test PVA-phosphate for inorganic controlled nucleation studied within the scope of the thesis by Britta Hering (ACI Hannover). PVA being uncharged was modified to be highly negatively charged by this modification. The reaction scheme followed was originally used for the conversion of polysaccharides and is generalized here to PVA.[14-15] The degree of substitution was calculated from the integral at 4.68 ppm representing the protons with phosphate substituted groups and found to be 46%. This amount of phosphate functionality into the polymeric chain is considered to be sufficient to impart a negatively charged character.

Poly DMEP-co-DMAEMA

Dimethyl(2-methacryloyloxethyl) phosphonate (DMEP) was copolymerized with 2-(dimethylamino)ethyl methacrylate (DMAEMA). DMEP is temperature sensitive and therefore requires distillation at reduced pressure in the range of 10^{-3} mbar. A typical ^{1}H-NMR spectrum for the copolymer is presented in Figure 5-9 where signals from both monomeric units can be identified.

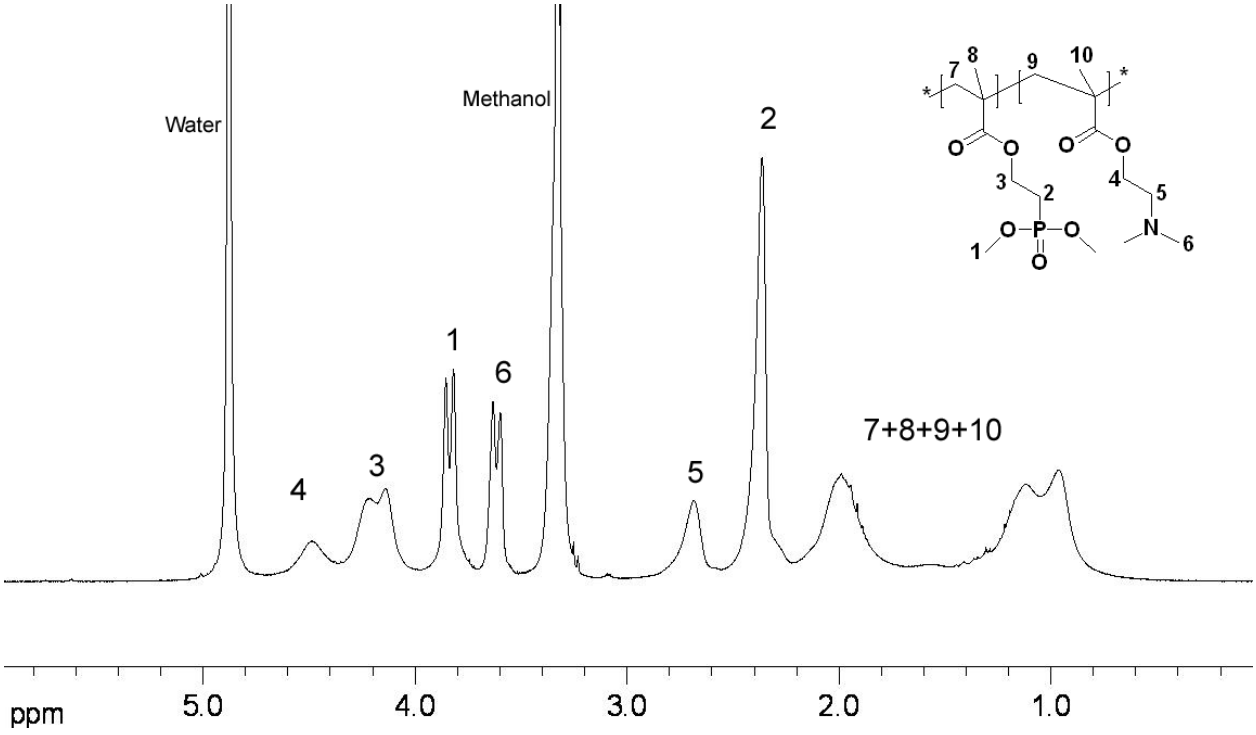

Figure 5-9: ^{1}H-NMR spectrum of p(DMEP-co-DMAEMA)

The synthesized copolymers were subjected to dealkylation with bromotrimethyl silane and alcoholysis with methanol. However, this procedure resulted in a gel like cross linked material. This could be due to the instability of phosphonic acid groups as stated by Boutevin et al.[16] The formation of a P-O-P link within the polymer has resulted in a cross linking reaction leading to a gel.

5.4 Conclusion

An unsaturated bisphosphonic acid ester was synthesized followed by dealkylation leading to an unsaturated bisphosphonic acid. Polyethyleneimine and polyallylamine were modified with different amounts of bisphosphonic acid via Michael addition and the reaction was verified by ^{1}H- and ^{31}P-NMR. Polyvinyl alcohol being uncharged was modified by phosphate groups to be highly negatively charged and the structure was verified by ^{1}H-NMR. These polymers are candidates as crystallization controlling agent to obtain platelets of either calcium or zirconium hydrogen phosphate. A copolymer of DMEP-co-DMAEMA was synthesized with different ratios of both monomers; however, the dealkylation of DMEP to

phosphonic acid was not successful. Additionally a cross linkable PVA was synthesized and characterized by ^{1}H-NMR. This kind of modified PVA is considered to be an interesting organic component in the synthesis of stiff composite materials according to layer-by-layer assembly.

References

[1] Sparidans, R. W.; Twiss, I. M.; Talbot, S., *Pharm. World Sci.*, (1998) **20**, 206.

[2] Murphy, M. B.; Hartgerink, J. D.; Goepferich, A.; Mikos, A. G., *Biomacromolecules*, (2007) **8**, 2237.

[3] Degenhardt, C. R.; Burdsall, D. C., *J. Org. Chem.*, (1986) **51**, 3488.

[4] Fishbein, I.; Alferiev, I. S.; Nyanguile, O.; Gaster, R.; Vohs, J. M.; Wong, G. S.; Felderman, H.; Chen, I.-W.; Choi, H.; Wilensky, R. L.; Levy, R. J., *Proc. Natl. Acad. Sci. U. S. A.*, (2006) **103**, 159.

[5] Tang, Z.; Wei, J.; Yung, L.; Ji, B.; Ma, H.; Qiu, C.; Yoon, K.; Wan, F.; Fang, D.; Hsiao, B. S.; Chu, B., *J. Membr. Sci.*, (2009) **328**, 1.

[6] Bressy-Brondino, C.; Boutevin, B.; Hervaud, Y.; Gaboyard, M., *J. Appl. Polym. Sci.*, (2002) **83**, 2277.

[7] Sykes; Peter, *Guidebook to Mechanism in Organic Chemistry*, Longman London: (1986).

[8] McBain, S. C.; Yiu, H. H. P.; El Haj, A.; Dobson, J., *J. Mater. Chem.*, (2007) **17**, 2561.

[9] Podsiadlo, P.; Kaushik, A. K.; Shim, B. S.; Agarwal, A.; Tang, Z.; Waas, A. M.; Arruda, E. M.; Kotov, N. A., *J. Phys. Chem. B*, (2008) **112**, 14359.

[10] Zhao, X.; Zhang, Q.; Hao, Y.; Li, Y.; Fang, Y.; Chen, D., *Macromolecules*, (2010) **43**, 9411.

[11] Podsiadlo, P.; Kaushik, A. K.; Arruda, E. M.; Waas, A. M.; Shim, B. S.; Xu, J.; Nandivada, H.; Pumplin, B. G.; Lahann, J.; Ramamoorthy, A.; Kotov, N. A., *Science*, (2007) **318**, 80.

[12] Podsiadlo, P.; Liu, Z.; Paterson, D.; Messersmith, P. B.; Kotov, N. A., *Adv. Mater.*, (2007) **19**, 949.

[13] Podsiadlo, P.; Tang, Z.; Shim, B. S.; Kotov, N. A., *Nano Lett.*, (2007) **7**, 1224.

[14] Whistler, R. L.; Towle, G. A., *Appl. Surf. Sci.*, (1969) **135**, 396.

[15] Chen, X.; Huang, R.; Pelton, R., *Ind. Eng. Chem. Res.*, (2005) **44**, 2078.

[16] Boutevin, B.; Hamoui, B.; Parisi, J.-P.; Ameduri, B., *Eur. Polym. J.*, (1996) **32**, 159.

6 Synthesis of Inorganic Particles under the Influence of Polymer Additives

6.1 Introduction

In nacre, aragonite crystal nucleation takes place via a protein assisted mechanism.[1] Calcium carbonate nucleation was studied by the addition of artificial peptides and alginates which were capable of controlling the morphology.[2-3] Different polymers synthesized and discussed in the previous chapters were used as morphology controlling agent for inorganic materials. A nacre like platelet structure was obtained in the presence of polyacrylic acid from potassium sulfate.[4] In matrix controlled inorganic nucleation, crystal surfaces do not grow equally. Controlled by the presence of added macromolecules, the growth results in a specific morphology. A mineralization process under the influence of added polymers requires specific interactions to an inorganic mineral.

Nucleation control using the synthesized polymers was investigated by Britta Hering at Institute of Inorganic Chemistry, Leibniz University Hanover. This chapter provides an overview of the synthesis of inorganic platelets which were used later in the fabrication of composite materials.

6.2 Calciumphosphate

Several polymorphs of calciumphosphate exist, showing different mechanical, chemical and thermal properties. They vary in the calcium/phosphate-ratio accounting for the solubility, which is an important factor concerning the application.[5-6]

Various researchers have reported on controlling the morphology of calciumphosphate using different substances.[6-9] CTAB (cetyltrimethylammonium bromide) was used to obtain spherical hydroxyapatite particles instead of needles during a hydrothermal synthesis.[10] Reaction time, pH and temperature are the parameters to tailor the morphology. The

influence of different types of additives on the crystallization of calciumphosphate has been summarized in a review article.[6]

Hydroxyethylstarch substituted with L-3,4-dihydroxyphenylalanine (HES-DOPA) (Intermediate of which HES-DG was kindly given by A. Bertz*) was synthesized and used as additive in a hydrothermal synthesis. A detailed synthesis of the HES-DOPA is described in chapter 9. Calciumphosphate was selected as inorganic component for the synthesis of biocompatible composites. HES-DOPA could facilitate a change in the crystal growth of calcium phosphate in order to obtain platelets or structures similar to that found in nacre. Added polymer may act electrostatically with the growing surface of hydroxyapatite.[7, 11]

The synthesis was performed according to an established method with slight modifications and replacement of CTAB with HES-DOPA.[12] The addition of HES-DOPA had a considerable influence on the morphology of the resulting product depending highly on the concentration.

Products with different Ca/DOPA ratios were investigated and interesting morphologies were found at Ca/DOPA ratio of 18:1 and 28:1. In Figure 6-1, SEM-images exhibit the morphology of such different calciumphosphates. At a ratio of 18:1, blocks were formed consisting of stacked thin lamellae. This morphology resembles the structure of nacre. For a lower amount of the polymer, comparable piles were observed, but the platelets were much thicker.

* Institute for Technical Chemistry, TU Braunschweig

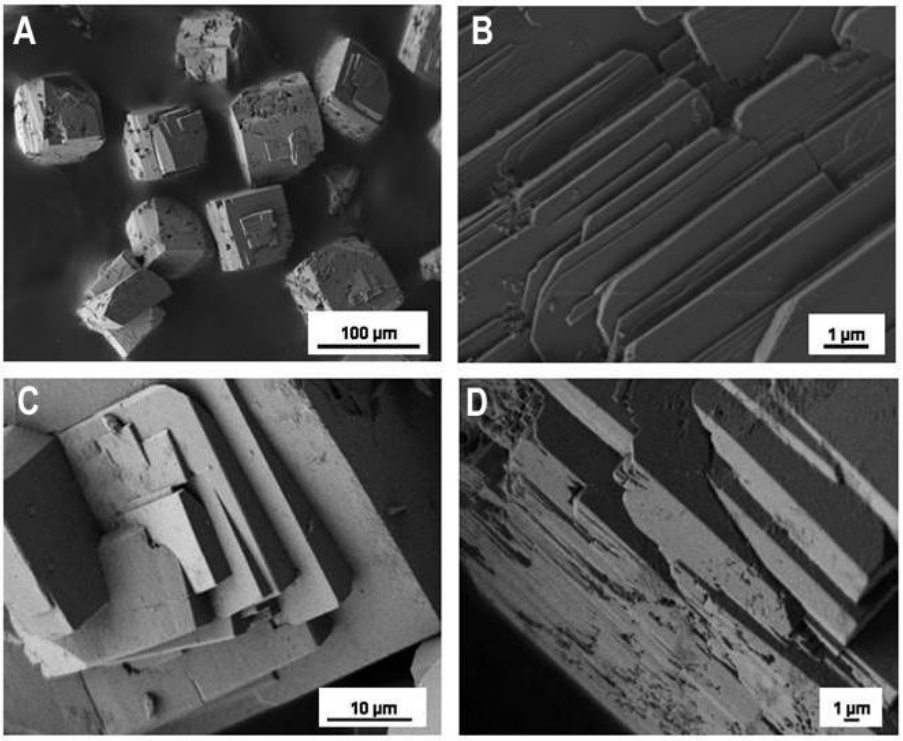

Figure 6-1: SEM of products synthesized with HES-DOPA at Ca/DOPA-ratios of (A&B) 18:1 and (C&D) 28:1

By decreasing the content of polymeric additive down to a Ca/DOPA ratio of 58:1 elongated crystals of hydroxyapatite were observed in contrast to the stacked lamellar structure observed at higher content of additives. A change in the concentration of added HES-DOPA not only resulted in different morphology but also different modification of calcium phosphate namely monetite and hydroxyapatite. Up to Ca/DOPA ratio of 28:1, monetite was formed. However, a further decrease in the ratio precipitated the most stable calciumphosphate form, hydroxyapatite, as shown in Figure 6-2.

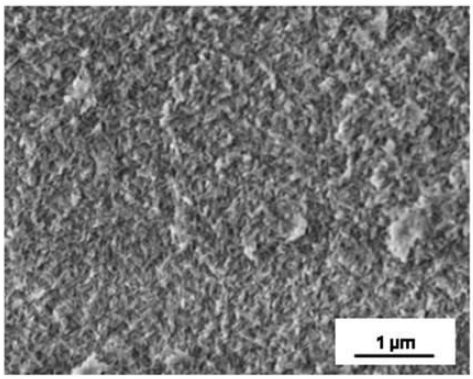

Figure 6-2: SEM image of hydroxyapatite with HES-DOPA at Ca/DOPA-ratio 39:1

These structural investigations were supported by XRD analysis of the products obtained at different times under different concentration of the additive. For detailed information on characterization and effect of reaction time on the morphological changes the reader is referred to the dissertation of B. Hering.[12]

Calciumphosphate particle morphology is strongly affected by the presence of the anionic polyelectrolytes.[6] Besides HES-DOPA, polyelectrolytes additives were used which resulted in different calciumphosphate morphologies as presented in Figure 6-3. Although platelet like structures as obtained in the presence of HES-DOPA were expected (Figure 6-1), all attempts with hydroxyapatite have resulted in different morphology.

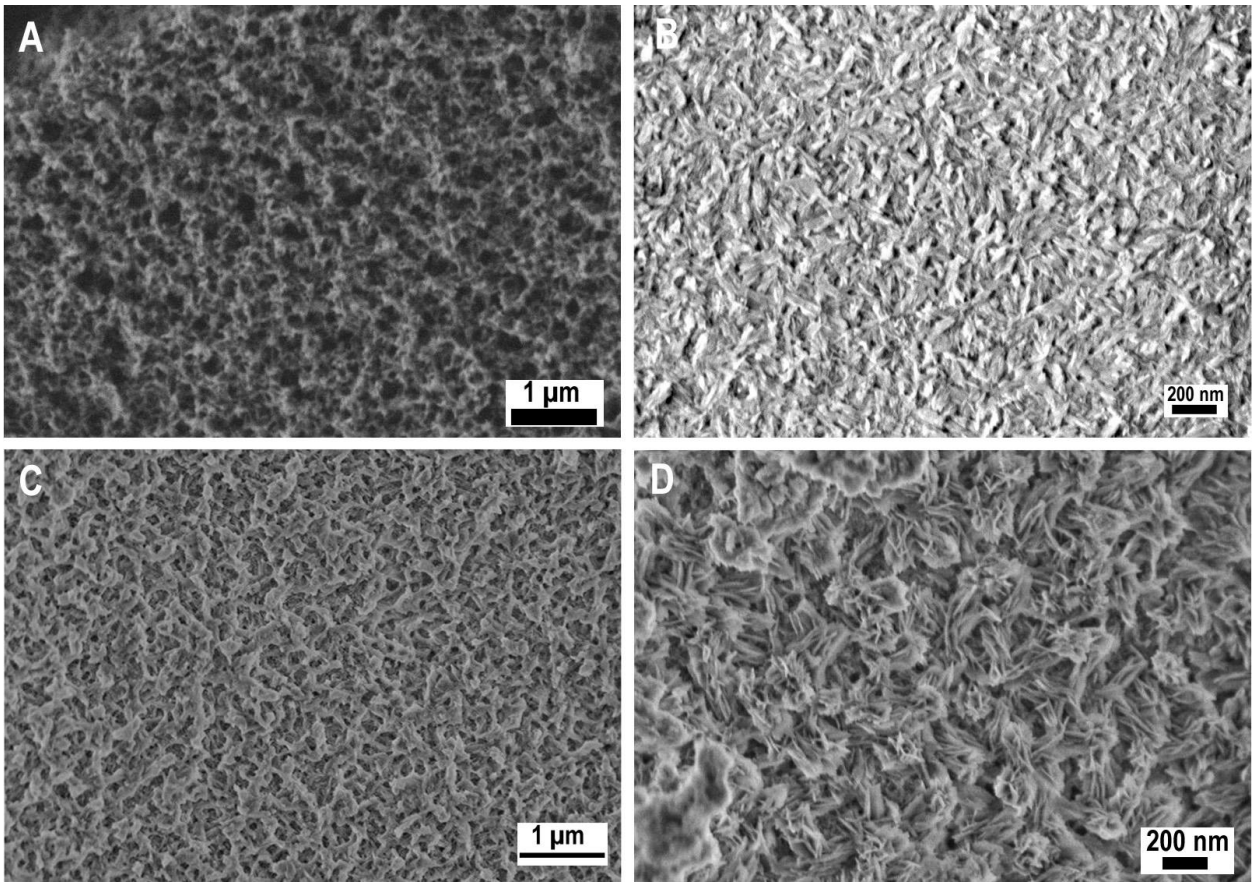

Figure 6-3: SEM images of HAP synthesized under the influence of (A) pMEPD Ca/P 2:1, (B) p($VPA_{0.29}$-co-$DMAA_{0.71}$) Ca/P 4:1, (C) p($VPA_{0.33}$-co-$AAM_{0.67}$) Ca/P 9.7:1, (D) p($EDOA_{0.64}$-co-$DMAA_{0.36}$) Ca/P 3.5:1

In the presence of pMEPD a porous material was obtained (Figure 6-3A). The pore size increases with an increasing polymer content as measured by nitrogen adsorption experiments. Maximum pore size was obtained at Ca/P ratio of 2:1, whereas no porosity was observed with polymer content lower than Ca/P ratio of 4:1.

Copolymer of VPA with DMAA resulted in elongated needles at Ca/P ratio of 4:1 (Figure 6-3B). With a lower concentration of copolymer particles of inconsistent morphology were formed.

A copolymer of VPA with AAM resulted in porous structures up to Ca/P ratio of 12.9:1. A further decrease in the copolymer content leads to the disappearance of the porosity. A higher content of the copolymer resulted in bigger pore size. To see the effect of copolymerizing unit such experiments were performed with pVPA alone. This leads to the small, fine, aggregated needles thus showing the effect of second monomer on crystallization control.

Long, thin needles of calcium phosphate were formed in the presence of p(EDOA-co-DMAA) at Ca/P 3.5:1. These morphologies are the result of the interaction of polymeric molecules to the growing crystal face. Modified polyamine with bisphosphonic acid and polyvinyl alcohol phosphate do not have any effect on the morphology when compared to experiment without any additives.

6.3 α-Zirconium Hydrogen Phosphate

α-Zirconium hydrogen phosphate (ZrP) possesses a layered structure and a controlled crystallization in the form of platelets is very likely.[13-15] Being biocompatible, ZrP has already been used on titanium and metal oxides resulting for enhancement of the mechanical properties.[16-18] It is well-known that polymers, especially charged ones, are capable of influencing the morphology of inorganic crystals by interaction with charged building units, either by influencing the nucleation process, complexation equilibria in solution or by specific adsorption to crystal surfaces. Polymers containing phosphate or phosphonate groups have been used extensively for controlling the formation of different calcium phosphates and other calcium-containing minerals. Also in biological systems, nucleation of ionic biominerals is often controlled by proteins or polysaccharides carrying anionic groups.[19-20]

Tailored synthetic polymers with anionic phosphonate groups $–P(=O)(O^-)_2$ have been evaluated for calcification experiments.[21] For the synthesis of α-zirconium hydrogen phosphate with high aspect ratio, the nucleation controlling property of phosphonic acid functional homo and copolymers as additives was exploited. Different (co-)polymers used in this study are depicted in Figure 6-4. The crystallization experiments with these polymers synthesized in this work have been carried out by B. Hering.[12]

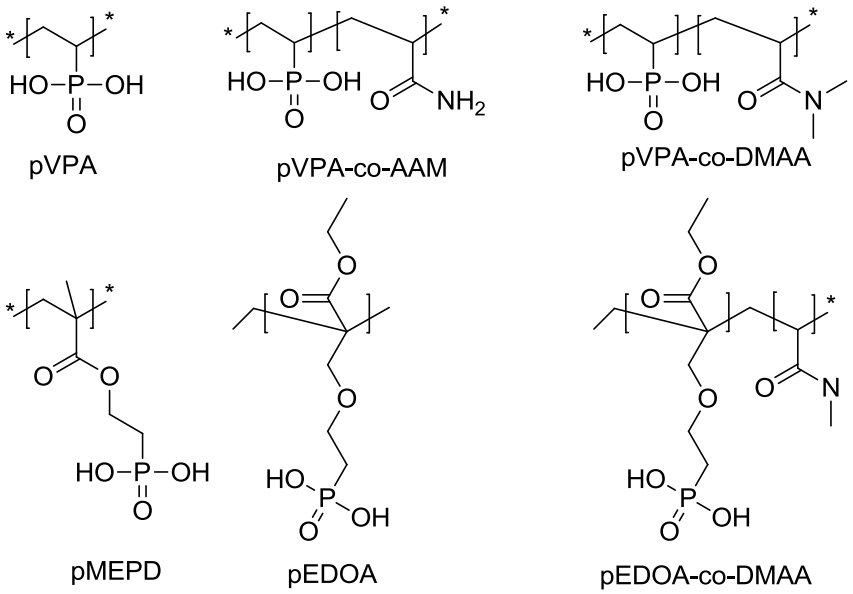

Figure 6-4: Polyelectrolytes used as additives in the synthesis of α-ZrP

Before synthesizing α-ZrP in the presence of polymers, a synthesis without any additive was performed. The resulting particles were partly aggregated and have different sizes (see Figure 6-5).

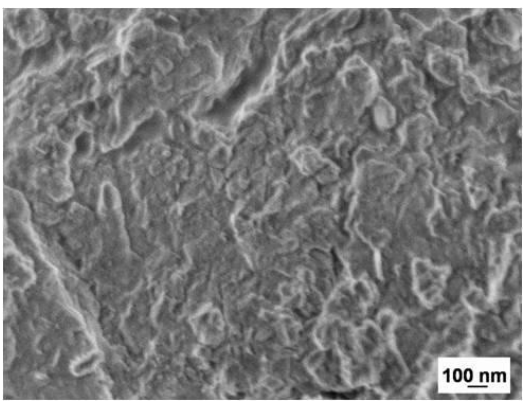

Figure 6-5: SEM images of α-ZrP synthesized without any additive

The addition of (co-)polymers had a considerable influence on the morphology of the resulting products. The crucial factors are the chemical structure of the additives and their concentration.

For pVPA-co-AAM, different copolymer compositions were used as additives. Figure 6-6 shows SEM images of α-ZrP samples synthesized under the influence of pVPA-co-AAM at different Zr/P ratios. It is obvious that the higher Zr/P ratio of 9.4:1 led to the formation of platelets of a diameter between 200 and 400 nm and high aspect ratio, whereas a higher concentration of the copolymer (Zr/P ratio of 4.7:1) resulted in unspecific particles comparable to those prepared without additives shown in Figure 6-5. Platelets (Figure 6-6A) can be dispersed by ultrasonication to makes a stable suspension of the inorganic platelets that can be used for the fabrication of composite material.

Furthermore it was observed that not only the content of phosphonic acid is important but also the monomer ratio within the copolymer is influencing the nucleation control.

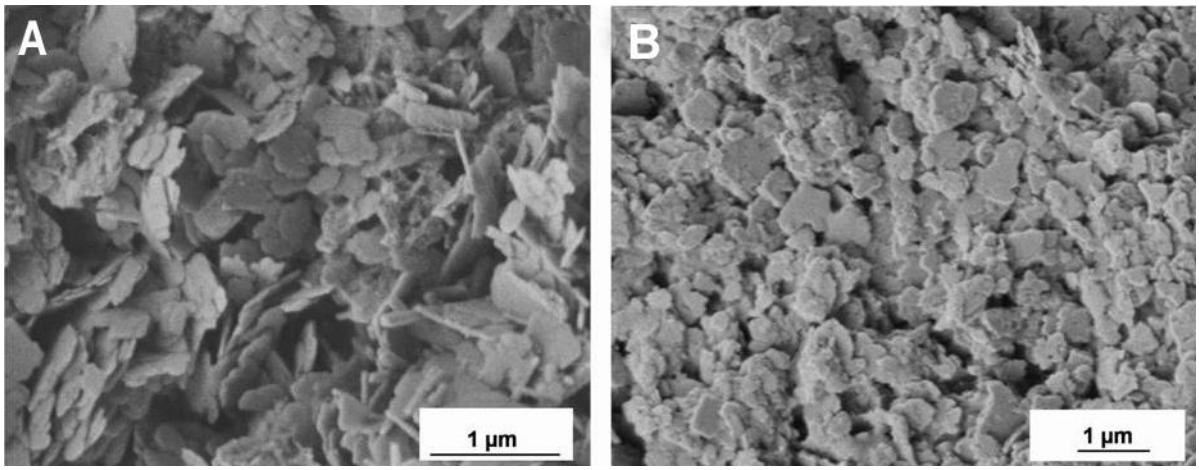

Figure 6-6: SEM images of α-ZrP synthesized under the influence of (A) $pVPA_{0.25}$-co-$AAM_{0.75}$ with Zr/P ratio of 9.4:1; (B) $pVPA_{0.33}$-co-$AAM_{0.67}$ at Zr/P ratio of 4.7:1

Probably, the copolymer influences the growth of the crystals because of interactions between its phosphonic acid groups and the growing crystal faces. By adsorption of the polymer onto a surface, further epitaxial growth would be inhibited. It is conceivable that at the surface zirconium cations are partly coordinated by phosphonate groups from the

copolymer instead of phosphate ions, as proposed by Alberti for the synthesis of MELS (molecularly engineered layers).[22] Because of interactions within the copolymer chains, these are adsorbed in a folding and not in a linear form on the crystal surface. The hindered access of ions to the occluded surface then precludes further growth of the crystals vertically to the layers, leading to platelets with high aspect ratio. A model based on these observations along with detailed discussion of the crystallization behaviour is discussed in detail by B. Hering.[12]

In order to ascertain whether the mere presence of phosphonic acid groups is sufficient to affect the morphology of ZrP crystals, the polymer pVPA was added in different Zr/P ratios between 3:1 and 5:1. SEM images showed that all products consisted of platelets with rough crystal surfaces. A difference lies in the smaller aspect ratios in comparison to the material obtained with p(VPA-co-AAM) (Figure 6-6A). In a similar experiment with pVPA-co-DMAA thick aggregated platelets were obtained as seen in the case of pVPA indicating a modest influence of the dimethyl acrylamide group within the copolymer (Figure 6-7).

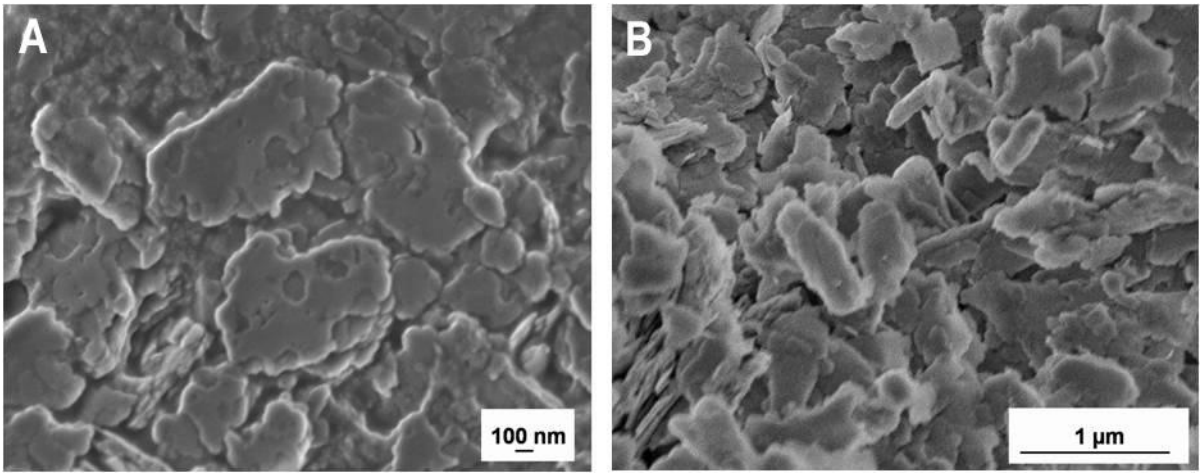

Figure 6-7: SEM images of α-ZrP synthesized under the influence of A) pVPA at Zr/P ratio 3:1 and B) pVPA-co-DMAA at Zr/P ratio of 12:1

To clarify the correlation between the constitution of the polymer and its influence on crystal formation pMEPD and p(EDOA-co-DMAA), were used. In pMEPD, ester groups connect the phosphonate groups to the polymer backbone, whereas in pEDOA they appear as independent side chain along with dimethyl acrylamide.

When pEDOA-co-DMAA was added at a Zr/P ratio of 11:1, the product morphology (Figure 6-8A) was quite similar to that observed for particles prepared in the presence of pVPA-co-DMAA (Figure 6-7B) with platelets showing diameters up to 1 µm and being partly aggregated. The additional presence of the ester groups thus does not appear to have any special effects here. pMEPD was added to the synthesis mixture at Zr/P ratios of 5:1 leading to small aggregated platelets as presented in Figure 6-8B. However, compared to previously described products, these platelets exhibited much smaller diameters of only few hundred nanometres.

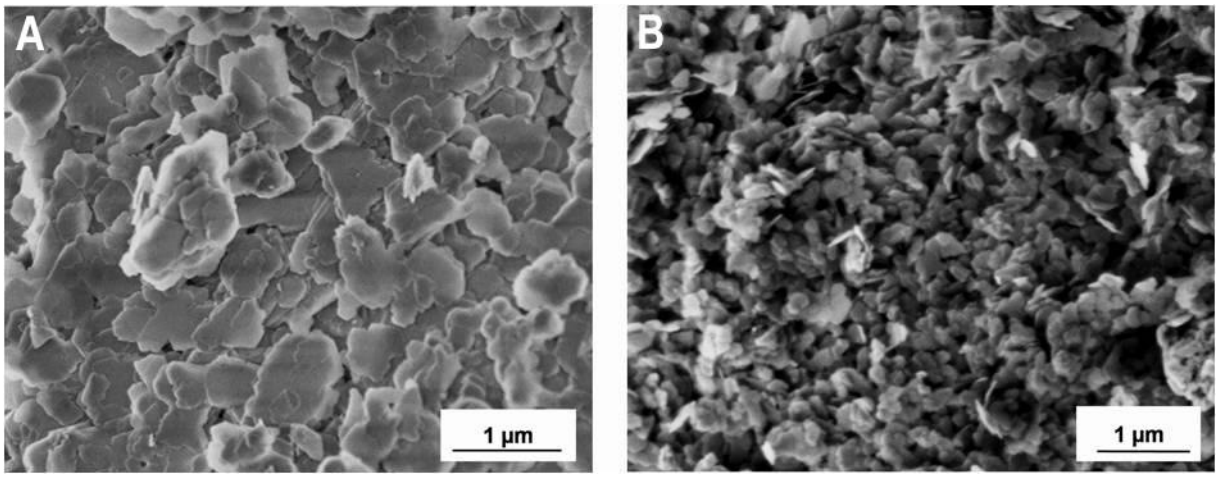

Figure 6-8: SEM images of α-ZrP synthesized under the influence of A) pEDOA-co-DMAA at Zr/P ratio 11:1 and B) pMEPD at Zr/P ratio of 5:1

6.4 Conclusion

Morphology of calciumphosphate and α-zirconium hydrogen phosphate was controlled under the influence of polyelectrolytes. Calciumphosphate nucleation has resulted in a porous material in presence of pMEPD and p(VPA-coAAM). Elongated needle like structures were formed under the influence of p(VPA-co-DMAA) and p(EDOA-co-DMAA). Mussel inspired HES-DOPA has resulted in a layered structure as found in nacre. A change in the amount of polymer lead to the formation of different structures. Thick aggregated platelets of α-zirconium hydrogen phosphate were formed under the nucleation control of different polyelectrolytes. For a platelet morphology with high aspect ratio, a copolymer of VPA and AAM was very prominent. The copolymer amount and composition were critical structure orienting parameters.

References

[1] Lin, A.; Meyers, M. A., *Mater. Sci. Eng., A*, (2005) **390**, 27.

[2] Wang, T.; Leng, B.; Che, R.; Shao, Z., *Langmuir*, (2010) **26**, 13385.

[3] Gebauer, D.; Verch, A.; Boerner, H. G.; Coelfen, H., *Cryst. Growth Des.*, (2009) **17**, 2678.

[4] Oaki, Y.; Imai, H., *Angew. Chem., Int. Ed.*, (2005) **44**, 6571.

[5] Dorozhkin, S. V.; Epple, M., *Angew. Chem., Int. Ed.*, (2002) **41**, 3130.

[6] Schweizer, S.; Taubert, A., *Macromol. Biosci.*, (2007) **7**, 1085.

[7] Walsh, D.; Kingston, J. L.; Heywood, R.; Mann, S., *J. Cryst. Growth*, (1993) **133**, 1.

[8] Suzuki, S.; Whittaker, M. R.; Grondahl, L.; Monteiro, M. J.; Wentrup-Byrne, E., *Biomacromolecules*, (2006) **7**, 3178.

[9] Kim, Y. K.; Gu, L.-s.; Bryan, T. E.; Kim, J. R.; Chen, L.; Liu, Y.; Yoon, J. C.; Breschi, L.; Pashley, D. H.; Tay, F. R., *Biomaterials*, (2010) **31**, 6618.

[10] Wang, Y.; Chen, J.; Wei, K.; Zhang, S.; Wang, X., *Mater. Lett.*, (2006) **60**, 3227.

[11] Huq, N. L.; Cross, K. J.; Reynolds, E. C., *J. Mol. Model. Chem*, (2000) **6**, 35.

[12] Hering, B., Dissertation Leibniz Universität Hannover (2010).

[13] Clearfield, A.; Smith, G. D., *Inorg. Chem.* , (1969) **8**, 431.

[14] Losilla, E. R.; Aranda, M. A. G.; Bruque, S., *J. Solid State Chem.*, (1996) **125**, 261.

[15] Brandão, L. S.; Mendes, L. C.; Medeiros, M. E.; Sirelli, L.; Dias, M. L., *J. Appl. Polym. Sci.*, (2006) **102**, 3868.

[16] Zhang, J.; Jiang, D.; Kotobuki, N.; Maeda, M.; Hirose, M.; Ohgushi, H.; Iwasa, M., *Appl. Phys. Lett.*, (2006) **89**, 183902.

[17] Kijima, T.; Ueno, S.; Goto, M., *J. Chem. Soc., Dalton Trans.*, (1982), 2499.

[18] Knabe, C.; Berger, G.; Gildenhaar, R.; Klar, F.; Zreiqat, H., *Biomaterials*, (2004) **25**, 4911.

[19] Dogan, O.; Oner, M., *Langmuir*, (2006) **22**, 9671.

[20] Murphy, M. B.; Hartgerink, J. D.; Goepferich, A.; Mikos, A. G., *Biomacromolecules*, (2007) **8**, 2237.

[21] Chirila, T. V.; Zainuddin, *React. Funct. Polym.*, (2007) **67**, 165.

[22] Alberti, G.; Vivani, R.; Marmottini, F.; Zappelli, P., *J. Porous Mater.*, (1998) **5**, 205.

7 Preliminary Dipping Experiments

To establish the layer-by-layer deposition method for preparation of composites and to evaluate the suitability of different analytical methods for fabricated composites, two different model systems were choosen. First a system from the literature was selected, whereas the choice for second experiment was based on a new set of components. Thicknesses of the layered material were determined with AFM and ellipsometry while nanoindentation was chosen as a method for mechanical characterization. Composite morphology was analyzed with the help of SEM.

7.1 Materials and Methods

7.1.1 Chitosan/Montmorillonite Composites

A typical system reported by Podsiadlo et al. constituting chitosan with clay particles of montmorillonite (MTM) was choosen as a model system.[1] As reported a 0.1% solution of chitosan was prepared in acetic acid by overnight stirring and pH was adjusted to 3 with 1 M NaOH solution. MTM suspension with a concentration of 0.5% was prepared in deionized water under vigorous stirring for a week and pH was adjusted with 1 M HCl solution. Detailed procedure can be found in the literature.[1] The substrates used were one-side polished silicon wafers, cut into rectangles of 3x1.3 cm. Before dipping experiment the substrates were wiped with acetone, dried in nitrogen flow and treated by plasma-cleaning for 30 minutes. According to literature this treatment results in a negatively charged silicon oxide layer on the surface.[2-3]

Multilayers were assembled on the silicon wafer by dipping into a commercially available chitosan (Mw 190,000 – 310,000) solution for 5 minutes followed by 1 minute rinsing in water twice. After deposition of the polymer the wafer was dried in a gentle flow of compressed air from an automated nozzle. Next the wafer was dipped into MTM suspension for 5 minutes, rinsed for 1 minute in water twice and air dried. This procedure constituted one

bilayer. Substrates were dipped into beakers of diameter 2.4 cm up to depth of 2.5 cm with the help of a dipping robot (Riegler & Kirstein GmbH, Berlin, Germany).

7.1.2 ZrP/PDDA Composites

ZrP platelets were synthesized in the presence of a copolymer of vinylphosphonic acid with acrylamide in the form of platelets by B. Hering.[4] PDDA available commercially (Mw 100 000 – 200 000) was used as a 0.1 wt% solution in Millipore water while inorganic platelets were used as a 0.2 wt% suspension which was stabilized by 30 minutes of sonication. Layers were constructed according to layer-by-layer assembly starting with PDDA on a plasma cleaned silicon wafer. Substrate was dipped in PDDA solution for 5 minutes followed by 2 minutes of rinsing and drying. Subsequently it was dipped in the ZrP suspension for 5 minutes with second rinsing in water for 2 minutes and finally drying in a gentle air flow. Composites with increasing number of layers were fabricated with dipping robot.

Thickness of the composites was determined using a multiscope (Optrel, Germany) in the ellipsometry mode, AFM XE-100 (Park Systems) or DekTak 8 stylus profilometer from Veeco, Germany. SEM investigations were done employing a field-emission scanning electron microscope type JSM-6700F from Jeol (Eching, Germany) with an acceleration voltage of 2 kV and a working distance of 3 or 8 mm. The mechanical properties of the layered composites were investigated by nanoindentation with a Nano Indenter XP from MTS Nano Instruments (Oak Ridge, Tennessee) equipped with a Berkovich indenter.

7.2 Results and Discussion

7.2.1 Composites of CH/MMT

Multilayers of CH/MMT were assembled up to 900 cycles and characterized for their thickness and mechanical behavior. Thickness profile was linear with respect to dipping cycles until 320 layers as determined by ellipsometry, presented in Figure 7-1 and Table 7-1.

Beyond this limiting number of layers it was difficult to apply ellipsometry because of the stronger light scattering of the film.

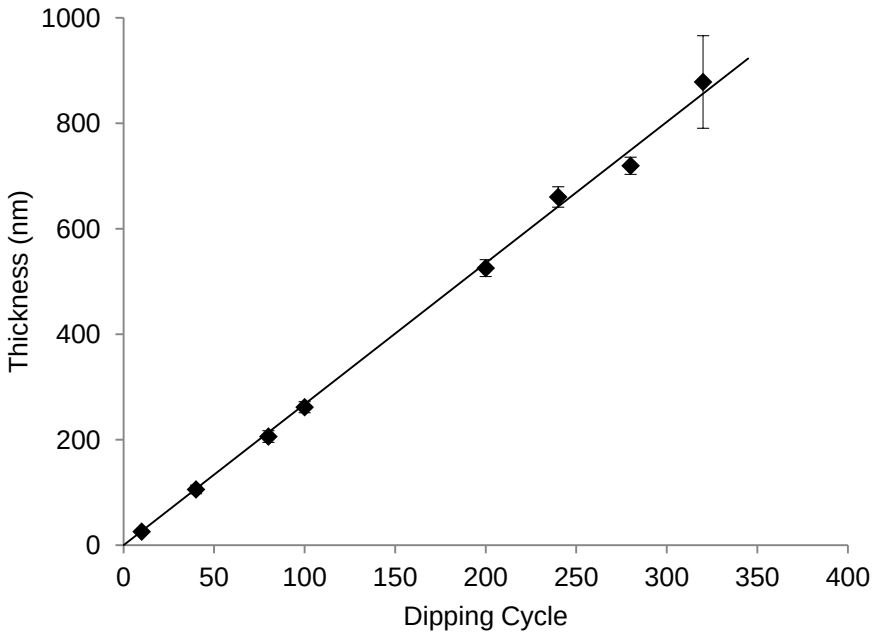

Figure 7-1: Thickness of the CH/MMT films as function of the number of dipping cycles

At initial stages the error of the measurement as indicated by the error bars was smaller but increased gradually with increasing number of layers. This is indicative of increasing roughness with increasing number of dipped layers.

Table 7-1: Thickness increment with number of layers

Layers	Thickness (nm)	Std. Dev.
10	25.8	2.1
40	105.8	8.2
80	206.1	11
100	261.7	10.5
200	525.4	16.0
240	660.3	19.3
280	719.5	16.3
320	878.3	87.7

This characterization has revealed an average thickness of 2.7 nm for each bilayer which is close to the reported bilayer thickness of 3 nm.[1]

Composite thickness was determined by AFM* after 580 cycles as an alternative method for the thickness measurement. By this way height of 27 points in three rows were measured starting in the uncoated area. The height difference of 1.7 µm between coated and uncoated area was utilized as thickness of the composite film. Based on the ellipsometric thickness measurements for one bilayer, 580 cycles were expected to have a total thickness of 1.56 µm which is almost close to the thickness measured by AFM.

Composites with 760 and 900 bilayers were subjected to nanoindentation for the determination of modulus and hardness as shown in Table 7-2.

Table 7-2: Nanoindentation data of the composites

Sample	Dipping Cycles	Modulus (GPa)	Hardness (GPa)
CH-MTM	760	6.7	0.27
CH-MTM	900	9.21	0.36
Nacre[5]	-	69.88	4.57

Composite material made up of 760 bilayers has shown values of 6.7 and 0.27 GPa for the modulus and hardness respectively. Increasing the number of bi-layers to 900 resulted in an increased modulus of 9.21 GPa and hardness of 0.36 GPa. Modulus value at 760 bilayers are close to those (6.1 GPa) given by Podsiadlo.[1] While making comparison we must remind that the analysis performed by Podsiadlo was according to standard stretching and getting stress vs. strain plots. However, these values are not comparable to those of nacre. New combinations of the materials are required to achieve the desired mechanical properties as found in our model system nacre. For fabricated composites thickness measurement with ellipsometry is not a suitable method. This is particularly important for samples with higher surface roughness. Although AFM was applied for the thickness measurement of films

* Institute for Particle Technique, TU Braunschweig

deposited on the silicon wafer, it was tedious and cantilever could not scan the surface because of roughness. Therefore, still there is a need for a suitable, quick and accurate method for the thickness measurement of the composite materials.

7.2.2 Composites of ZrP/PDDA

A composite material made up of poly(diallyldimethyl ammonium chloride) (PDDA, Mw 100 000-200 000) with ZrP platelets was fabricated and tested for the mechanical properties with nanoindenter and thickness measurement with a profilometer. Different combinations of two components were tested as shown in Table 7-3.

Table 7-3: Composite of ZrP/PDDA

Dipping Cycle	PDDA conc.%	ZrP (wt%)
200	0.2	0.2
200	0.1	0.2
200	0.01	0.2

SEM of the fracture surfaces of the composites prepared has revealed the better result, that is a nicely layered structure at PDDA concentration of 0.1 wt%.

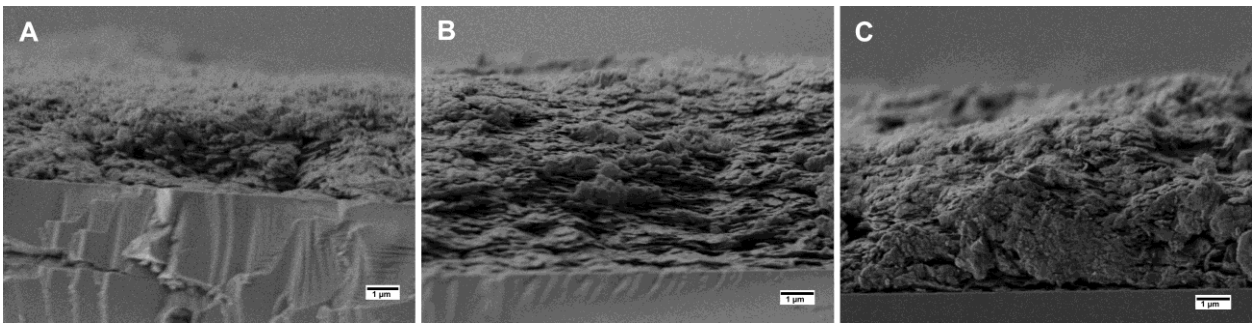

Figure 7-2: SEM of fracture surfaces of composites prepared at different concentrations of ZrP with PDDA after 200 cycles at (A) 0.01%, (B) 0.1% and (C) 0.2%

Utilizing the optimal combination of two components further composites were fabricated with increasing number up to 220 layers. High light scattering was observed due to the opaque nature of constituting components thus making thickness measurement with ellipsometry inappropriate. As an alternative method of thickness measurement, profilometer was used. Mechanical properties were determined with nanoindenter. For a variety of materials, nanoindentation has been applied to determine properties like modulus and hardness.[2, 6-7] This method was found suitable here too and applied to determine the modulus and hardness as given in Table 7-4.

Table 7-4: Thickness and mechanical properties of ZrP/PDDA composite

Dipping Cycle	Thickness (µm)	Modulus (GPa)	Hardness (GPa)
70	3.45 ± 0.22	5.40 ± 0.8	0.16 ± 0.04
100	5.47 ± 0.30	3.80 ± 0.7	0.10 ± 0.03
130	6.65 ± 0.29	2.59 ± 0.6	0.08 ± 0.03
160	8.85 ± 0.55	2.10 ± 0.7	0.05 ± 0.02
190	11.88 ± 0.67	5.38 ± 0.9	0.16 ± 0.04
220	12.37 ± 0.78	2.50 ± 0.6	0.10 ± 0.04

The highest values for modulus and hardness measured were 5.4 GPa and 0.16 GPa respectively. No correlation was found between the mechanical properties and the thickness of the film.

A regular increase in the thickness was observed as depicted in Figure 7-3. With increasing number of dipping cycles particularly from 160 onward, higher standard deviations in the thickness were observed. The increasing standard deviations can be rationalized to be a consequence of a decreasing quality of alignment of the ZrP platelets.

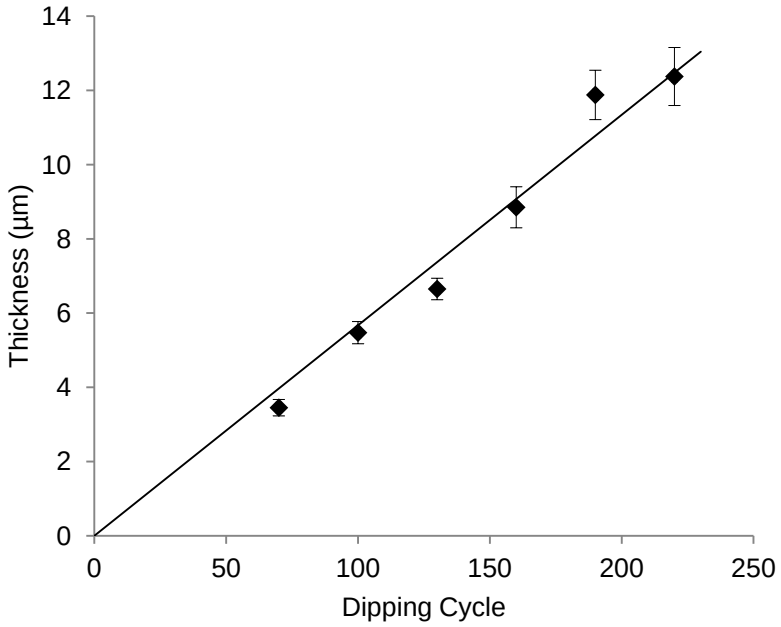

Figure 7-3: Thickness of the ZrP/PDDA films as function of the number of dipping cycles

The micro structure of the composites was investigated by SEM. The images of fractured surfaces indicate a layered structure for the composites, with no significant influence of the number of dipping cycles (Figure 7-4). Fabricated composites are similar in alignment to that found in nacre.

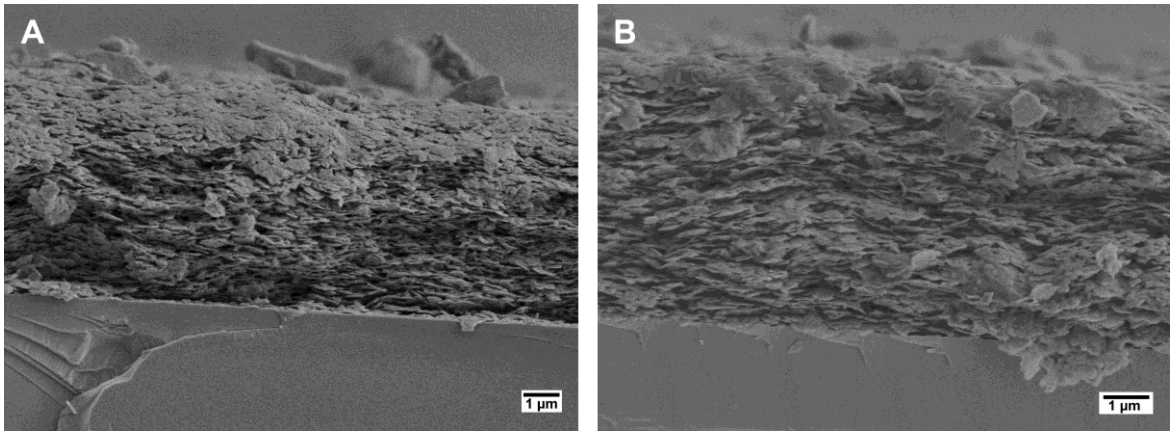

Figure 7-4: SEM of ZrP/PDDA composites at (A) 160 cycles (B) 220 cycles

7.3 Conclusion

Model experiments were performed to synthesize and analyze the composite materials and to observe the applicability of different analytical methods. For thickness measurement profilometery is best suited in comparison to ellipsometer or AFM. AFM cantilever could not scan the surface because of roughness at the surface. Similarly ellipsometry was not applicable as the surface was not reflecting enough light to be measured accurately by the sensor of the instrument. Nanoindentation was found to be a good method for fabricated composites where reliable and reproducible results could be obtained.

References

[1] Podsiadlo, P.; Tang, Z.; Shim, B. S.; Kotov, N. A., *Nano Lett.*, (2007) **7**, 1224.

[2] Zlotnikov, I.; Gotman, I.; Gutmanas, E. Y., *Appl. Surf. Sci.*, (2008) **255**, 3447.

[3] Kim, H.-N.; Keller, S. W.; Mallouk, T. E.; Schmitt, J.; Decher, G., *Chem. Mater.*, (1997) **9**, 1414.

[4] Hering, B., Dissertation Leibniz Universität Hannover (2010).

[5] Denkena, B.; Koehler, J.; Moral, A., *J. Mater. Process. Technol.* , (2010) **210**, 1827.

[6] Zhao, X.; Zhang, Q.; Hao, Y.; Li, Y.; Fang, Y.; Chen, D., *Macromolecules*, (2010) **43**, 9411.

[7] Wang, J.; Li, W.-Z.; Li, H.-D.; Shi, B.; Luo, J.-B., *Thin Solid Films*, (2000) **366**, 117.

8 Fabrication and Characterization of Biocompatible Nacre-like Structures from α-Zirconium Hydrogenphosphate Hydrate and Chitosan*

8.1 Abstract

Composite materials with an ordered layered structure resembling that of nacre were fabricated by layer-by-layer assembly making use of pre-synthesized α-zirconium hydrogenphosphate hydrate (ZrP) platelets and chitosan. These two biocompatible materials were chosen in view of possible applications in the biomedical field, e.g. as bone or joint replacement implants. The effect of different concentrations of the inorganic ZrP platelets and the organic components (chitosan) on the composite assembly and structure was investigated. A high concentration of chitosan (0.1 wt%) resulted in a misalignment of the inorganic platelets, while at very low concentrations (0.001 wt%) the substrate was not fully covered by the polymer, again leading to misalignment. Also the concentration of the α-ZrP platelets affected the composite assembly and structure. The number of dipping cycles was varied between 70 and 220, yielding a maximum thickness of approximately 6 µm. The pH value of the chitosan solution was also varied to investigate its influence on the composite assembly. The mechanical properties of the composites were tested with a nanoindenter. For samples prepared with the same number of dipping cycles, higher values of Young´s modulus and hardness were obtained with improved alignment of the platelets in the samples. For samples prepared with 220 dipping cycles, a Young's modulus of 2.6 GPa and a hardness of 70 MPa was observed. Important general relationships are recognized between the preparation parameters, the degree of order within the nacre-like films and the resulting mechanical properties.

Keywords: layer-by-layer assembly, nacre, chitosan, mechanical properties

* Waraich, S. M.; Hering, B.; Burghard, Z.; Bill, J.; Behrens, P.; Menzel, H., *J. Colloid Interface Sci.*, (2012) **367**, 74.

8.2 Introduction

Mimicking natural composites which show exceptional mechanical properties due to their hierarchical organization is an excellent starting point for the design of a new generation of synthetic materials. Nacre, the material of the inner shells of mollusk shells is a particular case. Owing to its excellent mechanical properties and its comparatively simple morphology, nacre has attracted considerable attention. High toughness and strength in nacre result from its hierarchical structure, where bioorganic polymers (chitin and proteins, 10 to 50 nm thick) and aragonite platelets (200-900 nm thick) form an ordered, "brick and mortar"-like structure. The polymeric part provides elasticity and adhesion while the aragonite tablets act as rigid building blocks.[1-2] Due to this structure nacre is 3000 times tougher than its main component, namely aragonite[3], although the organic material situated in between the platelets corresponds to a volume fraction of only 5 percent.[4] Various mechanisms have been proposed for this high toughness, namely platelet sliding, organic material adhesion, presence of asperities and, importantly, the waviness of the aragonite platelets which generates progressive locking, hardening and spreading of non-linear deformation around defects and cracks. The cracks are arrested before they can lead to failure of the material by dissipating the crack energy at the interfaces between the tablets. In nacre, a crack cannot move through the platelets but has to travel around them, the resulting increased crack length then being responsible for an enhanced work of fracture.[5-6] The nanometer size of the mineral crystals in nacre is important to ensure optimum fracture strength and maximum tolerance of flaws. For nacre the calculations show that the mineral crystals should have a minimum thickness of 200 nm.[7]

The attractive mechanical properties of nacre have provoked the development of organic-inorganic composite materials which are inspired by its morphology.[8-13] However, synthetically mimicking nacre requires special fabrication procedures in order to obtain a similar structure and morphology. Deville et al. synthesized a layered composite material by making use of controlled freezing of a suspension of alumina. After freeze-drying the resulting structure, a porous scaffold of the ceramic particles was obtained, which subsequently was filled with an organic phase.[14] The resulting material was structurally analog to nacre and showed better mechanical properties than the natural model, due to crack deflection. The chemical bath deposition method was employed by Burghard et al. to fabricate bio-inspired nanocomposite films which were made up of alternating layers of TiO_2

and ZnO as inorganic component and polyelectrolytes as organic component. In this approach the inorganic layer is deposited from a precursor solution and careful control of the parameters is necessary to control the size of the crystallites and the thickness of the layers.[15-16]

A well-established and convenient way for the production of layered materials is the layer-by-layer (LbL) deposition method[17], which can be employed for the fabrication of polymer-polymer as well as polymer-inorganic composites. This procedure consists of coating a substrate alternately with two different substances, for example by dipping into two different solutions or suspensions, possibly with intermittent washing steps.

Especially when the two components are oppositely charged, strong adhesion between the layers results from electrostatic adhesion. Negatively charged carboxymethylated cellulose nanofibrils and cationic polyethyleneimine have been used to assemble free standing films and their mechanical and structural properties have been investigated.[18] In the same way an artificial nanostructure resembling nacre was fabricated by Tang et al. by alternately dip-coating montmorillonite clay platelets and poly(diallyldimethylammonium) chloride (PDDA), a cationic polyelectrolyte.[9] With up to 200 alternating layers a thickness of 4.9 µm was obtained. The mechanical properties of the artificial materials can be improved by a load transfer from the polymer to the inorganic component in the composite material. By replacing PDDA with polyvinyl alcohol for the preparation of a composite with montmorillonite and by crosslinking the polymer with glutaraldehyde after each 10 dipping cycles, high-strength composites were obtained. The dense covalent and hydrogen bonding network of the organic material enhanced the load transfer from the polymer to the platelets.[19] Adhesion of the polymer to the clay platelets and thus increasing the load transfer was achieved by using polymers containing 3,4-dihydroxyphenylalanine (DOPA) groups. The introduction of these groups was inspired by bio-adhesives of marine organisms, which can adhere very strongly to almost all kinds of substrates. The DOPA groups can also be cross-linked by complex formation with Fe^{3+} ions. Employing this self cross-linking mechanism, an improvement in the mechanical properties of the corresponding composites was observed.[20-21]

Bonderer et al. deposited alumina platelets together with chitosan by combining dip- and spin-coating techniques.[22] By using alumina platelets, which are stronger than clay platelets, materials possessing very good mechanical properties were obtained. However, the content of organic material in the composite prepared by this method is very high (85 to 90%), quite

unlike to nacre. The good mechanical properties were attributed to the favorable aspect ratio, which favors fracture mechanism by platelet pullout. Kim et al. reported the preparation of LbL-Films from poly(allylamine hydrochloride) PAH and α-zirconium hydrogen phosphate (α-ZrP) platelets. The platelets were prepared by exfoliation of α-ZrP with butylammonium hydroxide resulting in crystallites with less than 1.5 nm thickness.[23] Despite the small thickness of each layer, the films show sharp boundaries between the different layers, as has been proven by the absence of any energy transfer between fluorescence probes built into the film.[24] The mechanical properties of these films were not investigated.

Here we report on the LBL deposition preparation of a nacre-type material which is constructed from biocompatible components. Such a material has potential applications in bone replacement and joint implantology. We have chosen α-zirconium hydrogenphosphate hydrate (α-ZrP) as the inorganic component. This material can be prepared in the form of platelets with suitable size and aspect ratio. Chitosan, a cationic polysaccharide was chosen as the polymer component. Chitosan is a well investigated biocompatible, antibacterial and environmentally friendly polymer used in biomedical devices, optically active films, biosensors, coatings for improvement of cytocompatibility and microcapsule implants for controlled release in drug delivery.[25-28] Chitosan is prepared from chitin (poly(β-(1-4)-N-acetyl-D-glucosamine)), which is a naturally occurring polysaccharide, by deacetylation. Above a degree of deacetylation of 50% the chitin becomes soluble in acidic aqueous media (pH < 6) and is called chitosan. Chitosan is soluble in aqueous solutions, but the solubility depends on the degree of deacetylation.[28-30] Due to the polysaccharide backbone chitosan is regarded to be a semi-rigid polymer, which adopts an extended conformation. The conformation is pH-dependent as expected for a weak polyelectrolyte.[30] Even in acetic acid solutions aggregates of chitosan molecules have been detected by fluorescence, static and dynamic light scattering.[31-33] Anthonsen et al. suggested that only a small fraction of the total weight of the samples contributes to the high molecular weight aggregates. It was also postulated that some sequences of acetylated units along the chitosan backbone are the origin for the aggregates.[32]

Biocompatibility of zirconium phosphate has already been shown. Corresponding coatings on zirconium oxide or titanium did not only improve the mechanical properties of these materials but also the adhesion and proliferation of osteoblasts as well as of fibroblasts.[34-36] Due to the layered structure of α-ZrP[37-39], it was expected that the crystallization could

result in particles with a platelet-like morphology when being influenced by specific morphology-directing agents.

8.3 Experimental

8.3.1 Materials

Chitosan of low molecular weight (190,000 – 310,000 Da) with a degree of deacetylation 75-85% was purchased from Aldrich and used as received without further purification. By NMR the degree of deacetylation was determined to be ~ 83%. Acetic acid for dissolution of the chitosan was purchased from Fluka. Sodium hydroxide used to adjust the pH of the solution was obtained from Carl Roth GmbH, Karlsruhe, Germany. α-Zirconium hydrogenphosphate hydrate (α-ZrP) platelets were synthesized with poly(vinylphosphonic acid-co-acrylamide) ($pVPA_{0.25}$-co-$AAM_{0.75}$) as morphology directing agent (see supporting info). All solutions and suspensions were prepared with Millipore water of resistivity 17 MΩ.

8.3.2 Preparation of Solutions and Suspensions

A 0.1% solution of chitosan was prepared by as described in ref.[40] by dissolving 1 g of the polymer in 1 L of Millipore water, adding a few drops of acetic acid, and stirring over night. Other concentrations were prepared by appropriate dilution with Millipore water and the pH was adjusted with 1M NaOH. Suspensions of α-ZrP platelets were prepared by addition of the required amount of platelets to Millipore water and sonication for 1 hour prior to use in the dipping experiments. The suspension was used as prepared having a pH of 3.7, no further pH adjustment was necessary, because there is no change of the zeta potential with pH in the range investigated here.

8.3.3 Substrates

The substrates used were one-side polished silicon wafers cut into rectangles of 3x1.3 cm. These silicon wafers were wiped with acetone after cutting, dried in a nitrogen flow and

treated by plasma-cleaning for 30 minutes. In this way a negatively charged silicon oxide layer is formed.[23, 41]

8.3.4 Layer-by-Layer Deposition

Multilayers were assembled on the silicon wafer by first dipping into the corresponding chitosan solution (pH = 4, 5, or 6 respectively) for 5 minutes followed by 2 minutes rinsing in water. After deposition of the polymer the wafer was dried in a gentle flow of compressed air from an automated nozzle. Next the wafer was dipped into a α-ZrP platelet suspension for 5 minutes, rinsed for 2 minutes in water and air-dried. This procedure completes one dipping cycle and the formation of a bilayer. Substrates were dipped into beakers of diameter 2.4 cm up to depth of 2.5 cm with the help of a dipping robot (Riegler & Kirstein GmbH, Berlin, Germany). Sonication of the suspension in sonication bath before the dipping kept the α-ZrP platelets well dispersed during the process.

8.3.5 Characterization

Zeta potentials of both components were investigated by a Zetasizer Nano ZS from Malvern Instruments (Worcestershire, UK). The thickness of the LbL samples was measured by a DekTak 8 stylus profilometer from Veeco, Mannheim, Germany. The stylus tip radius was 5 µm at force of 3 mg. The morphology of the product was investigated via SEM. Small pieces were cut out of the center of the wafers by a diamond blade and glued on cross-section-holders. To improve the conductivity silver-glue was used. Loose particles were removed. Images were collected on a field-emission scanning electron microscope type JSM-6700F from Jeol (Eching, Germany) with an acceleration voltage of 2 kV and a working distance of 3 or 8 mm.

The mechanical properties of the layered composites were investigated by nano-indentation with a Nano Indenter XP from MTS Nano Instruments (Oak Ridge, Tennessee) equipped with a Berkovich indenter. All measurements were performed in the continuous stiffness mode (CSM). Each sample was investigated at 30 points with a constant deformation rate of $5 \cdot 10^{-5}\ s^{-1}$. In order to avoid an influence of the substrate on the results, the deformation was restricted to one fourth of the thickness of the composite. Young's modulus and hardness

were derived from the loading curve of the graph in dependence of the penetration depth according to the Oliver and Pharr method.[42] Average values and standard deviations were calculated with the software Analyst.

8.4 Results and Discussion

8.4.1 Preparation and Characterization of the Platelet Suspension and the Chitosan Solution

Platelets of α-zirconium hydrogenphosphate hydrate were synthesized under the influence of poly vinylphosphonic acid-co-acrylamide.[43] The synthesis resulted in well separated, individual particles of few hundred nanometer in diameter and a few nanometer thickness as shown by SEM (Figure 8-1).

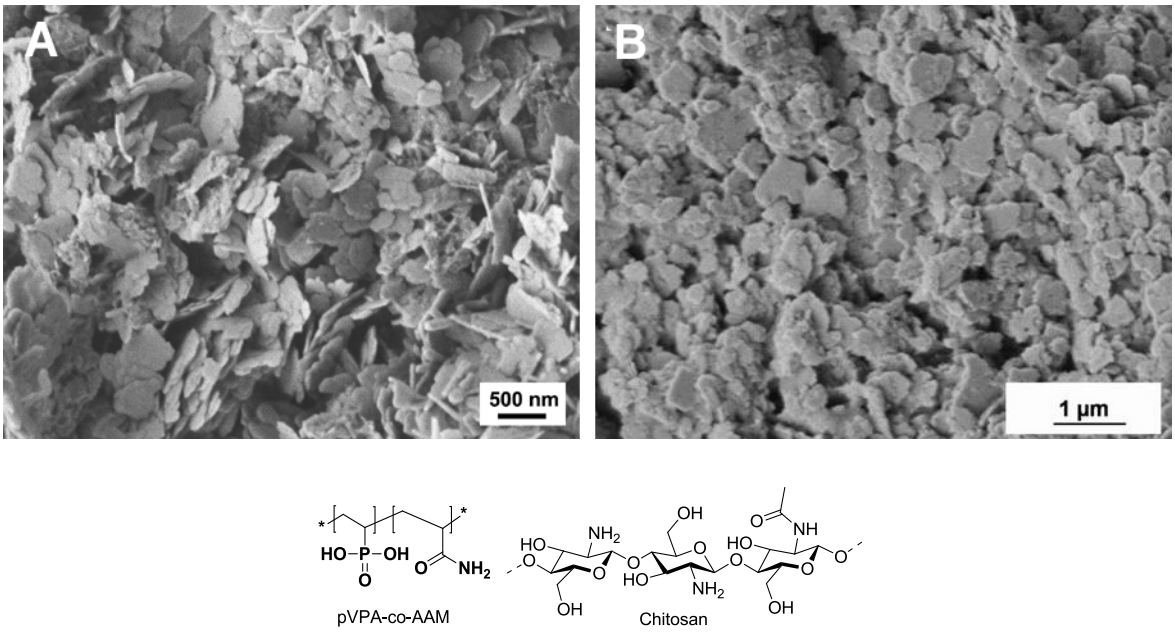

Figure 8-1: SEM images of α-ZrP nanoparticles synthesized under the influence of a p($VPA_{0.25}$-co-$AAM_{0.75}$) copolymer with a Zr to P ratio of (A) 9.4 : 1 and (B) p$VPA_{0.33}$-co-$AAM_{0.67}$ at Zr/P ratio of 4.7:1, the structural formula of which is given. The structural formula of chitosan is also given.

All syntheses produced as the only crystalline compound α-zirconium hydrogenphosphate hydrate (α-ZrP). The XRD patterns of α-ZrP synthesized without any polymeric additive and of the products of the syntheses with pVPA-co-AAM which were obtained at different Zr/P ratios, namely at 9.4:1 and 4.7:1, have been compared to reference data.[37] The similarity of the diffraction patterns shows that the addition of (co-)polymers did not have an influence on the crystal structure. (see supporting info.).

The zeta potentials of the nanosized α-zirconium hydrogenphosphate hydrate platelets and of chitosan were determined in water as function of the pH. Thus pH-values most suitable for the LbL deposition process, i.e. the pH value where there is a mutual electrostatic attraction can be determined. The results (Figure 8-2) show strongly opposed charges for the two components for the complete range of pH values investigated. The α-ZrP particles show a strong negative zeta potential whereas chitosan as a cationic polyelectrolyte shows a very strongly positive zeta potential at least up to a pH value of 5. Above pH = 5 the charge of the polymer decreases due to the reduced number of protonated amino groups (pK_a = 6.0 for chitosan[28]). The last data point at pH = 6.5 might be due to a metastable situation or aggregates of the polymer chains. A pH value of 5 was chosen for the LbL deposition experiments.

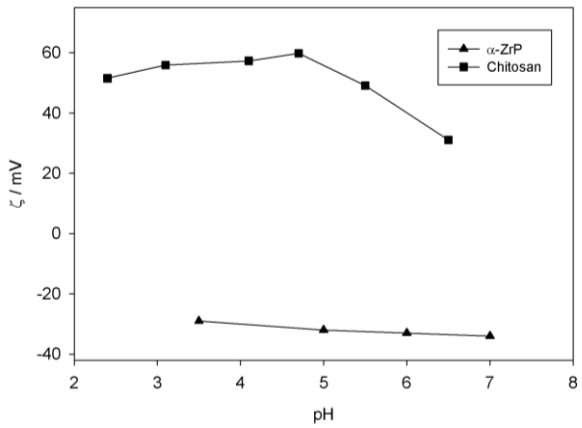

Figure 8-2: Zeta potentials of chitosan and α-ZrP as function of the pH value

8.4.2 Influence of Different Concentrations on LbL Deposition

Initially the effect of different concentrations of the two components on the LbL deposition process was investigated. For this purpose chitosan was used in three different concentrations

of 0.001 wt%, 0.01 wt% and 0.1 wt% and α-ZrP platelets suspensions were prepared in concentrations of 0.1 wt% and 0.2 wt%. Since the substrate is negatively charged after the pretreatment [41], the LbL deposition process was always started using the chitosan solution for the formation of the first layer. The dipping is followed by a washing step to get rid of superfluous material. Overcompensation of the negative surface charge leads to a net positive surface charge of the first layer.[17] The substrate with the first layer is then dipped into the suspension of the α-ZrP platelets. The negatively charged platelets adsorb to the surface. The net charge of the assembly is then again negative[17], so that, after rinsing to remove non-bound platelets, the cycle can be repeated.

In Figure 8-3 cross section SEM images of the LbL assemblies prepared with different concentrations of the chitosan solution and the α-ZrP suspension are compiled. The substrate can be seen beneath the layered material in all images. Using a α-ZrP suspension with a concentration of 0.1% and a chitosan solution with a concentration of 0.1% in the dipping process results in an LbL assembly in which the stacking is irregular and the platelets are not clearly visible, but appear to be covered. This overcoat might be chitosan (Figure 8-3A). An increase in the concentration of the α-ZrP suspension from 0.1% to 0.2% resulted in a slightly better ordered structure (Figure 8-3B). Here, the individual tiles are better visible and not as obscured as in the previous case.

Reducing the concentration of the chitosan solution to 0.01% and keeping the α-ZrP suspension concentration at 0.2%, a regular structure with only minor corrugation and with uniform thickness was obtained (Figure 8-3D). In this image only a few platelets at the edge appear to be displaced. However, this is probably an artefact caused by the cutting procedure in the sample preparation necessary to obtain the cross section. A further dilution of the chitosan solution to a concentration of 0.001% produced structures with only partially ordered arrangement (Figure 8-3F). In this case, although most of the platelets are oriented parallel to the substrate, also platelets oriented perpendicularly can be observed. It can be assumed that at this low chitosan concentration the amount of polymer available to interact with the platelets is not sufficient. Correspondingly, a decrease of the concentration of the α-ZrP suspension to 0.1% at a chitosan concentration of 0.01% also resulted in a well-organized structure (Figure 8-3E).

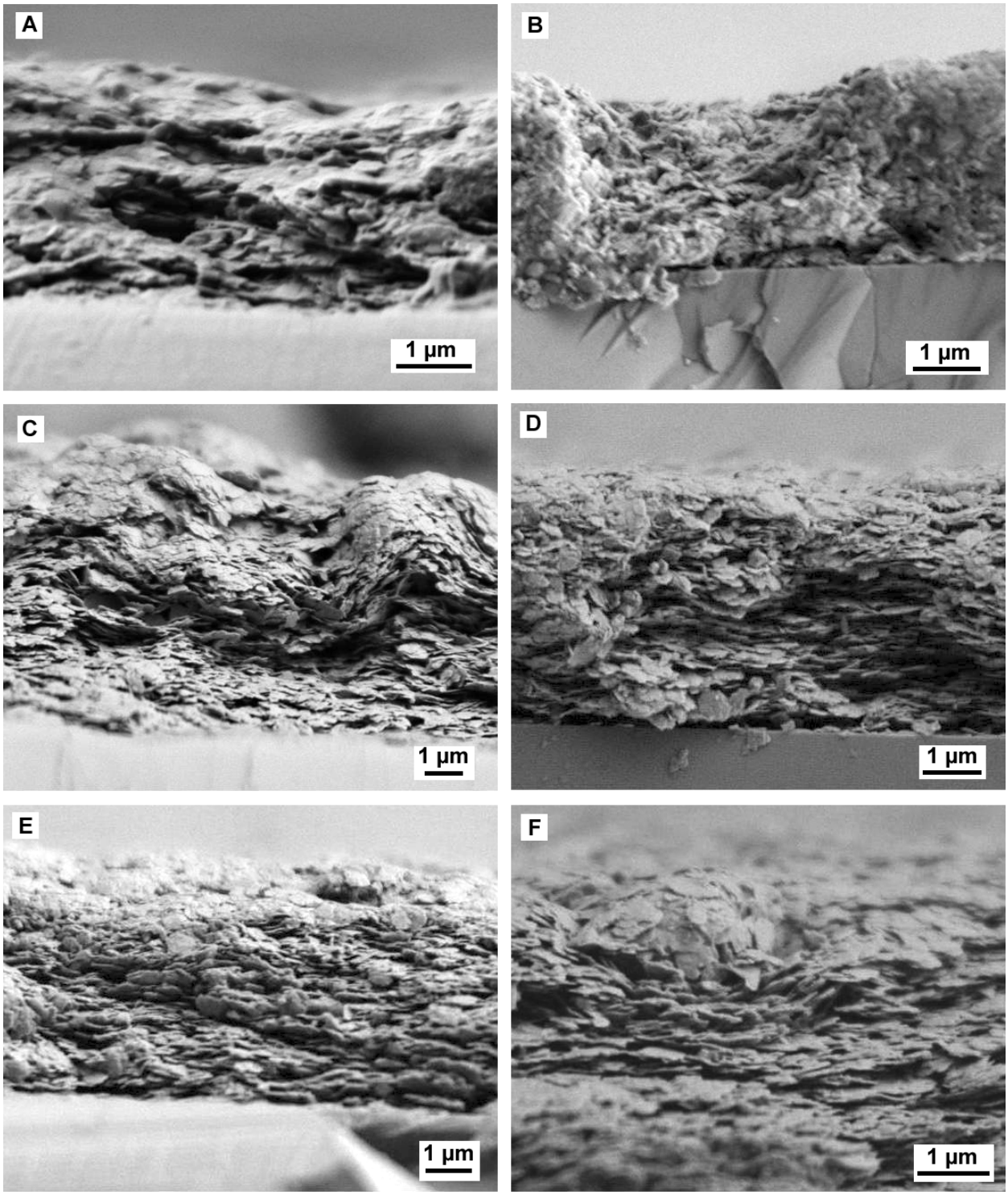

Figure 8-3: SEM images of cross sections of LbL assemblies prepared from chitosan and α-ZrP. The concentrations of the α-ZrP suspension and of the chitosan solution were varied as well as the number of dipping cycles. (A) α-ZrP concentration 0.1%, chitosan concentration 0.1%, 107 cycles; (B) α-ZrP concentration 0.2%, chitosan concentration 0.1%, 120 cycles; (C) α-ZrP concentration 0.2%, chitosan concentration 0.1%, 220 cycles; (D) α-ZrP concentration 0.2%, chitosan concentration 0.01%, 220 cycles; (E) α-ZrP concentration 0.1%, chitosan concentration 0.01%, 107 cycles; (F) α-ZrP concentration 0.2%, chitosan concentration 0.001%, 215 cycles.

The concentration dependence of the order within the LbL assembled composite film can be rationalized as follows (Figure 8-4). Using a low (0.001%) concentration of chitosan only a smaller amount of chitosan is adsorbed. This might be because the adsorption equilibrium is not reached within the dipping time or because there are less aggregates present at the lower concentration. The smaller amount of adsorbed chitosan might result in a non-uniform positive charge density at the surface of the substrate. Consequently, in the next step there is no uniform adhesion of α-ZrP platelets, but a somewhat irregular profile is obtained. For the composites fabricated with a higher concentration of chitosan (0.1%), the surface of the substrate is completely covered by chitosan. Subsequently, α-ZrP platelets can adhere uniformly to the complete area of substrate. This results in a smooth surface, at least for lower numbers of dipping cycles. Experimentally it was observed, that the corrugation of the films increased with the number of deposited layers (see Figure 8-3B and C). For example, the image of the film prepared in 220 dipping cycles depicted in Figure 8-3C suggests that in the lower third of the LbL assembled film, the platelets are oriented in a parallel fashion to the substrate, while in the upper part of the film, there is strong corrugation. As depicted in the model in Figure 8-4 this effect is probably caused by the presence of superfluous chitosan, being adsorbed in thicker and non-flat layers. In the following dipping step, several α-ZrP platelets can then adsorb at such a site due to the increased positive charge. Such a multi-adsorption can result in a non-parallel arrangement with some particles even being oriented perpendicularly to the substrate.

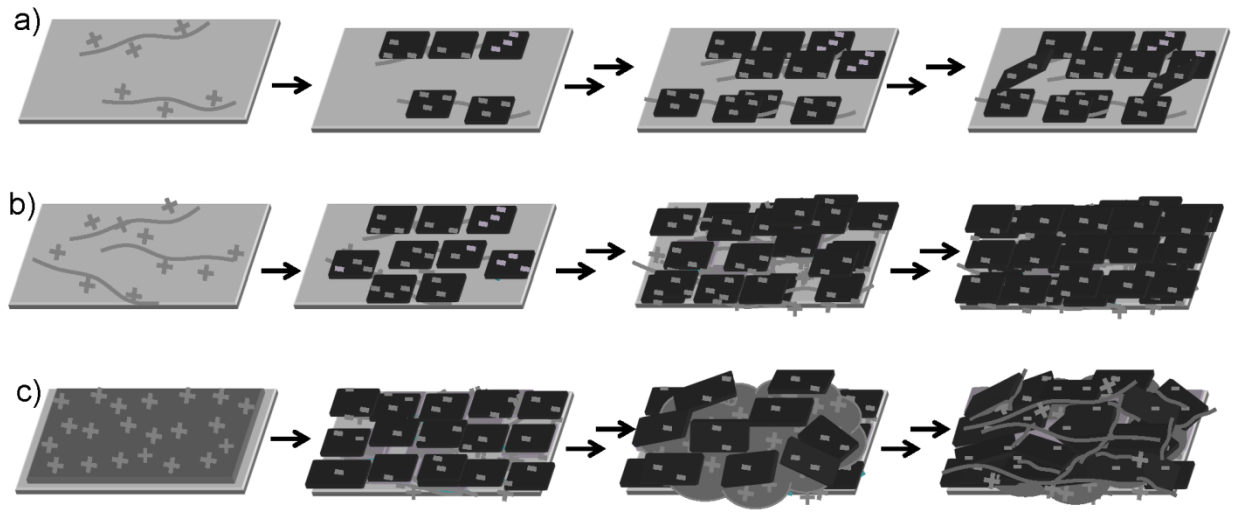

Figure 8-4: Schematic presentation of the assembly of composite materials at different chitosan concentrations: (a) low concentration of chitosan resulting in inhomogeneous layers of chitosan and surfaces not fully covered, (b) medium concentration of chitosan resulting in thin but homogeneous layers of chitosan and highly ordered platelets, (c) high concentration of chitosan resulting in thick layers of chitosan and an inhomogeneous, less ordered deposition of the platelets.

The effect of the concentration of the chitosan solution can be also discerned by a comparison of Figure 8-3A and F. For the preparation of the LbL assembly shown in Figure 8-3A, a high chitosan concentration of (0.1%) was used. Here the platelets appear to be covered by an amorphous layer, most likely a chitosan layer. The structural order of the platelets is low. In contrast, with the 0.001% chitosan solution (Figure 8-3F), the concentration seems to be neither sufficient to cover the substrates surface in the beginning (as described above) nor to fully enwrap the platelets at later dipping stages.

Although further investigations are necessary to clarify the reasons, it is apparent that the concentrations have an influence on the order of the LBL-assembly. Furthermore from the experiments described above it becomes evident that the concentration of the chitosan solution is influencing the order of the LbL assembly more strongly than the concentration of the α-ZrP suspension. A concentration of 0.1% or 0.2% for the α-ZrP suspension and a chitosan solution concentration of 0.01% are optimal for the fabrication of LbL assemblies with an ordered nacre-like structure. These conditions were used to investigate the influence of the pH value of the solution/suspension and the increase of the layer thickness with the number of dipping cycles.

8.4.3 Thickness of LbL Assembled Composites

Thickness measurement with the help of SEM is difficult due to possibly non-perpendicular cutting and orientation of the sample as well as to artifacts produced by this procedure, resulting in large uncertainties. The thickness was thus determined employing a profilometer. The force acting on the stylus of the profilometer while moving over the surface was adjusted such as not to penetrate the material but to only scan the upper surface. Three scans were performed on each sample.

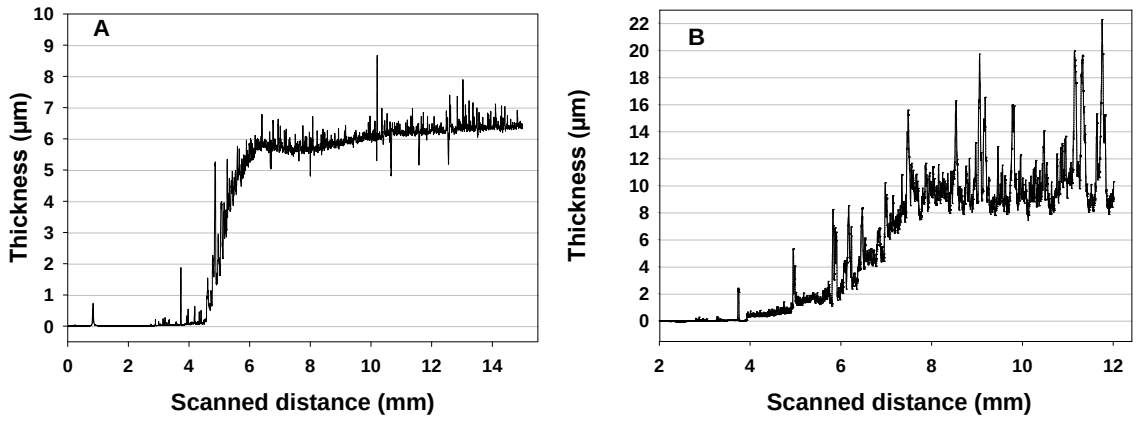

Figure 8-5: Thickness and roughness profile of an LbL assembled composite film. Curve A was measured on a sample prepared under the following conditions: α-ZrP concentration: 0.2%, chitosan concentration: 0.01%; pH = 5; 220 dipping cycles; a cross-section SEM of this sample is presented in Figure 8-3D. Curve B was measured on a sample prepared under the following conditions: α-ZrP concentration: 0.2%, chitosan concentration: 0.1%; pH = 5; 220 dipping cycles; a cross-section SEM of this sample is presented in Figure 8-3C.

A profilometer scan, as shown exemplarily in Figure 8-5A, shows three regions. The measurement starts on the naked surface of the silicon wafer which was never inserted into the dipping solutions. This region is very flat and was used to define zero height. Then a gradual increase can be observed (between 4 to 6 mm scanned distance) where the coated area begins. Minor variations of the fluid level occurring during the cyclic dipping process are responsible for the fact that the increase in thickness occurs gradually. Finally a plateau is reached where the thickness is almost constant. In this region (from 6 mm to 14 mm in Figure 8-5A) the thickness of the film was determined. The spiking in the profilometer scans

probably corresponds to single misaligned platelets or a few dust particles. The "noise" in the profilometer signal is indicative of a certain roughness of the LbL assemblies.

The thickness profile of a material obtained at a high concentration of chitosan of 0.1% (concentration of α-ZrP 0.2%, 220 dipping cycles) is presented in Figure 8-5B. It shows very strong spiking and also strong fluctuations of the thickness. This corresponds very well to the cross section SEM image shown in Figure 8-3C.

In order to observe the increase in the thickness of the LbL assembled composite films, a series of films was fabricated with the number of dipping cycles varying between 70 and 220 with increments of 30 dipping cycles. For this investigation, the concentrations were 0.01% for the chitosan solution, 0.2% for the α-ZrP suspension, and the pH was adjusted to 5. The thickness of each sample was determined from the profilometer scans on each film; the scans were averaged in the plateau region and the standard deviation as error of the measurement is a measure of the fluctuations in the thickness. The results are given in Table 8-1 and are plotted in Figure 8-6.

Table 8-1: Thickness of the composite layers as measured by a profilometer. The number of dipping cycles was varied as well as the pH value. For this investigation, the concentrations were 0.01% for the chitosan solution and 0.2% for the α-ZrP suspension.

Number of dipping cycles	pH	Thickness (µm)	Thickness per double layer (nm)
70	5	2.57 ± 0.19	36.7
100	5	3.95 ± 0.34	39.5
130	5	4.36 ± 0.22	33.5
160	5	5.34 ± 0.44	33.3
190	5	6.07 ± 0.34	31.9
220	5	6.06 ± 0.69	27.5
240	4	3.54 ± 0.45	14.7
240	6	6.80 ± 0.24	28.3
240	7[a]	5.64 ± 0.32	23.5

[a] Chitosan is not soluble above pH=6, thus the solution is not stable

There is a continuous increase in the thickness with additional dipping cycles. For small numbers of dipping cycles, the increase in thickness per dipping cycle is somewhat larger than at higher numbers of cycles, corresponding to a kind of saturation behavior and the thickness reaching a kind of plateau. From the thickness of the films, also the thickness of one double layer (chitosan + α-ZrP) can be calculated (see Table 8-1). These data also illustrate the smaller thickness increase per dipping cycle for thicker films. At the beginning the average thickness of the one double layer is around 33 nm. However, above approximately 160 dipping cycles the average thickness per double layer decreases. The reason for this behavior is not clear: It could be caused by a reduced efficiency of polymer and platelet adsorption, or by the continuous increase in electrostatic interactions which of course become stronger when more and more positive polymer chains and negative crystallites are added. Non linear increase of the layer thickness has been described before for the LbL assembly.[44]

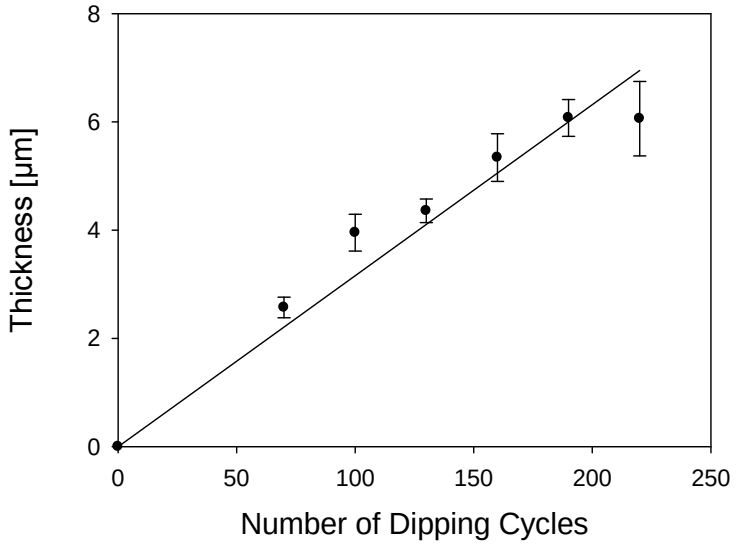

Figure 8-6: Thickness of the composite layers as a function of the number of dipping cycles for 70 to 220 dipping cycles, as measured by a profilometer. For this investigation, the concentrations were 0.01% for the chitosan solution, 0.2% for the α-ZrP suspension, and the pH was adjusted to 5.

Table 8-1 also provides thickness values for samples prepared at different pH values. It is well-known that the difference in the zeta potential is an important parameter for the deposition of a polyelectrolyte and nanoparticles in the LbL assembly process. For the system

chitosan/α-ZrP, the difference in zeta potentials is highest at a pH value of 5 (see Figure 8-2), but also at pH values between 4 and 6.5, this difference is large enough to allow for the construction of an LbL deposition assembly. However, such subtle changes as a change in the pH value can influence the structure of the assembled film significantly, in particular close to the solubility limit of chitosan at pH = 6. Therefore, in the experiments described in the following, the pH value was varied. These were performed with a concentration of the α-ZrP suspension of 0.2% and a concentration of the chitosan solution of 0.01%. The chitosan solution was adjusted to a pH value of 4, 5, or 6, respectively, and films were deposited with 220 or 240 cycles. Furthermore, some experiments were carried out at pH = 7, where chitosan should precipitate and the solution is not stable anymore. The layer thickness decreases for samples prepared at the lowest and the highest pH value. As already pointed out, at the highest pH the chitosan solution is not stable and therefore the polymer is no longer completely available for adsorption. However, it is interesting to note that a LbL-film could be produced at pH = 7. The small value observed for the sample prepared at the lowest pH value may be caused by the more extended conformation due the increased number of protonated amino groups with decreasing pH. In summary, these experiments show that the LbL assembly at pH 5 gives the best results, namely the best structural order as indicated by the low surface roughness and the largest thickness.

8.4.4 Mechanical Properties

The mechanical properties of the composite films are not only of interest for possible future applications, but they also reflect the composition and the structural ordering and are thus important for the evaluation of composites prepared under various conditions. Since the composites are films of several micrometers thickness only, the Young's modulus and hardness have been determined by nano-indentation. The indentation depth was restricted up to 200 nm for the thinner and to up to 600 nm for the thicker samples, respectively, in order to avoid any influence of the underlying substrate. The results summarized in Table 8-2 indicate a strong influence of the chitosan concentration on the mechanical properties.

Table 8-2: Mechanical properties of chitosan/**α**-ZrP composites produced at pH 5 by LbL assembly.

Entry	Concentration (chitosan wt.%)	Concentration (α-ZrP wt.%)	Number of cycles	pH	Young's modulus (GPa)	Hardness (MPa)
1	0.001 wt%	0.2 wt%	215	5	0.66	33
2	0.010 wt%	0.1 wt%	107	5	0.80	26
3	0.010 wt%	0.2 wt%	100	5	1.15	48
4	0.100 wt%	0.1 wt%	107	5	1.76	46
5	0.010 wt%	0.2 wt%	70	5	1.34	49
6	0.010 wt%	0.2 wt%	100	5	1.15	48
7	0.010 wt%	0.2 wt%	130	5	1.75	50
8	0.010 wt%	0.2 wt%	160	5	2.46	71
9	0.010 wt%	0.2 wt%	190	5	2.30	55
10	0.010 wt%	0.2 wt%	220	5	2.60	70
11	0.100 wt%	0.2 wt%	120	5	2.15	59
12	0.100 wt%	0.2 wt%	240	5	1.04	25

For samples prepared using a concentration of 0.001% chitosan, the values for the Young's modulus (0.66 GPa) and hardness (33 MPa) are very low. As has already been proposed, at this low chitosan concentration the amount of polymer adsorbed was probably not sufficient to enwrap all the particles and to fill all the gaps between the platelets. Thus, there is only minor contribution of the polymer to the properties of the composite. Expectedly, increasing the chitosan concentration during sample preparation to 0.01% or 0.1% improves the mechanical properties (see Table 8-2, entries 2, 3 and 4). However, the concentration of α-ZrP platelets in the suspension is important, too. This fact can be noticed when comparing entry 2 and 3 in Table 8-2. Although the SEM images suggested very similar well-ordered structures (see Figure 8-3A and B, respectively), the material obtained at an α-ZrP concentration of 0.2% shows higher values for the Young's modulus and the hardness than the LbL assembly produced with a lower concentration of α-ZrP platelets. Thus both components interact more effectively when the concentrations are carefully adjusted. It has been shown previously that adjusting the conformation of the polymer is necessary for maximizing the interaction with the nanoscale platelet.[40] The conformation of the adsorbed polymer depends on the degree of protonation (and with that on the pH), but also on parameters like concentration and adsorption kinetics.

As an optimal combination a chitosan concentration of 0.01% and a α-ZrP suspension concentration of 0.2% have been found here. These concentrations were used to investigate the influence of the number of dipping cycles used in the preparation (and thus of the thickness of the composite films) on the mechanical properties. As can be seen from the data presented in Table 8-2 (entries 5-10) and Figure 8-7 an increase of the number of cycles improves the mechanical properties of the composites. The increase of the Young's modulus is more pronounced. However, the linear regression drawn in Fig. 8 might be somewhat misleading and the data for the films prepared with more than 160 dipping cycles can be also considered as a kind of a saturation behavior. The hardness is not changing so strongly with the number of dipping cycles.

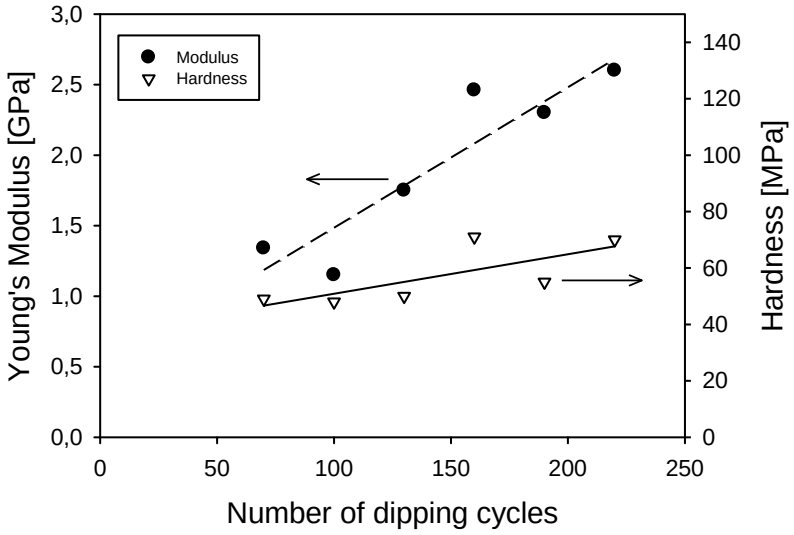

Figure 8-7: Young's modulus and hardness of the composite layers as a function of the number of dipping cycles for 70 to 220 dipping cycles, as measured by nano indentation. For this investigation, the concentrations were 0.01% for the chitosan solution, 0.2% for the α-ZrP suspension, and the pH was adjusted to 5.

Samples with similarly good mechanical properties (Young's modulus > 2 GPa and hardness > 50 MPa) can also be obtained with a higher concentration of the chitosan solution of 0.1%, but only when a small number of dipping cycles (120) is used (Table 8-2, entry 11). For a thicker film obtained after 240 dipping cycles (Table 8-2 entry 12) the values are clearly inferior. This observation can be rationalized when the ordering in the sample is taken into account. A comparison of the SEM images in Figure 8-3B and C showed that the LbL

assembly prepared using 120 cycles are nicely ordered, whereas after 220 cycles the composite film exhibited stronger corrugation. The concentrations identified here to yield optimal mechanical properties (α-ZrP suspension concentration of 0.2% and a chitosan solution concentration of 0.01%) also have been shown to give the most regular structure and the thickest films with the lowest roughness.

It can be expected that the change in the polymer conformation and the structural differences found for LbL assemblies prepared at different pH values also influence the mechanical properties. Thus the Young's modulus and hardness of LbL assemblies obtained after 240 cycles at different pH values of the chitosan solution (4, 5, 6) were measured and are summarized in Table 8-3. It is evident that the values for these properties are significantly lower for the sample assembled at a pH of 4 compared to the films deposited at pH values of 5 and 6. This reflects the small thickness of the sample prepared at a pH of 4 as reported in Table 8-1. In any case, as stated already above, there appears to be an optimum pH of the chitosan solution when used for the preparation of chitosan/α-ZrP composites, which lies around 5.

Table 8-3: Mechanical properties of chitosan/α-ZrP composites prepared with different pH-values of the chitosan solution.

Entry	Concentration (chitosan wt.%)	Concentration (α-ZrP wt.%)	Number of cycles	pH	Young's modulus (GPa)	Hardness (MPa)
1	0.01 wt%	0.2 wt%	240	4	1.05	19
2	0.01 wt%	0.2 wt%	220	5	2.60	70
3	0.01 wt%	0.2 wt%	240	6	2.55	75

In the work presented here, the best mechanical properties for a LbL assembled composite film were obtained with 220 double layers prepared from a 0.01% chitosan solution and a 0.2% α-ZrP suspension. The values of Young's modulus of 2.6 GPa and a hardness of 70 MPa are not exceptional in comparison to similar nacre-like assemblies which had been reported before. Podsiadlo et al. described for free standing film of a composite material of chitosan-montmorillonite with an Young's modulus of 6.1 GPa and an ultimate strength of 900 MPa whereas the pure chitosan showed Young's modulus of 1.9 GPa and a ultimate

strength of 31.6 MPa.[40] These authors used chitosan of an average molecular mass of 6 300 000 Da which is 25 times higher than the material used in this work. The higher molecular mass of the polymer could be a reason for the improved mechanical properties, but another aspect to be considered in the comparison of such values is the analytical method employed. Podsiadlo et al. determined the mechanical properties from stress strain curves of a free standing film while here nano-indentation was used. The same group has also investigated composites of montmorillonite (MTM) with poly(diallyldimethylammonium) chloride (PDDA). The Young's modulus and hardness for PDDA-MTM composites were better than for the chitosan-MMT composites despite the fact that PDDA is a much weaker polymer than chitosan.[25] This can be reasoned by taking into account the different molecular structures. The density of potentially charged amino groups is significantly higher for PDDA. Therefore a stronger interaction between the polymer chains and the nanoparticle surface can occur. The cohesive strength in the PDDA-MTM composite was estimated to be 4 times higher than in the chitosan-MTM composite film.[25] Furthermore, the more flexible PDDA backbone can be stretched upon stress which could contribute to stress dissipation. Chitosan as a polysaccharide has a stiffer polymer backbone than PDDA.[40] Therefore, replacement of chitosan by other polymers with higher molecular weight and stronger interactions with the inorganic platelets might significantly improve the mechanical properties of the LbL assemblies with α-ZrP nanoparticles. In some cases, the biocompatibility of other polymers may first have to be established with regard to the biomedical applications envisaged.

8.5 Conclusion

Layered composites of α-zirconium hydrogenphosphate hydrate (α-ZrP) platelets and chitosan were prepared by layer-by-layer assembly. The growth and structural features of the composite films were studied along with their mechanical properties. A concentration of 0.2 wt% for the α-ZrP suspension and 0.01 wt% for the chitosan solution was found to be optimal for the deposition of a layered composite material consisting of around 200 bilayers. A higher concentration of chitosan (0.1 wt%) was ideal for composites up to 120 bilayers. Lower concentrations of both components resulted in an inferior alignment of the platelets and lower values for Young's modulus and hardness. Best results were obtained when the chitosan solution had a pH value of 5 or 6. Composites obtained with chitosan solutions at pH

4 showed inferior alignment of the particles and reduced mechanical properties. The limited solubility of the chitosan at pH > 6 and the extended conformation at lower pH might be reason for non optimal interaction with the nanoscale α-ZrP platelets. This results in only moderate mechanical properties.

8.6 Acknowledgments

We are thankful to M. Boettger and Prof. W. Kowalsky (LEO, Braunschweig University of Technology) for the possibility to perform profilometer measurements. Financial support from the DFG within the framework of SFB 599 is gratefully acknowledged. The authors wish to thank all colleagues in work package D9.

8.7 Supporting Information

Synthesis of the morphology-directing polymer

Poly(vinylphosphonic acid-co-acrylamide) ($pVPA_{0.25}$-co-$AAM_{0.75}$) was synthesized as described elsewhere.[45] Briefly, dibenzoyl peroxide was used as initiator (0.7 wt% based on monomers) and the polymerization was carried out in dioxane at 80 °C. Care was taken to keep the conversion below 25% in order to obtain well-defined copolymers.

Synthesis of α-zirconium hydrogenphosphate hydrate

α-Zirconium hydrogenphosphate hydrate (α-ZrP) was prepared according to a modified two-step method, consisting of a precipitation and a crystallization step.[46] Zirconyl chloride octahydrate was dissolved in 20 mL deionized water and added to cooled phosphoric acid (1 M) containing $pVPA_{0.25}$-co-$AAM_{0.75}$. The concentration of the copolymer was adjusted in a way that the number of zirconium cations to phosphonic acid groups of the copolymer (Zr/P ratio) was 9.4:1. The solid precipitate was isolated by centrifugation, washed with phosphoric acid (5%) and water and then dried at 55 °C. In a second step, this primary product was dispersed in phosphoric acid (10%) and stirred for 200 h at 115 °C. The solid was recovered by centrifugation, washed with water until neutrality, and finally dried at 55 °C. It was identified as α-zirconium hydrogenphosphate hydrate using powder X-ray diffraction.

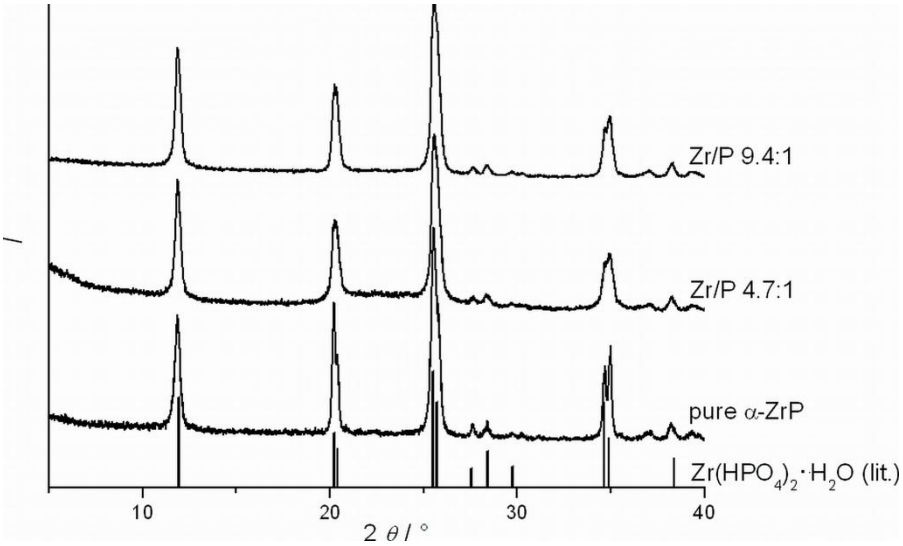

Figure 8-8: XRD patterns of the products of syntheses carried out without any polymeric additive (pure α-ZrP) and of the products of syntheses carried out with pVPA-co-AAM (Zr/P ratios of 4.7:1 and 9.4:1, respectively) in comparison to data from ref.[37]

References

[1] Chen, R.; Wang, C.-A.; Huang, Y.; Le, H., *Mater. Sci. Eng., C* (2008) **28**, 218.

[2] Oaki, Y.; Imai, H., *Angew. Chem., Int. Ed.*, (2005) **44**, 6571.

[3] Wegst, U. G. K.; Ashby, M. F., *Philos. Mag.*, (2004) **84**, 2167.

[4] Luz, G. M.; Mano, J. F., *Philos. Trans. R. Soc. London, Ser. A* (2009) **367**, 1587.

[5] Jackson, A. P.; Vincent, J. F. V.; Turner, R. M., *J. Mater. Sci.*, (1990) **25**, 3173.

[6] Espinosa, H. D.; Rim, J. E.; Barthelat, F.; Buehler, M. J., *Prog. Mater. Sci.*, (2009) **54**, 1059.

[7] Gao, H.; Ji, B.; Jager, I. L.; Arzt, E.; Fratzl, P., *Proc. Natl. Acad. Sci. U. S. A.*, (2003) **100**, 5597.

[8] Kato, T., *Adv. Mater.*, (2000) **12**, 1543.

[9] Tang, Z.; Kotov, N. A.; Magonov, S.; Ozturk, B., *Nat. Mater.*, (2003) **2**, 413.

[10] Li, Y.-C.; Schulz, J.; Grunlan, J. C., *ACS Appl. Mater. Interfaces*, (2009) **1**, 2338.

[11] Podsiadlo, P.; Paternel, S.; Rouillard, J. M.; Zhang, Z.; Lee, J.; Lee, J. W.; Gulari, E.; Kotov, N. A., *Langmuir*, (2005) **21**, 11915.

[12] Lu, C.; Donch, I.; Nolte, M.; Fery, A., *Chem. Mater.*, (2006) **18**, 6204.

[13] Bennadji-Gridi, F.; Smith, A.; Bonnet, J.-P., *Mater. Sci. Eng., B* (2006) **130**, 132.

[14] Deville, S.; Saiz, E.; Nalla, R. K.; Tomsia, A. P., *Science*, (2006) **311**, 515.

[15] Burghard, Z.; Tucic, A.; Jeurgens, L. P. H.; Hoffmann, R. C.; Bill, J.; Aldinger, F., *Materials Research Society Symposium Proceedings*, (2007) **1007**,

[16] Burghard, Z.; Tucic, A.; Jeurgens, L. P. H.; Hoffmann, R. C.; Bill, J.; Aldinger, F., *Adv. Mater.*, (2007) **19**, 970.

[17] Decher, G.; Schlenoff, J. B., *Multilayer Thin Films*, Multilayer Thin Films, Wiley-VCH: Weinheim: (2003).

[18] Karabulut, E.; Wågberg, L., *Soft Matter*, (2011) **7**, 3467.

[19] Podsiadlo, P.; Kausshik, A. K.; Aruda, E. M.; Waas, A. M.; Shim, B. S.; Xu, J.; Nandivada, H.; Pumplin, B. G.; Lahann, J.; Ramamoorthy, A.; Kotov, N. A., *Science*, (2007) **318**, 80.

[20] Podsiadlo, P.; Liu, Z.; Paterson, P.; Messersmith, P. B.; Kotov, N. A., *Adv. Mater.*, (2007) **19**, 949.

[21] Lee, H.; Lee, Y.; Statz, A. R.; Rho, J.; Park, T. G.; Messersmith, P. B., *Adv. Mater.*, (2008) **20**, 1619.

[22] Bonderer, L. J.; Studart, A. R.; Gauckler, L. J., *Science*, (2008) **319**, 1069.

[23] Kim, H.-N.; Keller, S. W.; Mallouk, T. E.; Schmitt, J.; Decher, G., *Chem. Mater.*, (1997) **9**, 1414.

[24] Kaschak, D. M.; Mallouk, T. E., *J. Am. Chem. Soc.*, (1996) **118**, 4222.

[25] Podsiadlo, P.; Tang, Z.; Shim, B. S.; Kotov, N. A., *Nano Lett.*, (2007) **7**, 1224.

[26] Sezer, A. D.; Akbuga, J., *Journal of Microencapsulation*, (1999) **16**, 687.

[27] Bartkowiak, A.; Hunkeler, D., *Chem. Mater.*, (1999) **11**, 2486.

[28] Rinaudo, M., *Prog. Polym. Sci.*, (2006) **31**, 603.

[29] le Dung, P.; Milas, M.; Rinaudo, M.; Desbrières, J., *Carbohydr. Polym.*, (1994) **24**, 209.

[30] Sogias, I. A.; Khutoryanskiy, V. V.; Williams, A. C., *Macromol. Chem. Phys.*, (2010) **211**, 426.

[31] Philippova, O. E.; Volkov, E. V.; Sitnikova, N. L.; Khokhlov, A. R.; Desbrières, J.; Rinaudo, M., *Biomacromolecules*, (2001) **2**, 483.

[32] Anthonsen, M. A.; Vårum, K. M.; Hermansson, A. M.; Smidsrød, O.; Brant, D. A., *Carbohydr. Polym.* , (1994) **25**, 13.

[33] Buhler, E.; Rinaudo, M., *Macromolecules*, (2000) **33**, 2098.

[34] Zhang, J.; Jiang, D.; Kotobuki, N.; Maeda, M.; Hirose, M.; Ohgushi, H.; Iwasa, M., *Appl. Phys. Lett.*, (2006) **89**, 183902.

[35] Kijima, T.; Ueno, S.; Goto, M., *J. Chem. Soc., Dalton Trans.*, (1982), 2499.

[36] Knabe, C.; Berger, G.; Gildenhaar, R.; Klar, F.; Zreiqat, H., *Biomaterials*, (2004) **25**, 4911.

[37] Clearfield, A.; Smith, G. D., *Inorg. Chem.* , (1969) **8**, 431.

[38] Losilla, E. R.; Aranda, M. A. G.; Bruque, S., *J. Solid State Chem.*, (1996) **125**, 261.

[39] Brandão, L. S.; Mendes, L. C.; Medeiros, M. E.; Sirelli, L.; Dias, M. L., *J. Appl. Polym. Sci.*, (2006) **102**, 3868.

[40] Podsiadlo, P.; Tang, Z.; Shim, B. S.; Kotov, N. A., *Nano Letters*, (2007) **7**, 1224.

[41] Zlotnikov, I.; Gotman, I.; Gutmanas, E. Y., *Appl. Surf. Sci.*, (2008) **255**, 3447.

[42] Oliver, W. C.; Pharr, G. M., *J. Mater. Res.*, (1992) **7**, 1564.

[43] Hering, B., Dissertation Leibniz Universität Hannover (2010).

[44] Elzbieciak, M.; Kolasinska, M.; Zapotoczny, S.; Krastev, R.; Nowakowska, M.; Warszynski, P., *Colloids Surf., A*, (2009) **343**, 89.

[45] Chen, X.; Huang, R.; Pelton, R., *Ind. Eng. Chem. Res.*, (2005) **44**, 2078.

[46] Brauer, G., *Handbuch der Präparativen Anorganischen Chemie*, Ferdinand Enke Verlag: Stuttgart, (1978); Vol. Band 2.

9 Nacre Inspired Assembly of Organic- Inorganic Composites, Characterization and Mechanical Properties

9.1 Introduction

Combining the properties of organic and inorganic components in the form of hybrid composite is a matter of interest because of the improved mechanical properties. In nature biological materials can be found build up by organic and inorganic components with modest mechanical performance, however, showing surprisingly high toughness, strength and modulus.[1] Thanks to their complex hierarchical structure their mechanical properties are exceptional. Nacre the inside layer of mussels is a striking example. Due to superior mechanical properties along with bio-compatibility seashell nacre is a material of interest. A peculiar microstructure described as a "brick and mortar" arrangement of the aragonite platelets (200-900 nm thick) bonded by protein layers (10 to 50 nm) has resulted in superior strength and toughness e.g. fracture toughness is 3000 times higher than that of the pure mineral.[2-3] These exceptional properties are because of different mechanisms such as platelet sliding, organic material adhesion, presence of asperities and, importantly, the waviness of the aragonite platelets which generates progressive locking, hardening and spreading of non-linear deformation around defects and cracks.[4] In nacre, a crack cannot move through the platelets but has to travel around them, the resulting increased crack length then being responsible for an enhanced work of fracture.[4-5] The structural pattern found in nacre has inspired scientist to design new biomimetic materials.[6-11]

Controlled freezing is one way of getting such hybrid materials. A porous scaffold of the ceramic particles was obtained by controlled freezing of a suspension of alumina followed by filling with organic component.[12] Burghard et al. has employed chemical bath deposition to produce nano-composite films which were made up of alternating layers of TiO_2 and ZnO as inorganic component and polyelectrolytes as organic component.[13-14]

A simple and well-established method to synthesize layered materials is the layer-by-layer-deposition.[15] This procedure is limited not only to polyelectrolytes but nearly any type of

macromolecular species, inorganic clusters, nanoparticles and plates, polysaccharides and proteins can be successfully used as building blocks.[16] This technique can be applied for the fabrication of multilayer films of variable thickness and composition. Using delaminated montmorillonite and solutions of chitosan or poly(diallyldimethylammonium) chloride a layered composite material with better mechanical properties is reported by Tang and Podsiadlo et al.[7, 17] A composite material with an ordered layered structure resembling that of nacre is fabricated by layer-by-layer assembly making use of pre-synthesized α-zirconium hydrogenphosphate hydrate (ZrP) platelets and chitosan.[18] In general most of LBL deposition methods exploit electrostatic interaction arising from the opposite charge of the constituting components[19-20], however, LbL films have been constructed with hydrogen bonding too.[21-22]

Bonderer et al. deposited alumina platelets together with chitosan by combining dip- and spin-coating techniques.[22] By using alumina platelets, which are stronger than clay platelets, materials possessing very good mechanical properties were obtained. However, the content of organic material in the composite prepared by this method is very high (85 to 90%), quite unlike to nacre. The good mechanical properties were attributed to the favorable aspect ratio, which favors fracture mechanism by platelet pullout.

Mussels are capable of adhesion to stones and other water submerged objects by secreting proteins rich in catechol and amine functionalities.[23] These proteins serve the role of cement and help in adherence. A mimic of the mussel adhesive proteins is synthesized by copolymerizing dopamine methacrylate with methoxyethyl acrylate presenting adhesion under wet and dry conditions.[24] Based on this biomaterial, it has been reported that dopamine forms thin films on the surface of a variety of organic and inorganic materials like metal oxides, polymers, noble metals and ceramics via coordination, covalent or hydrogen bond.[25-26] Lee et al. have investigated the interaction of dopamine with organic and inorganic surfaces with the help of dopamine modified tip of AFM. Dopamine adheres strongly and reversibly to the titanium surface via coordination bonds. No hysteresis between approach and pull off curves was observed by replacing dopa with PEG on the tip of cantilever indicating that only dopa interacts with the titanium surface. Bond dissociation energy determined was close to the bond formed between dopamine and titanium oxide. Additionally the same tip of AFM was tested with an amine substituted silicon surface. From

the calculation of pull off force it has been revealed that a covalent bond is formed between dopa and amine at the surface.[26]

Adhesion of the polymer to the clay platelets and thus increasing the load transfer was achieved by using polymers containing 3,4-dihydroxyphenylalanine (DOPA) groups. The DOPA groups can also be cross-linked by complex formation with Fe^{3+} ions. Employing this self cross-linking mechanism, an improvement in the mechanical properties of the corresponding composites was observed.[27-28]

Based upon these observations it has been proposed that there should be a possible interaction between HES modified with dopamine and aluminium oxide platelets which were modified with terminal amine functionality. Here we report on the LBL preparation of nacre like material which is constructed from alumina platelets and hydroxyethyl starch modified with dopamine. Alumina platelets used have close resemblance to aragonite as found in nature and their aspect ratio is also close to that found for the platelets in nacre. It is expected that this combination of polymer and inorganic component should result in a composite with interesting mechanical properties.

9.2 Materials and Methods

Hydroxyethyl starch (Mw 130 000) was obtained from Fresenius Kabi (Bad Homburg, Germany). 4-(dimethylamino)pyridine (DMAP, purum), diglycolicanhydride (DGA, >90%), dopamine (DA, 99%), N,N′-dicyclohexylcarbodiimide (DCC, 99%), dimethylsulfoxide (DMSO, puriss), (3-aminopropyl)triethoxysilane (ATES, 98 %) and 2-(3,4-dihydroxyphenyl)ethylamine (dopamine, DA, 99%**)** were purchased from Sigma-Aldrich (Steinheim, Germany). Dimethylformamide (DMF, HPLC grade) and N-hydroxysuccinimid (NHS, 98%) were purchased from Acros Organics. Methanol 99.8 % was obtained from Fisher Scientific. Roth ZelluTrans dialysis tubes with a MWCO of 12000-14000 were used for purification. Aluminium oxide platelets (alusion) were obtained from advanced nanotechnology limited (Australia). Glass slides were used as substrate with dimensions 3.7x2.5 cm. A plasma cleaner “Femto” from Plasma Surface Technology Germany was used to clean the substrate surface.

9.2.1 Synthesis of Hydroxyethyl starch-diglycol (HES-DG)

The reaction scheme for the modification of dextran was generalized for HES.[29] HES (50 g, 271.49 mmol) was dissolved in 1 L DMF (HPLC grade) at RT under nitrogen. After cooling to 0 °C (8.28 g, 67.8 mmol) DMAP and one hour later (7.795 g, 67.9 mmol) DGA were added to the solution and stirred over night under nitrogen. Contents of the reaction were dialysed for 3 days followed by freeze drying. This process has resulted a white HES-DG with a conversion of 67%. A modified HES-DG was kindly provided by A. Bertz*.

^{1}H-NMR (D_2O, 300 MHz): δ 3.41-4.08 (8H, HES glucosidic protons), 4.34-4.39 (4H, -CH_2-O-CH_2-), 5.43 and 5.70 (4H, HES ethyl protons) ppm.

IR (KBr, cm^{-1}): 3400 (υ_{COOH}), 2900 (υ_{CH2}), 1740 and 1230 (υ_{COOR}), 1150 (υ_{CO}).

9.2.2 Synthesis of of Hydroxyethyl starch-diglycol-dopamine (HES-DG-DA)

HES-DG (2 g, 7.5 mmol) was dissolved in 80 mL DMSO at RT under nitrogen. DCC (0.784 g, 3.8 mmol), NHS (0.518 g, 4.5 mmol) and dopamine (4.5 g, 0.89 mmol) were added to the solution and the mixture was stirred at RT under nitrogen for 24 h. The product was purified by dialysis and isolated by freeze-drying as a white powder. yield, 1.23 g (57%).

^{1}H-NMR (D_2O, 400 MHz): δ 6.55-6.94 (3H, DA aromatic protons), 5.83 and 5.13 (4H, HES ethyl protons), 4.35 (4H, -CH_2-O-CH_2-), 4.28-3.11 (8H, HES glucosidic protons), 2.91-2.58 (4H, -CH_2-CH_2-)

Elemental Analysis: H, 6.71; C, 44.88; N, 0.97

DS (elemental analysis): 21 %

* Institute for Technical Chemistry, TU Braunschweig.

9.2.3 Surface Modification of Alumina Platelets

The chemical nature of inorganic platelets was modified with (3-aminopropyl)triethoxysilane (ATES).[22] To 37.7 ml of water 12.6 ml of methanol was added in a volume ratio of 3:1. To this solution 5.02 ml of ATES was added and stirred for about an hour to hydrolyze ATES. To this solution 2 g of alusion (aluminium oxide) were added and the mixture was brought to ultrasonication for 5 minutes. The contents were heated at 40 °C for 30 minutes with stirring. The platelets were separated by centrifugation at 3800 rpm and washed five times with ethanol. Finally modified platelets were diluted with ethanol to prepare 1 vol. % suspension of modified alusion.

9.2.4 Fabrication of Composite Material

Glass slides were cleaned with acetone and dried in a flow of nitrogen. The surface of the slides was made free of organic impurities by a treatment with a plasma cleaner for 30 minutes. Dopamine substituted HES-DG-DA solution 0.5 volume % was prepared in millipore water. Modified platelets were suspended on the air water surface in a glass vessel of 11 cm diameter. This was done by hand shaking the platelet stock solution followed by uptake of 2 ml of this suspension with the help of a syringe. The suspension from syringe was added carefully onto the water surface. Initially platelets were not evenly distributed however an ultrasonication for 30 minutes made a homogenous Langmuir film at the surface. For the construction of composite the glass slide was dipped into the polymer solution for 2 hours and dried in oven at 50 °C. In the next step glass slide was held horizontally with tweezers and brought carefully under the water to transfer platelets to the glass substrate and dried again at 50 °C. This procedure makes one layer and is repeated until the desired number of transferred layers is reached.

9.2.5 Characterization

The mechanical properties of the fabricated composites were investigated by nano-indentation with a Nano Indenter XP from MTS Nano Instruments (Oak Ridge, Tennessee) equipped with a Berkovich indenter. All measurements were performed in the continuous stiffness mode (CSM). Modulus (E) and hardness (H) were derived from the loading curve of

the graph in dependence of the penetration depth. Average values and standard deviations were calculated with the software Analyst. Thicknesses of the LbL samples were measured by a DekTak 8 stylus profilometer from Veeco, Mannheim, Germany. The stylus tip radius was 5 µm at force of 3 mg. The morphology of the product was investigated via SEM. Images were collected on a field-emission scanning electron microscope type JSM-6700F from Jeol (Eching, Germany) with an acceleration voltage of 2 kV and a working distance of 3 or 8 mm.

9.3 Results and Discussion

Adhesive proteins found in mussel are rich with cathechol and amine functionality and therefore are capable of adhering to almost all organic and inorganic surfaces. Synthetic polymers modified with these functionalities have a potential to be used as building block in LbL assemblies. HES was modified with dopamine from an ester containing diglycolic group in a two step synthesis as illustrated in Figure 9-1.

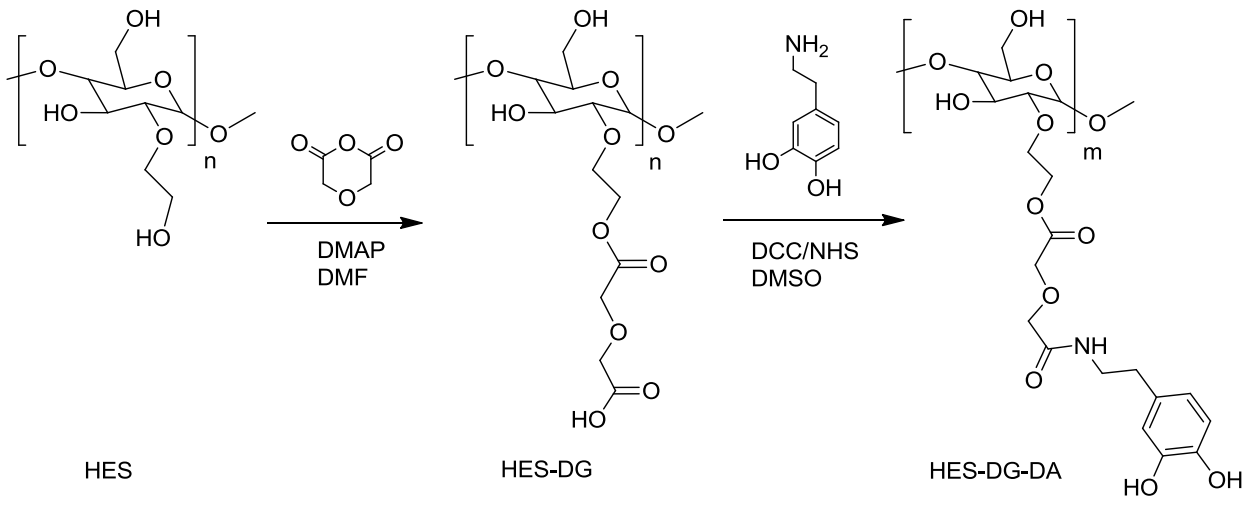

Figure 9-1: Synthetic scheme for HES-DG-DA

Diglycolicanhydride (DGA) was reacted with HES in the first step yielding carboxylic end groups. A degree of substitution of 67 % was achieved calculated from the ^{1}H-NMR integrals (not shown here). In the next step HES-DG was modified with dopamine where amino group of dopamine was coupled to the carboxyl groups of HES-DG. This coupling took place by the activation of carboxyl group using DCC and NHS. Dialysis of the reaction contents has removed any unreacted species. ^{1}HNMR of freeze dried polymer is given in Figure 9-2.

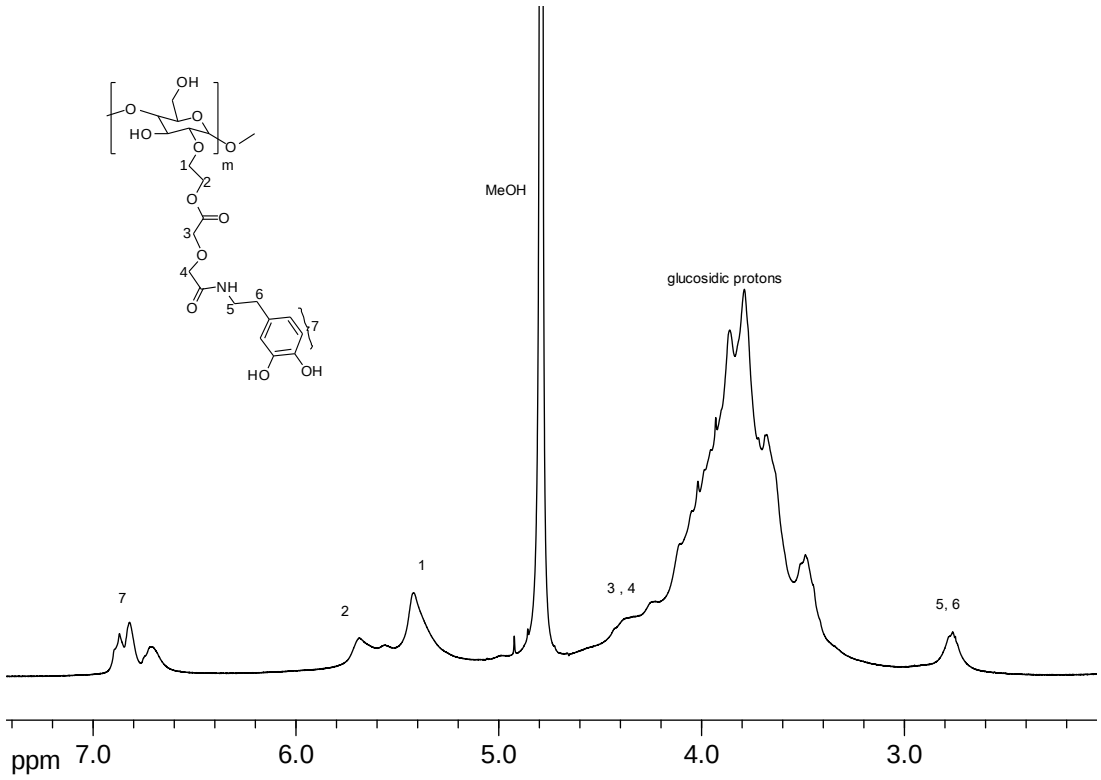

Figure 9-2: ^{1}H NMR spectra of HES-DG-DA

The aromatic hydrogen signals around 6.5 to 6.9 are indicative of the successful addition of dopamine to the polymer. The degree of substitution was 21 % determined from nitrogen to carbon ratio from elemental analysis.

Size measurements of the alusion platelets were performed on two different composite materials with a top view in SEM shown in Figure 9-6. Data was analyzed with image processing and analysis software “Image J”. Randomly 69 different platelets on the surface of two different samples were selected for this purpose. Aluminium oxide platelets are in the range of 2.2 µm to 13.6 µm with an average diameter of 7.11 ± 2.82 µm. Beside smallest

platelets of 2.2 µm there were smaller particles in the form of debris. In a similar way thickness of the individual platelet was also calculated from the side view of the fracture surface of the composite material. Altogether platelets at 17 different points were analyzed resulting in 329±58 nm thickness. It is noteworthy that thickness measurement by this way is not an absolute method however it can be used as a rough estimate. The reason lies in that during SEM, neither the sample under investigation is lying exactly at vertical position to the viewing angle nor the cutting edge of the substrate is exactly perpendicular.

A stable suspension of α-ZrP platelets with a diameter of few hundred nanometers was prepared by ultrasonication.[18] As alusion platelets were of comparatively bigger size than α-ZrP platelets, it was not possible to make a suspension by simple ultrasonication of the platelets as received. They need to be modified to disperse them so that can be used in the fabrication of a layer composite. The surface was modified with hydrophobic silane species containing amine terminated functionality.[22] ATES is a well established reagent to modify glass surfaces. The terminal amine group at the so modified surfaces can be used to attach proteins, drug molecule and DNA.[30-31] This modification also allows to spread the platelets at the air water surface.[22] Platelets were not fully dispersed when added to the water in the beginning; however, ultrasonication of the suspension has resulted in evenly distributed layer (Figure 9-3). After the formation of very smooth and highly oriented platelets, they can be transferred to a glass substrate by a dipping procedure.

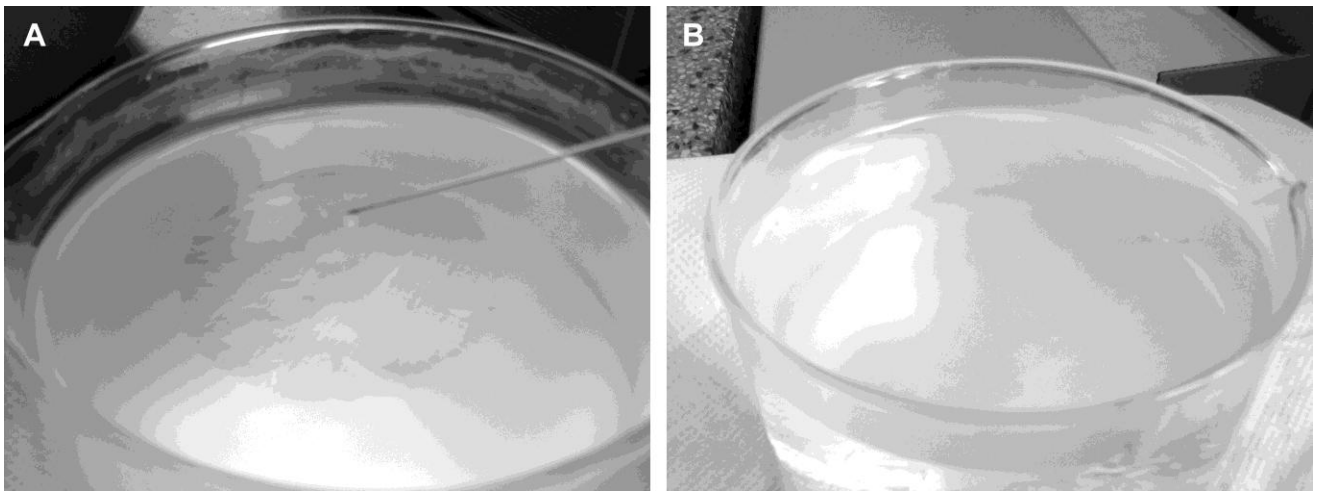

Figure 9-3: Modified aluminum oxide platelets (A) as transferred (B) after sonication

The choice of dopamine modification is inspired by mussels adhesive proteins. Based on this bio material, it has been reported that dopamine form thin films on the surface of a variety of organic and inorganic materials like metal oxides, polymers, noble metals and ceramics via coordination, covalent or hydrogen bonding.[23,25-26]

Lee et al. have investigated the interaction of dopamine with organic and inorganic surfaces with the help of dopamine modified tip of AFM. Dopamine adheres strongly and reversibly to the titanium surface via coordination bonds. No hysteresis between approach and pull off curves was observed by replacing DOPA with PEG on the tip of cantilever indicating that only DOPA interacts with the titanium surface. The determined bond dissociation energy was close to the bond formed between dopamine and titanium oxide. Additionally the same tip of AFM was tested with an amine substituted silicon surface. From the calculation of pull off force it has been revealed that a covalent bond is formed between DOPA and amine at the surface.[26] Based upon these observations it has been proposed that there should be a possible interaction between HES modified with dopamine and aluminium oxide platelets which were modified with terminal amine functionality. This modification achieved by ATES serve two important functions. Firstly hydrophobic modification help to orient platelets at the air water surface and secondly amines are available for an interaction with the dopamine groups. A covalent bond is expected between dopamine and surface bound amine. As mentioned earlier dopamine is also capable of interacting directly to the titanium oxide surface and a similar mechanism can be thought of for aluminium oxide surface. A schematic illustration of possible adhesion mechanism is given in Figure 9-4.

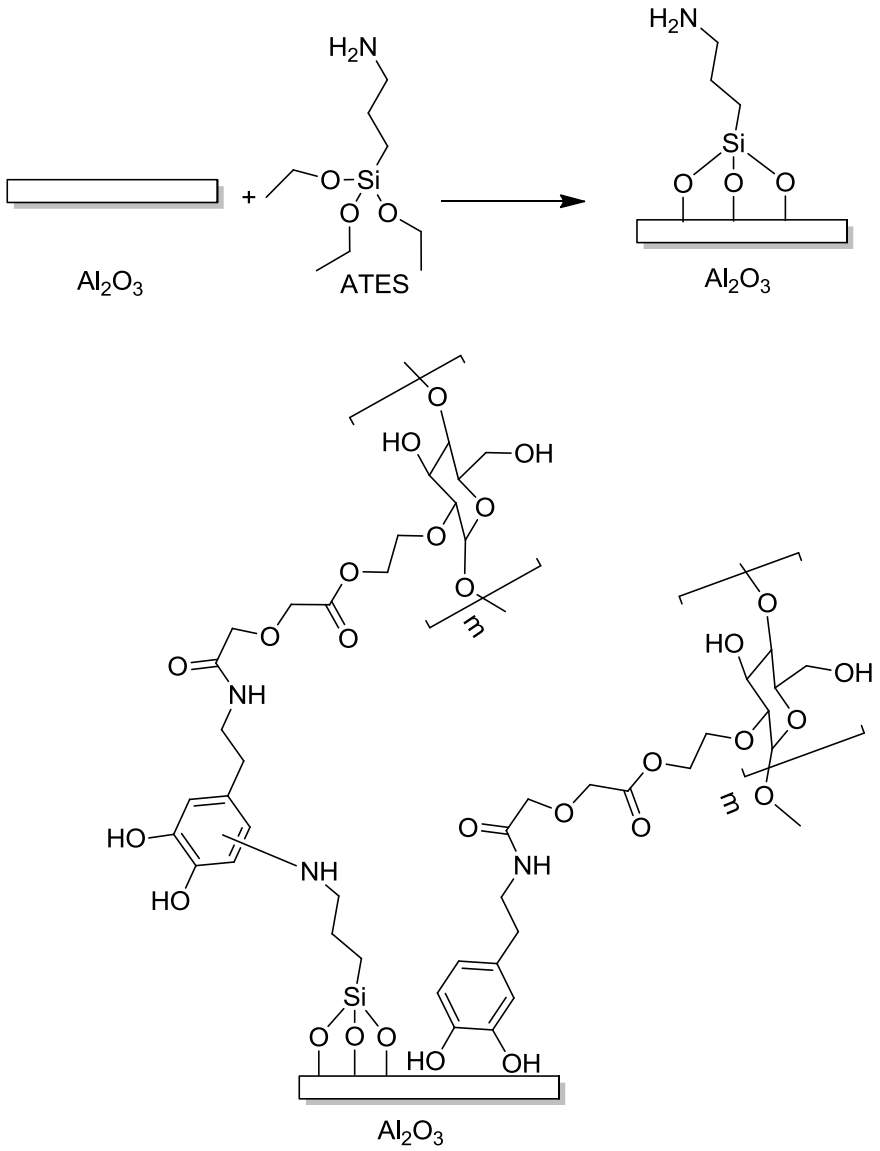

Figure 9-4: Schematic illustration of possible interaction mechanisms HES-DG-DA with alusion

Composites were constructed on glass slides with up to 9 layers of alusion and polymer. SEM images of fabricated composite materials are given in Figure 9-5.

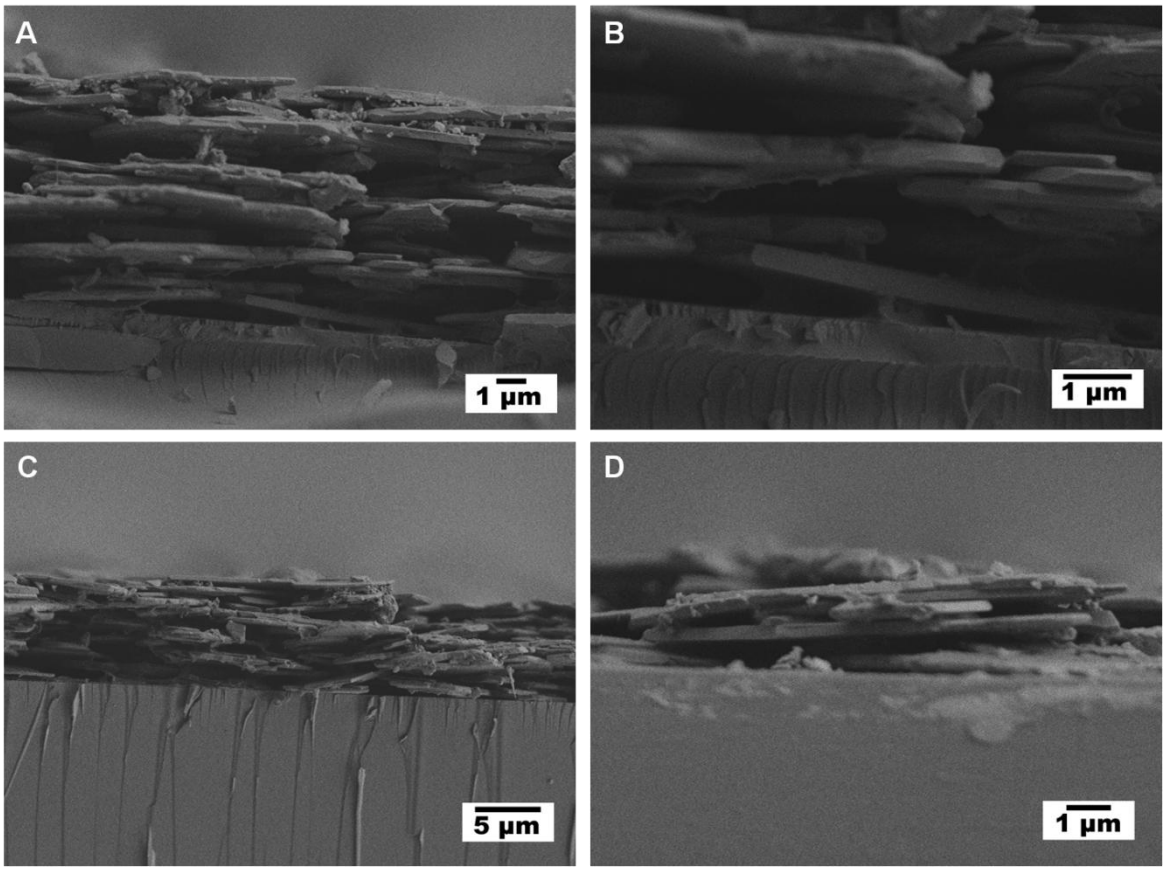

Figure 9-5: SEM of hybrid composite material (A) and (B) 8 layers, (C) 9 layers, (D) 2 layers

On the SEM images the glass substrate can be seen at the bottom. Inorganic platelets are stacked upon the glass substrate according to brick and mortar assembly. As found in nacre some of the platelets are overlapping on the neighbouring platelets as can be seen in Figure 9-5B. Beside major platelets there is debris found in between the layers. In Figure 9-6 a top view of a 8 layer composite is presented. Homogenously distributed platelets are found at the top surface, however, there are few voids which are more visible at higher magnification shown in Figure 9-6B.

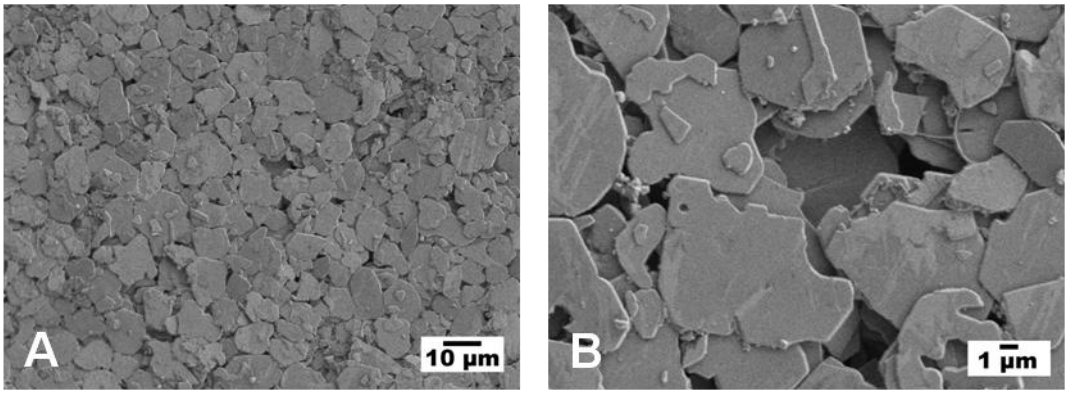

Figure 9-6: SEM top view of fabricated composite 8 layers

These blank areas might appear during the transfer of platelets from the water surface although care has been taken to shift the platelets without disturbing their alignments during this manual transfer to glass slide. A void at one particular point is covered by the under lying layer. Layer deposition was always started and ended with polymer layer by dipping into the dopamine substituted polymer. The surface topology was also verified by AFM as illustrated in Figure 9-7. Non alignment at the platelets can be seen here. Furthermore, the gaps between the platelets are visible here too.

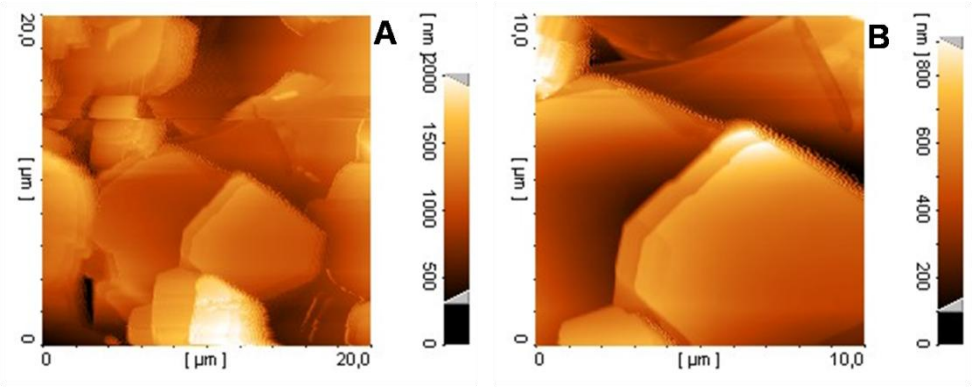

Figure 9-7: AFM surface analysis of composite

As discussed earlier, SEM is not an exact method for determining the thickness from side view. As an alternative a profilometer was used for this purpose which is a non destructive method for thickness measurement with higher accuracy for the kind of samples used here.

The vertical depth was measured along a horizontal length with a stylus force of 3 mg so as not to destroy the surface and scan only the surface coated material. In general two scans were performed on each sample at different places. Thickness profiles of two composite materials are shown exemplarily in Figure 9-8.

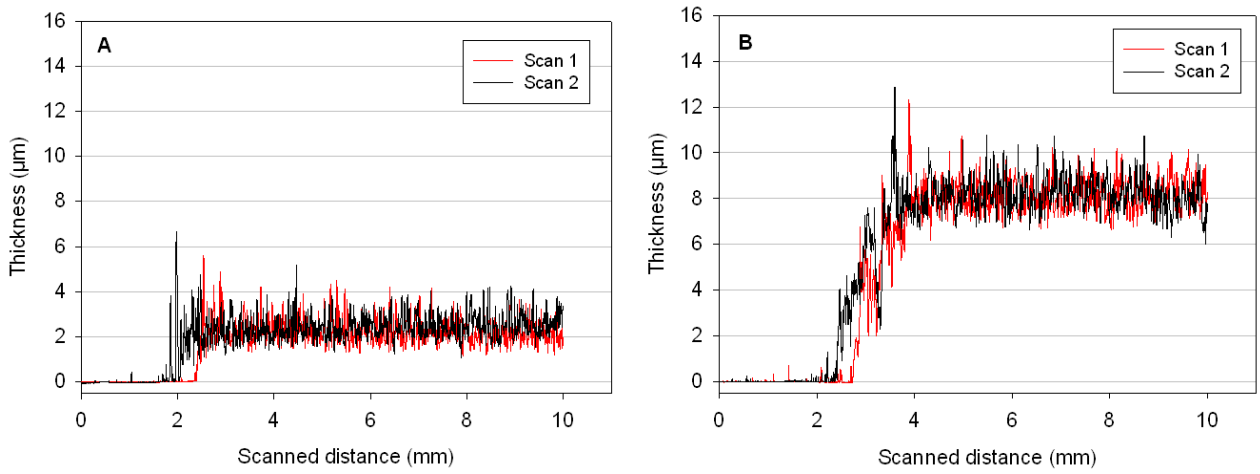

Figure 9-8: Thickness and roughness profile of composite film (A) 2 layers (B) 9 layers

The measurement starts on the naked surface of the glass slide. This region is very flat and was used to define zero height. Then a gradual increase can be observed (between 2 to 4 mm scanned distance) where the coated area begins. In the flat region (from 4 to 10 mm for example in Figure 9-8B) the thickness of the film was determined. The spiking in the profilometer scans corresponds to misaligned platelets and the "noise" in the profilometer signal is indicative of a certain roughness of the LbL assembled material.

In order to observe the increase in the thickness of the LbL assembled composite films, a series of composites was fabricated with the number of layers varying between 2 to 9. The thickness of each sample was determined from the profilometer scans on each film; the scans were averaged in the plateau region and the standard deviation was used as error of the measurement and is a measure of the fluctuations in the thickness.

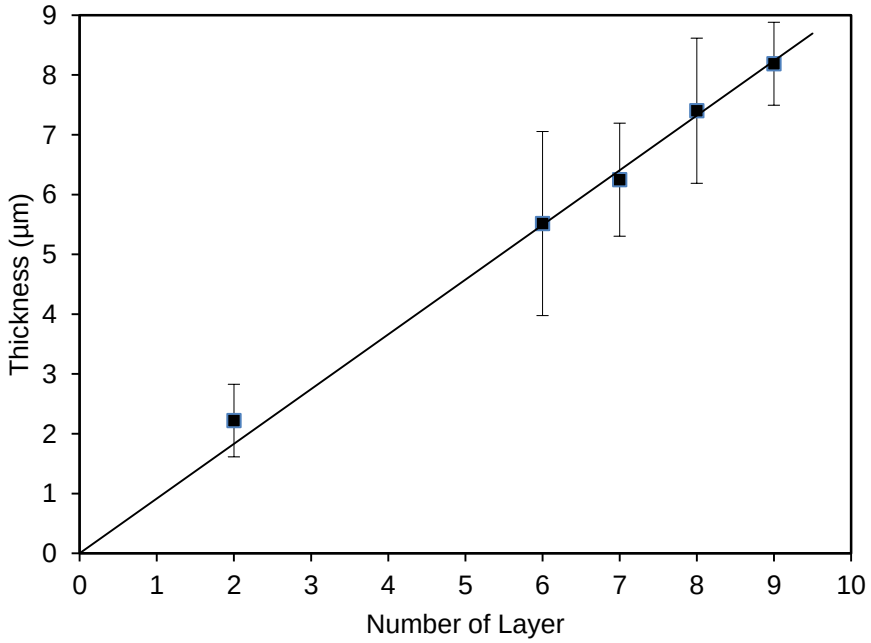

Figure 9-9: Thickness of the composite as measured by a profilometer

There is a continuous increase in the thickness with additional layers being deposited and trend line was drawn passing through zero. All samples are lying on a straight line with continuous addition of polymer and inorganic platelets.

In spite of the fact that SEM does not provide accurate information about thickness it was additionally estimated with SEM images for three samples for a general comparison purpose as summarized in Table 9-1.

Table 9-1: Thickness and roughness profile from profilometer and SEM

Layers	Thickness µm (Profilometer)	Std. Dev.	Thickness µm (SEM)
2	2.22	0.61	2.03
6	5.51	1.54	
7	6.25	0.95	5.93
8	7.40	1.21	
9	8.19	0.69	8.17

The data obtained from SEM are slightly different in comparison to the profilometer but within the standard deviation. Profilometer measurements were performed along the surface with thousands of data point while SEM was restricted only to five to six spots.

9.3.1 Mechanical Testing

The composite films fabricated were in the range of 8 µm thickness making nano-indentation an appropriate method for determining the mechanical properties. Samples were tested in an array of 5x5 µm at a distance of 25 µm at two different places. Typical load (P) displacement curves are presented in Figure 9-10.

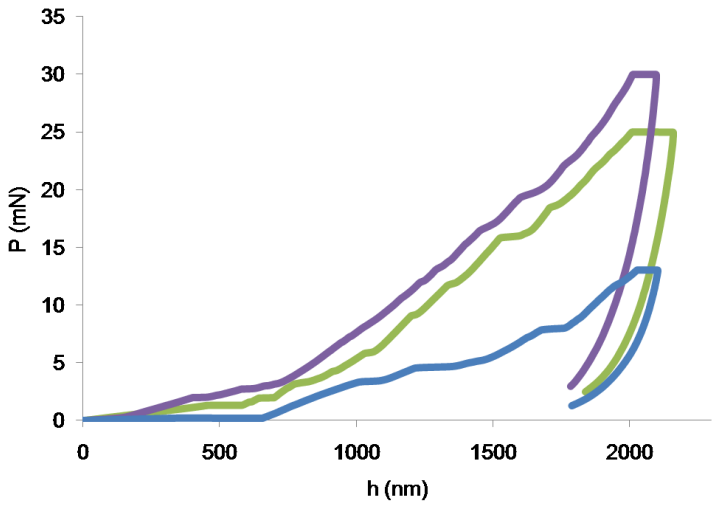

Figure 9-10: Load displacement curves in nanoindentation experiments

From these curves values of hardness (H) and Young's modulus (E) can be determined as reported by Burghard et al.[32] This mode of measurement is affected greatly and very sensitively by the substrate on which indentation takes place. This is particularly true for indentation depth greater than 20 % of the total thickness of the sample under observation.[33] Because of the surface roughness indents were performed on smoother areas and limited to 200 nm depth. The data obtained was analyzed with the method of Olive and Pharr[34] and results are summarized in Table 9-2. A composite with 9 layers has shown highest values of

10.8 GPa for modulus a hardness of 0.35 GPa. In comparison, composite with 7 layers gave a hardness of 0.53 GPa, however, it is important to note that the hardness of sample 7 has shown double of standard deviation than sample with 9 layers. Therefore within the error of the measurement the data is comparable. The values obtained for 9 layered sample with E modulus of 10.8 GPa and a hardness (H) of 0.35 GPa are comparable to and often better than similar nacre-like assemblies which had been reported. Young's modulus of DOPA-Lys-PEG with montmorillonite has a reported value of 4.6 GPa for modulus which has increased to 6.8 GPa after crosslinking.[35] The values presented here are even better than previously reported composites of chitosan with ZrP (E=2.60 GPa, H=70 MPa).[18] In another report using alusion with chitosan a modulus of 9.6 GPa has been given.[22]

Table 9-2: Mechanical properties of composite with different number of layers

Layers	Modulus (E) GPa	Hardness (H) GPa
6	7.8 ± 2.23	0.34 ± 0.11
7	9.6 ± 3.78	0.53 ± 0.22
8	6.2 ± 2.56	0.31 ± 0.17
9	10.8 ± 3.11	0.35 ± 0.10

The good mechanical properties indicate a strong interaction between polymer and platelets, being responsible for the load transfer. This is a similar mechanism as found in nacre. Fabricated composite material looks very similar to the nacre structure (Figure 9-11). The significance of interlocking of platelets has been described as the most important phenomenon beside nano scale structure.[36] In fabricated composite piling up can be seen along with interlocking where platelets are overlapping partially at their edges.

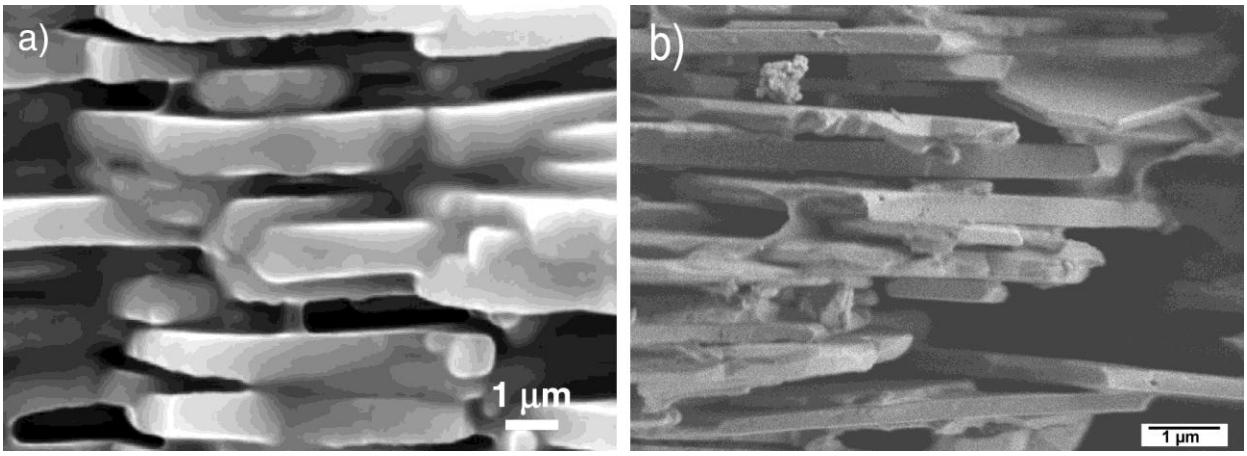

Figure 9-11: SEM images of (a) nacre[36] (b) fabricated composite

9.3.2 Thermogravimetric Analysis

TGA was performed with a heating rate of 10 °C to make a comparison between the constituting components and the composite made out of them. Pure aluminium oxide platelets show only 4.4 % mass loss while HES-DG-DOPA was fully degraded upon heating to 690 °C. The composite material shows a mass loss of 28.7 %. Mass loss curve of the composite is similar to that of pure polymeric content. A major dip can be seen between 220 to 300 C°, and followed by a second degradation step in the temperature range from 300 to 410 C° (Figure 9-12).

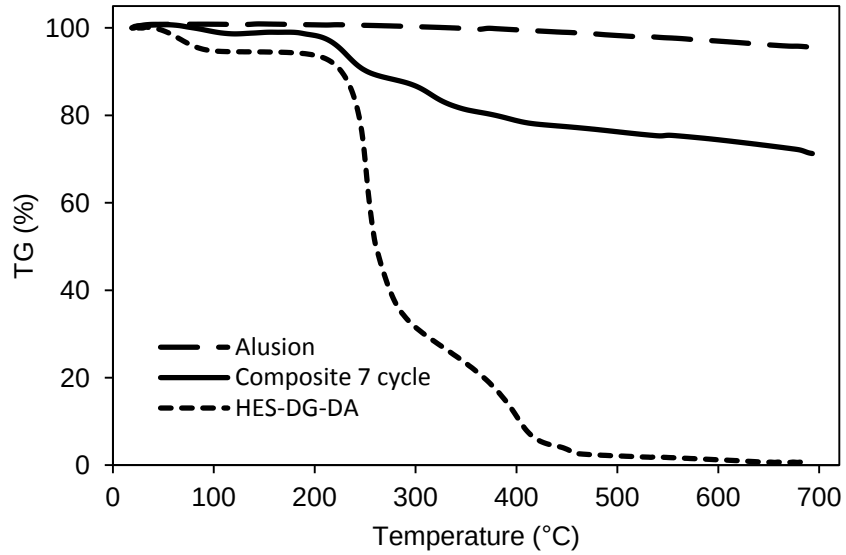

Figure 9-12: Thermogravimetric analysis of pure polymer, alusion and composite material

From TGA curves, mass content of the pure polymeric part within composite can be estimated by subtracting relative mass change due to alusion from the total mass change of composite. In this way pure polymer content was found to be around 27 % of the whole composite material. This load of organics in the construction is comparable to other fabricated films of this kind.[17, 37] However, the polymeric protein part found in nacre is around 5 % only.[5]

9.4 Conclusion

Layered composites of hydroxyethyl starch-diglycol-dopamine (HES-DG-DA) and aluminium oxide platelets (alusion) were prepared by layer-by-layer assembly. Alumina platelets were surface modified with (3-aminopropyl)triethoxysilane (ATES) while hydroxyethyl starch was modified with dopamine for better adhesion. Composite films were constructed with up to 9 bilayers of alusion and polymer. The growth and structural features were studied along with their mechanical properties. Fabricated composite material looks morphologically similar to the nacre microstructure. Inorganic platelets were stacked according to brick and mortar assembly with some of the platelets overlapping on the neighbouring platelets which provide interlocking. A continuous increase in the thickness with additional layers being deposited was observed with a maximum thickness of 8.2 µm. Composite with 9 bi-layers has shown values of 10.8 GPa for E-modulus and 0.35 GPa for hardness. These values were found comparable and often better to similar nacre-like assemblies. Polymeric content of the fabricated composite was found around 27 %.

References

[1] Barthelat, F.; Tang, H.; Zavattieri, P. D.; Li, C. M.; Espinosa, H. D., *J. Mech. Phys. Solids*, (2007) **55**, 306.

[2] Chen, R.; Wang, C.-A.; Huang, Y.; Le, H., *Mater. Sci. Eng., C* (2008) **28**, 218.

[3] Currey, J. D., *Proc. R. Soc. London, B*, (1977) **196**, 443.

[4] Espinosa, H. D.; Rim, J. E.; Barthelat, F.; Buehler, M. J., *Prog. Mater. Sci.*, (2009) **54**, 1059.

[5] Jackson, A. P.; Vincent, J. F. V.; Turner, R. M., *J. Mater. Sci.*, (1990) **25**, 3173.

[6] Kato, T., *Adv. Mater.*, (2000) **12**, 1543.

[7] Tang, Z.; Kotov, N. A.; Magonov, S.; Ozturk, B., *Nat. Mater.*, (2003) **2**, 413.

[8] Li, Y.-C.; Schulz, J.; Grunlan, J. C., *ACS Appl. Mater. Interfaces*, (2009) **1**, 2338.

[9] Podsiadlo, P.; Paternel, S.; Rouillard, J. M.; Zhang, Z.; Lee, J.; Lee, J. W.; Gulari, E.; Kotov, N. A., *Langmuir*, (2005) **21**, 11915.

[10] Lu, C.; Donch, I.; Nolte, M.; Fery, A., *Chem. Mater.*, (2006) **18**, 6204.

[11] Bennadji-Gridi, F.; Smith, A.; Bonnet, J.-P., *Mater. Sci. Eng., B* (2006) **130**, 132.

[12] Deville, S.; Saiz, E.; Nalla, R. K.; Tomsia, A. P., *Science*, (2006) **311**, 515.

[13] Burghard, Z.; Tucic, A.; Jeurgens, L. P. H.; Hoffmann, R. C.; Bill, J.; Aldinger, F., *Materials Research Society Symposium Proceedings*, (2007) **1007**,

[14] Burghard, Z.; Tucic, A.; Jeurgens, L. P. H.; Hoffmann, R. C.; Bill, J.; Aldinger, F., *Adv. Mater.*, (2007) **19**, 970.

[15] Decher, G.; Schlenoff, J. B., *Multilayer Thin Films*, Multilayer Thin Films, Wiley-VCH: Weinheim: (2003).

[16] Podsiadlo, P.; Michel, M.; Lee, J.; Verploegen, E.; Wong Shi Kam, N.; Ball, V.; Lee, J.; Qi, Y.; Hart, A. J.; Hammond, P. T.; Kotov, N. A., *Nano Lett.*, (2008) **8**, 1762.

[17] Podsiadlo, P.; Tang, Z.; Shim, B. S.; Kotov, N. A., *Nano Lett.*, (2007) **7**, 1224.

[18] Waraich, S. M.; Hering, B.; Burghard, Z.; Bill, J.; Behrens, P.; Menzel, H., *J. Colloid Interface Sci.*, (2012) **367**, 74.

[19] Bulwan, M.; Zapotoczny, S.; Nowakowska, M., *Soft Matter*, (2009) **5**, 4726.

[20] Fujii, N.; Fujimoto, K.; Michinobu, T.; Akada, M.; Hill, J. P.; Shiratori, S.; Ariga, K.; Shigehara, K., *Macromolecules*, (2010) **43**, 3947.

[21] Lutkenhaus, J. L.; Hrabak, K. D.; McEnnis, K.; Hammond, P. T., *J. Am. Chem. Soc.*, (2005) **127**, 17228.

[22] Bonderer, L. J.; Studart, A. R.; Gauckler, L. J., *Science*, (2008) **319**, 1069.

[23] Waite, J. H.; Andersen, N. H.; Jewhurst, S.; Sun, C., *J. Adhes.*, (2005) **81**, 297

[24] Glass, P.; Chung, H.; Washburn, N. R.; Sitti, M., *Langmuir*, (2009) **25**, 6607.

[25] Lee, H.; Dellatore, S. M.; Miller, W. M.; Messersmith, P. B., *Science*, (2007) **318**, 426.

[26] Lee, H.; Scherer, N. F.; Messersmith, P. B., *Proc. Natl. Acad. Sci. U.S.A.*, (2006) **103**, 12999.

[27] Podsiadlo, P.; Liu, Z.; Paterson, P.; Messersmith, P. B.; Kotov, N. A., *Adv. Mater.*, (2007) **19**, 949.

[28] Lee, H.; Lee, Y.; Statz, A. R.; Rho, J.; Park, T. G.; Messersmith, P. B., *Adv. Mater.*, (2008) **20**, 1619.

[29] Jin, R.; Hiemstra, C.; Zhong, Z.; Feijen, J., *Biomaterials*, (2007) **28**, 2791.

[30] Warner, W. S.; Tenge, B. J.; Hungerford, J. M.; Honigs, D. E., *Anal. Biochem.*, (1989) **176**, 137.

[31] Hermanson, G. T.; Mallia, A. K.; Smith., P. K., *Immobilized Affinity Ligand Techniques*,, Academic Press, Inc.San Diego, CA.: (1992).

[32] Burghard, Z.; Zini, L.; Srot, V.; Bellina, P.; Aken, P. A. v.; Bill, J., *Nano Lett.*, (2009) **9**, 4103.

[33] Wang, J.; Li, W.-Z.; Li, H.-D.; Shi, B.; Luo, J.-B., *Thin Solid Films*, (2000) **366**, 117.

[34] Oliver, W. C.; Pharr, G. M., *J. Mater. Res.*, (1992) **7**, 1564.

[35] Podsiadlo, P.; Liu, Z.; Paterson, D.; Messersmith, P. B.; Kotov, N. A., *Adv. Mater.*, (2007) **19**, 949.

[36] Katti, K. S.; Katti, D. R., *Mater. Sci. Eng., C* (2006) **26**, 1317.

[37] Yao, H.-B.; Tan, Z.-H.; Fang, H.-Y.; Yu, S.-H., *Angew. Chem., Int. Ed.*, (2010) **49**, 10127.

10 Summary and Outlook

Aim of this thesis was to mimic structural features found in nacre to fabricate composite materials as a tough ceramic material and to explore the mechanical properties. Structural pattern found in nacre at micro level, so called “brick and mortar” assembly is formed in the presence of a mixture of proteins rich in acidic amino acids. Calcium carbonate in the form of aragonite is deposited in the form of platelets with polymeric material in between serving as gluing agent. To mimic this hierarchical pattern, an appropriate inorganic material and an adhesive polymeric partner are required.

Specific polymers are required that can be used as crystallization controlling agents in order to synthesize inorganic platelets. For this purpose different phosphonic acid functional polymers and copolymers were synthesized. Properties of the basic polymer chains were altered by copolymerization with different monomers to get desired properties. Vinylphosphonic acid (VPA) was copolymerized with acrylamide (AAM), dimethylacrylamide (DMAA) and vinylimadazole (VI). (Ethyl 2-[4-(dihydroxyphosphoryl)-2-oxabutyl]acrylate)-co-(dimethylacrylamide) (EDOA) was homo- and copolymerized with dimethylacrylamide (DMAA). Another phosphonic acid functional monomer vinylbenzyl phosphonic acid (VBP) was copolymerized with 4-vinylpyridine (VP). The copolymerization reactivity parameters were determined by establishing the relationship between the compositions of the copolymers and the different monomer concentrations. Results indicated alternative and statistical copolymers. Additionally some phosphonic acid homopolymers, phosphonate ester, bisphosphonate and phosphate functional polymers were synthesized. Inspired by the adhesive proteins of mussels a mimic was synthesized where hydroxyethyl starch was modified with 2-(3,4-dihydroxyphenyl)ethylamine (dopamine), (HES-DG-DA).

These polymers were tested for the controlled crystallization of hydroxyapatite, with a close resemblance to natural bone material and α-Zirconium hydrogenphosphate hydrate, a biocompatible material which exhibits a layered structure. These experiments were conducted by B. Hering (ACI, University Hannover). HES-DG-DA (hydroxyethyl starch substituted with dopamine) addition had a considerable influence on the morphology of the hydroxyapatite depending strongly on the concentration. The product prepared with Ca/DOPA ratio of 18:1 has shown an interesting morphology in the form of blocks consisting

of stacked thin lamellae. The structure already resembles the structure of nacre. For a lower amount of the polymer comparable piles were observed, but the platelets were much thicker. A change in the concentration of added HES-DG-DA not only resulted in different structures but also different forms of calcium phosphate namely monetite and hydroxyapatite. A phosphonic acid homo polymer (2-methacryloyloxyethyl) phosphonic diacid (pMEPD) has resulted in a porous hydroxyapatite whereas needle like structures of different orientation were obtained under the influence of other copolymers. Within the scope of this study only inorganic material in the form of platelets was of interest to be used in the fabrication of composite material.

Furthermore for controlled crystallization of α-Zirconium hydrogenphosphate hydrate, it was observed that not only the content of phosphonic acid but also the monomer ratio within the copolymer is influencing the nucleation control. A copolymer of $pVPA_{0.25}$-co-$AAM_{0.75}$ (poly vinylphosphonic acid-co-acrylamide) in a Zr/P ratio of 9.4:1 led to the formation of platelets with a diameter between 200 and 400 nm and a high aspect ratio. Under the influence of other polymeric materials for example pVPA-co-DMAA poly (vinylphosphonic acid)-co-(dimethyl acrylamide) either partly aggregated or thick aggregated material was obtained as verified by SEM. The crystal modification was verified in all cases by XRD.

For the construction of nacre like composites layer-by-layer assembly was chosen because of simplicity and good control on the architecture. First experiments were carried out with chitosan / montmorillonite and poly(diallyldimethyl ammonium chloride) / α-zirconium hydrogen phosphate in order to establish the preparation and analytical methods. Thicknesses of the layered material were determined with AFM and ellipsometry while nanoindentation was chosen as a method for mechanical characterization i.e. determination of the E-modulus and the hardness. Ellipsometry (because of strong light scattering) and AFM (because of high surface roughness) were not found to be suitable for the thickness determination at higher number of dipping cycles. However, profilometry can be employed for composite thickness measurement with high reproducibility.

Layered composites of α-zirconium hydrogenphosphate hydrate (α-ZrP) platelets and chitosan were prepared by layer-by-layer assembly. The growth and structural features of the composite films were studied along with their mechanical properties with reference to the number of dipping cycles, concentration and pH. A concentration of 0.2 wt% for the α-ZrP

suspension and 0.01 wt% for the chitosan solution are found to be optimal. Lower concentrations of both components have resulted in an inferior alignment of the platelets and lower values for modulus and hardness. Best results were obtained when the chitosan solution had a pH value of 5 resulting in modulus of 2.6 GPa and hardness of 70 MPa. Maximum thickness obtained was around 6 µm. Composites obtained with chitosan solutions at pH 4 showed inferior alignment of the particles and reduced mechanical properties. The limited solubility of the chitosan at pH > 6 and the extended conformation at lower pH might be reason for non optimal interaction with the nanoscale α-ZrP platelets, leading to only moderate mechanical properties.

Another LbL composite was constructed mimicking mussel proteins. Adhesive proteins found in mussels are rich in cathechol and amine functionality. They are capable to adhere to almost all organic and inorganic surfaces. A composite was prepared by LbL assembly using alumina platelets and hydroxyethyl starch. Alumina platelets used have close morphological resemblance to aragonite as found in nature and their aspect ratio is also close to as found in nacre. A continuous increase in the thickness of the composite layer was observed in profilometer measurement. Composite material with a thickness of 8 µm has resulted in modulus of 10.8 GPa with a hardness of 0.35 GPa. These values are comparable or even better as similar materials. Synthetic material looks very similar structurally to the original nacre as revealed by the SEM.

The experiments presented here have shown that it is possible to prepare materials which have a nacre-like structure and interesting mechanical properties. First structure-property-relationships were identified. However, with the methods used to prepare the materials it is not yet possible to obtain samples large enough to fabricate implants. For this purpose a fast method of material synthesis is required which can produce thicker composite material samples in short time. Controlled freezing of suspensions could be a method of choice for ordering the inorganic platelets. The porous scaffold obtained by this method can then be backfilled with an organic component thus resulting in a dense composite material. Synthesis of complex shapes with better mechanical properties should be possible with this technique.